Novel Design Approach for High Performance Waveguide Filters

by

Yifan Wang

A thesis

presented to the University of Waterloo

in fulfillment of the

thesis requirement for the degree of

Master of Applied Science

in

Electrical and Computer Engineering

Waterloo, Ontario, Canada, 2008

I hereby declare that I am the sole author of this thesis. This is a true copy of the thesis, including any required final revisions, as accepted by my examiners.

I understand that my thesis may be made electronically available to the public.

Abstract

This thesis provides design approaches for waveguide filter with prescribed transmission zeros. The emphasis is on a new class of filter, developed in recent years by utilizing non-resonating nodes (NRNs).

First, a novel circuit model of the coupling irises of waveguide filters is developed in order to aid the design of waveguide filters with NRNs for relatively wide band applications. Also, analytical solutions of the circuit parameters are presented and verified by experimental design.

Secondly, based on this new circuit model, a systematic approach for the design of filters with NRNs is developed and illustrated with two filters. The first has intermediate fractional bandwidth of 3.5%; Good results are obtained without performing global optimization. The second has a relatively wide fractional bandwidth of 8.33% and good results are achieved with very limited global optimization. The results are verified by EM simulations.

Furthermore, for choosing an empty waveguide to realize the NRNs, some novel criteria are proposed to improve the spurious free window of the filter.

Acknowledgements

I would like to thank my supervisor, Dr. Ming Yu for accepting me as candidate for M.A.Sc program in Electrical Engineering. His advice and support over the entire period of my study and research have been priceless.

I am also grateful to my co-supervisor, Dr. Raafat. R. Mansour, especially for his marvelous courses on microwave engineering and filter design which have provided me with a solid background for my research.

Finally, I would also express my appreciation to COM DEV International for supporting this research.

To my Parents

Table of Contents

List of Figures viii

List of Tables xi

1. Introduction 1

2. Design Filter with Coupling Matrix 6

2.1 Introduction 6
2.2 General Coupling Matrix 6
2.3 Synthesis of the Coupling Matrix from Filter Specification 9
2.3.1 Generating Chebychev Polynomials 9
2.3.2 Generating Coupling Matrix from Filter Polynomials 11
2.4 Design Example of Cross-Coupled Waveguide Filter 13
2.5 Conclusions 28

3. Filter with Non-Resonating Nodes 30

3.1 Introduction 30
3.2 Survey on Designs on Publications 31
3.3 Synthesis of Filter with Non-Resonating Nodes (NRNs) 32
3.4 Design of NRN Waveguide Filter with Intermediate Bandwidth 36
3.5 Conclusions 41

4. A Novel Circuit Model of Coupling Irises 42

4.1 Introduction 42
4.2 Circuit Model for Coupling Iris 42
4.3 Finding the Equivalent Coupling Coefficient of the Modified Circuit Model . 48
4.3.1 Single Resonator with Coupling Irises on Both Sides 49
4.3.2 Resonating Cavities in Series 53

5. Novel Design Approach of Waveguide Filters with NRNs 58

5.1 Introduction 58

5.2 Design Example with Intermediate Bandwidth 58

5.2.1 Circuit Model Optimization 59

5.2.2 Realize NRN 1 61

5.2.3 Realize NRN 2 65

5.2.4 Build 4-Pole Module 66

5.2.5 Build Entire Filter 69

5.3 Design NRN Filter with the Wide Bandwidth 71

5.3.1 Optimizing Parameters 71

5.3.2 Design Individual Modules 76

5.3.3 Entire Filter Response and Optimization 80

5.4 Summary of the Design Procedure 84

6. Conclusion and Future Work 86

References 87

List of Figures

Figure 2.1 Series-resonator band-pass prototype network 6

Figure 2.2 Terminated impedance network 11

Figure 2.3 Topology of 6-pole fold back cross coupled filter 15

Figure 2.4 6-pole cross coupled waveguide filter 15

Figure 2.5 HFSS model for direct coupling 17

Figure 2.6 Structure for tuning cavity 1 18

Figure 2.7 Frequency response of cavity 1 19

Figure 2.8 Structure to determine cross coupling M_{25} 20

Figure 2.9 Structure for adjust resonating frequency of cavity 2 21

Figure 2.10 Frequency response of cavity 2 with merely coupling M_{12} and M_{25} 21

Figure 2.11 Reduced filter with coupling matrix 2.38 22

Figure 2.12 Frequency response comparison of EM simulation and coupling matrix 23

Figure 2.13 Re-adjust resonating frequency of resonator 2 24

Figure 2.14 Frequency response of the structure in Figure 2.13 24

Figure 2.15 Structure for simulating the coupling M34 25

Figure 2.16 Structure to adjust length of cavity 3 and fine tune coupling M_{34} 26

Figure 2.17 Frequency responses of previous structure with that of coupling matrix 27

Figure 2.18 Frequency response of filter 28

Figure 2.19 Frequency response of filter with 350MHz bandwidth 29

Figure 3.1 Extracting a resonator from circuit 33

Figure 3.2 Extracting an NRN 35

Figure 3.3 Topology of 6-pole waveguide filter with two NRNs 37

Figure 3.4 Module of NRN1 (circuit topology and EM structure) 38

Figure 3.5 Frequency response comparison of NRN1 38
Figure 3.6 Frequency response comparison of NRN 2 39
Figure 3.7 Frequency response comparison of the entire filter 40
Figure 3.8 E-Field distribution of NRN1 at 6.75 GHz 41
Figure 4.1 Coupling iris between two empty waveguides 43
Figure 4.2 Amplitude of S21 of waveguide iris 43
Figure 4.3 Phase of S21 of waveguide iris 44
Figure 4.4 Admittance inverter prototype 44
Figure 4.5 Modified circuit model of inverter 45
Figure 4.6 Frequency response comparison of circuit model vs. HFSS 46
Figure 4.7 Amplitude of S21 (modified circuit model vs. HFSS) 47
Figure 4.8 Phase of S21 (modified circuit model vs. HFSS) 47
Figure 4.9 Equivalent circuit of modified circuit model of iris 48
Figure 4.10 Equivalent circuit of resonator with iris on both sides 49
Figure 4.11 Scaling the coupling coefficient of two coupled resonator to yield same response 50
Figure 4.12 Circuit models used to represent a coupled waveguide resonator 51
Figure 4.13 Frequency response comparison of circuit models vs. EM simulation 52
Figure 4.14 Circuit models for the structure with N resonators in series 53
Figure 4.15 Circuit models for two coupling resonators in series 55
Figure 4.16 Structure with two resonators in series 56
Figure 4.17 Frequency responses of different models of two resonators in series 57
Figure 5.1 Block diagram of circuit model 59
Figure 5.2 Frequency response of circuit model with original values from coupling matrix 60

Figure 5.3 Optimized circuit model response 61
Figure 5.4 Structure used to realize NRN1 62
Figure 5.5 Frequency response of NRN with arbitrary values 63
Figure 5.6 Circuit model of NRN1 63
Figure 5.7 Frequency responses after manual optimization 65
Figure 5.8 Frequency response of NRN2 66
Figure 5.9 Frequency response of 4-Pole module before optmization 67
Figure 5.10 Frequency response of 4-pole module 68
Figure 5.11 Compare of frequency responses of EM and circuit model 69
Figure 5.12 Frequency response of the filter after optimization 70
Figure 5.13 Frequency response of the filter with material of finite conductivity (copper) 71
Figure 5.14 Frequency response of the filter with original values 72
Figure 5.15 Frequency response of optimized filter with modified circuit model 72
Figure 5.16 Optimized frequency response with M23 limited 74
Figure 5.17 Frequency response of NRN 1 77
Figure 5.18 Frequency response of NRN2 78
Figure 5.19 Initial Frequency response comparison of 4-pole EM structure and circuit model 78
Figure 5.20 Frequency response comparison of 4-pole module after fine tuning 79
Figure 5.21 Frequency response after individual tuning 80
Figure 5.22 Frequency response of the filter after optimization 82
Figure 5.23 Frequency response of the filter with material of finite conductivity (copper) 83
Figure 5.24 Wider frequency range sweep (filter with copper) 83

List of Tables

Table 3.1 Survey of existing design examples of filter with non-resonating nodes 31

Table 5.1 Arbitrary values for NRN1 62

Table 5.2 Optimized parameters for NRN1 64

Table 5.3 Optimized sizes of NRN2 66

Table 5.4 Realizing coupling M45 67

Table 5.5 Tuning resonator no.4 and 5 67

Table 5.6 Optimized sizes for 4-Pole Module 68

Table 5.7 Realizing coupling M01 and M89 69

Table 5.8 Tune resonator no.1 and 8 69

Table 5.9 Optimizing sizes of last step 70

Table 5.10 ideal and optimized value of the filter 73

Table 5.11 Parameters of coupling matrix 75

Table 5.12 Relevent sizes of NRN1 76

Table 5.13 Relevant sizes of NRN2 77

Table 5.14 Relevant sizes of 4-Pole Module 79

Table 5.15 Relevant sizes of the filter in last step 80

Table 5.16 Filter sizes before and after global optimization 81

1. Introduction

Waveguide microwave filters are of great importance in many communication systems, particularly if a high power handling capacity and low insertion loss are desired. The waveguide filters with the Chebyshev class of the filtering function have, for a long time, been widely used in microwave terrestrial and space communication systems. The low insertion loss and equiripple amplitude in-band characteristics, together with the sharp cutoffs at the edge of the pass-band and high selectivity, make it possible to achieve an acceptable compromise between lowest signal degradation and highest noise rejection.

Moreover, the ability of building in prescribed transmission zeros for increasing the close-to-band rejection slops and linearizing the in-band group delay make these filters especially useful. Since the rapidly developing wireless and satellite communications industry is creating an increasingly crowded frequency spectrum, and in consequence, requires a very high close-to-band rejection of the channel filter to prevent the interference and noise from the neighboring channels.

Since 1970's, Atia and Williams have presented an efficient synthesis method using the coupling matrix [1] and [2]. The filters synthesized with such method can possess prescribed transmission zeros by introducing the cross coupling between non-adjacent resonators. Based on the coupling matrix theory, Cameron has developed some systematic approaches which can synthesize the coupling matrix of the filter efficiently with different topologies [3] and [4]. One of the most common topologies is the network with folded configuration. With such a configuration, the non-adjacent resonators can be located side by side so that it is possible to realize the cross coupling between these resonators. The design and optimization techniques of such filters are well covered in the literatures [3]-[11].

Nevertheless, in real applications, the cross coupling in folded configuration is not always desirable, since the generation of the transmission zeros at real frequencies usually requires the coupling coefficients of mixed signs, which increases the complexity of the structure of the filter; in addition, when the transmission zeros are close to the pass-band, the cross-coupling and direct-coupling are comparable in strength and may be difficult or even impossible to be implemented.

Some alternative layout of the filters with transmission zeros has been presented by Amari and some others [18]-[21]. This class of filters has transmission-zero-generating elements which are realized with a dedicated resonator coupled to a non-resonating node, which is, in waveguide filters, realized by a highly detuned waveguide cavity. The transmission-zero-generating elements are placed in cascade with other elements in in-line configurations.

Such filters have some advantages over the filters with cross-coupled resonators. First of all, they permit independent control of transmission zeros, since each one of the transmission zeros is generated and controlled by a dedicated resonator. Secondly, the signs of the coupling coefficients are inconsequential, which reduces the complexity in realizing the inter-resonator couplings. In addition, with the in-line configuration, it is easier to break the entire filter down to the individual modules, on which the optimizations are much less time consuming.

However, the design procedures, which are provided in the literatures [16]-[21], work well only for narrow band applications. The fractional bandwidth of the waveguide filters designed in those literatures ranged from 0.9% to 2.9%. Moreover, the spurious free window of the filter is also narrow because of the unwanted close-to-band resonances of NRNs.

Cogollos has presented a successful design of an eighth order waveguide filter with a fractional bandwidth as wide as 5.438% **Error! Reference source not found.**. However the procedure requires global optimization involving many parameters, which is very time consuming. The frequency dependence of the coupling iris and asymmetric structure of the filter make the design and optimization of the filter difficult, especially for intermediate and wide bandwidth applications with a fractional bandwidth larger than 3%.

In order to design the NRN filters more efficiently, a better circuit model of the coupling iris must be found since the frequency dependence of the coupling iris is the primary reason of degradation in frequency response of the band-pass filter, especially in the wide bandwidth application.

Improved iris models have been provided in recent researches [23] and [24], which took into consideration the frequency dependence of the coupling iris in waveguide filters. However, the design procedures based on those models are all developed for the pure Chebyshev filters without transmission zeros. The feasibility of utilizing such models to design waveguide filter with the NRNs is unknown.

In the first part of this thesis, the coupling matrix theory is briefly reviewed, and a design example of the waveguide filter with cross coupled resonators is illustrated and the limitations are addressed.

Then, together with a review of the extracting pole technique which is suitable to synthesis the filter in in-line configuration, a trial design of the waveguide filter with NRNs is performed basing on the existing procedures, the result illustrated that the circuit model that has been used to design such kind of filters is inadequate for intermediate and

wide bandwidth application. Moreover, some inspection is also done to prove the fact that the spurious within the interested band is actually generated by the unwanted resonance of the NRNs.

To design the filters with NRNs for wider bandwidth applications without excessive optimization, a novel circuit model for the coupling iris is introduced in this thesis. Compared to an ideal lumped element model, the proposed circuit model approximates the frequency dependence of the coupling iris more accurately. In addition, the analytical extraction of modeling parameters is provided.

A systematic design procedure is then developed, based on the novel circuit model, with two design cases. Compared to the existing design procedure, the new one requires much less optimization to realize a relatively wide bandwidth.

Moreover, in order to improve the spurious free window of the filter, some new criteria are developed, in both design cases, for choosing the optimum dimensions of an empty waveguides which are used as NRNs.

Chapter 2 reviews the methods to synthesize the microwave filters with the coupling matrices. A design case of a cross-coupled waveguide filter will be presented with an effort to minimize the usage of the EM simulation.

Chapter 3 presents a review of the extracted-pole method to synthesize the microwave filter with NRNs. A survey of existing designs is done, with a trial design based on the existing method; the limitations of designing waveguide filters with NRNs are discussed.

In Chapter 4, a new circuit model is proposed for the coupling irises in waveguide filters with a relatively wide bandwidth. After an analytical parameter extraction is demonstrated, the design examples of the coupled cavities are presented with a comparison of the results.

A new design procedure, which is developed basing on the new circuit model, is then introduced in Chapter 5. Two filters are realized with the modified circuit model. One of these filters has an intermediate bandwidth; the other has a relatively wide bandwidth. In addition, some new design criteria for choosing the waveguide dimension for NRNs are applied to realize a wider spurious free window of the filters.

Chapter 6 concludes the thesis and suggests some possible applications for the newly developed circuit model in an automatic filter design and optimization.

2. Design Filter with Coupling Matrix

2.1 Introduction

Firstly introduced in the early 1970s by Atia and Williams [1][2], the filter synthesis technique with a coupling matrix was highly developed and widely applied in microwave filter design[5]-[7].

In this chapter, the method of synthesis of microwave filter with a coupling matrix is reviewed. Some emphasis is put on the method provided by Cameron because of its simplicity [4] [7]. Also a waveguide filter design is included with a special effort made to avoid the intensive EM simulation for optimization.

2.2 General Coupling Matrix

Figure 2.1 illustrates a band-pass filter prototype which comprises of a series of resonators inter-coupled by a mutual inductance.

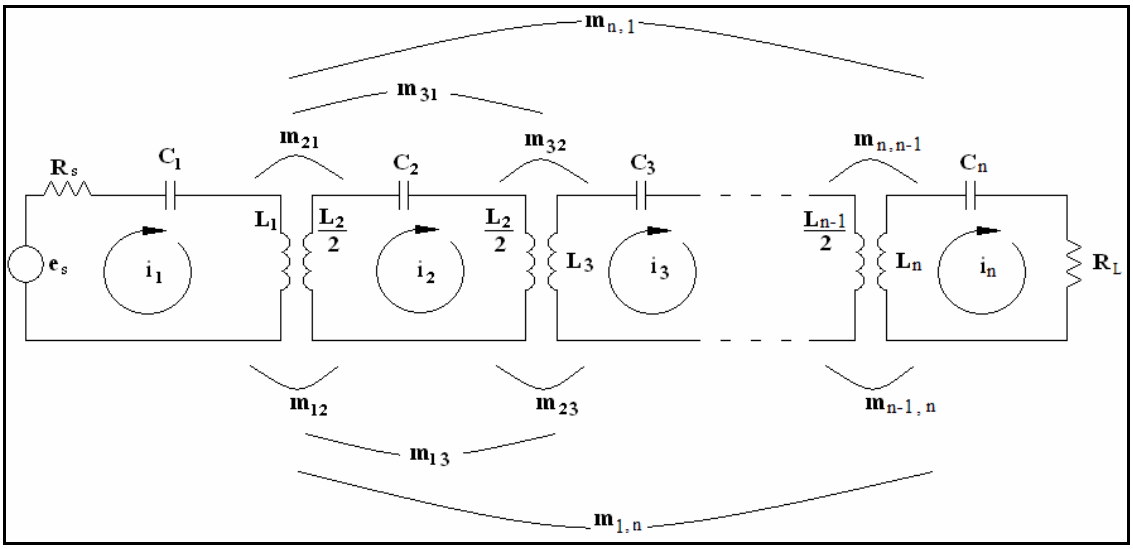

Figure 2.1 Series-resonator band-pass prototype network

The loop equation of this network is

$$\begin{bmatrix} R_S + j\omega L_1 + \dfrac{1}{j\omega C_1} & -j\omega L_{12} & \dots & -j\omega L_{1n} \\ -j\omega L_{21} & j\omega L_2 + \dfrac{1}{j\omega C_2} & \dots & -j\omega L_{2n} \\ . & . & \dots & . \\ . & . & \dots & . \\ . & . & \dots & . \\ -j\omega L_{n1} & -j\omega L_{n2} & \dots & R + j\omega L_n + \dfrac{1}{j\omega C_n} \end{bmatrix} \begin{bmatrix} i_1 \\ i_2 \\ . \\ . \\ . \\ i_3 \end{bmatrix} = \begin{bmatrix} e_S \\ 0 \\ . \\ . \\ . \\ 0 \end{bmatrix}. \quad (2.1)$$

Suppose that the resonators of the filter are synchronously tuned (resonate at the same frequency), then $\omega_0 = 1/\sqrt{LC}$ where $L = L_1 = L_2 = ... = L_n$, and $C = C_1 = C_2 = ... = C_n$, such that (2.1) is rewritten as

$$\omega_0 L \cdot \mathrm{FBW} \begin{bmatrix} \dfrac{R_S}{\omega_0 L \cdot \mathrm{FBW}} + p & -j\dfrac{\omega L_{12}}{\omega_0 L \cdot \mathrm{FBW}} & \dots & -j\dfrac{\omega L_{1n}}{\omega_0 L \cdot \mathrm{FBW}} \\ -j\dfrac{\omega L_{21}}{\omega_0 L \cdot \mathrm{FBW}} & p & \dots & -j\dfrac{\omega L_{2n}}{\omega_0 L \cdot \mathrm{FBW}} \\ . & . & & . \\ . & . & & . \\ . & . & & . \\ -j\dfrac{\omega L_{n1}}{\omega_0 L \cdot \mathrm{FBW}} & -j\dfrac{\omega L_{n2}}{\omega_0 L \cdot \mathrm{FBW}} & \dots & \dfrac{R_L}{\omega_0 L \cdot \mathrm{FBW}} + p \end{bmatrix} \begin{bmatrix} i_1 \\ i_2 \\ . \\ . \\ . \\ i_3 \end{bmatrix} = \begin{bmatrix} e_S \\ 0 \\ . \\ . \\ . \\ 0 \end{bmatrix}, \quad (2.2)$$

where $\mathrm{FBW} = \Delta\omega/\omega_0$ and $p = j\dfrac{1}{\mathrm{FBW}}\left(\dfrac{\omega}{\omega_0} - \dfrac{\omega_0}{\omega}\right)$.

Since the filter works in a narrow band, then $\dfrac{\omega}{\omega_0} \approx 1$, $\Delta\omega = 1$, $\omega_0 = 1$, and L=1 for the BPF prototype, (2.2) is now represented as follow:

$$\begin{bmatrix} R_S + p & -jm_{12} & \dots & -jm_{1n} \\ -jm_{21} & p & \dots & -jm_{2n} \\ . & . & & . \\ . & . & & . \\ . & . & & . \\ -jm_{n1} & -jm_{n2} & \dots & R_L + p \end{bmatrix} \begin{bmatrix} i_1 \\ i_2 \\ . \\ . \\ . \\ i_n \end{bmatrix} = \begin{bmatrix} e_S \\ 0 \\ . \\ . \\ . \\ 0 \end{bmatrix}, \tag{2.3}$$

where m_{ij} is defined as the normalized coupling coefficient, $m_{ij} = \dfrac{L_{ij}/L}{\mathrm{FBW}}$.

Therefore, the current-voltage relationship of the network is now

$$\underbrace{\left[j\left[-\underbrace{\begin{bmatrix} m_{11} & m_{12} & \dots & m_{1n} \\ m_{21} & m_{22} & \dots & m_{2n} \\ . & . & & . \\ . & . & & . \\ . & . & & . \\ m_{n1} & m_{n2} & \dots & m_{nn} \end{bmatrix}}_{[\mathrm{M}]} + \omega \underbrace{\begin{bmatrix} 1 & 0 & \dots & 0 \\ 0 & 1 & \dots & 0 \\ . & . & & . \\ . & . & & . \\ . & . & & . \\ 0 & 0 & \dots & 1 \end{bmatrix}}_{[\mathrm{I}]} - j \underbrace{\begin{bmatrix} R_S & 0 & \dots & 0 \\ 0 & 0 & \dots & 0 \\ . & . & & . \\ . & . & & . \\ . & . & & . \\ 0 & 0 & \dots & R_L \end{bmatrix}}_{[\mathrm{R}]} \right] \underbrace{\begin{bmatrix} i_1 \\ i_2 \\ . \\ . \\ . \\ i_n \end{bmatrix}}_{[\mathrm{I}]} \right]}_{[\mathrm{A}]} = e_S \underbrace{\begin{bmatrix} 1 \\ 0 \\ . \\ . \\ . \\ 0 \end{bmatrix}}_{[E]}, \tag{2.4}$$

and the loop current is calculated by

$$[\mathrm{I}] = -j[\mathrm{A}]^{-1}[\mathrm{E}]. \tag{2.5}$$

The S parameters of the two-port network are defined as

$$\mathrm{S}_{21} = 2\sqrt{R_S R_L} \cdot i_n \tag{2.6}$$

and

$$\mathrm{S}_{11} = 1 - 2R_S \cdot i_1. \tag{2.7}$$

By combining(2.5), (2.6) and (2.7), the S parameters can be calculated with the coupling matrix

$$S_{21} = -2j\sqrt{R_S R_L}\cdot[A]_{n1}^{-1} \tag{2.8}$$

and

$$S_{11} = 1 + 2jR_S \cdot [A]_{11}^{-1}. \tag{2.9}$$

2.3 Synthesis of the Coupling Matrix from Filter Specification

This section briefly reviews the method that is used to obtain the coupling matrix from any given specifications.

2.3.1 Generating Chebychev Polynomials

The recursive technique covered in [3] and [7] provides an effective way to generate Chebychev polynomial with transmission zeros in the finite frequency. The following is the outline of this technique.

For any general Chebychev filter of N order, the S parameters are expressed as

$$S_{11}(\omega) = \frac{F_N(\omega)}{\varepsilon_R E_N(\omega)} \tag{2.10}$$

and

$$S_{21}(\omega) = \frac{P_N(\omega)}{\varepsilon E_N(\omega)}. \tag{2.11}$$

The expression of $F_N(\omega)$ can be found as

$$F_N(\omega) = \frac{1}{2}\left(\prod_{n=1}^{N}(c_n + d_n) + \prod_{n=1}^{N}(c_n - d_n)\right) = \frac{1}{2}\left[G_N(\omega) + G_N{}'(\omega)\right] \tag{2.12}$$

where

$$c_n = \omega - \frac{1}{\omega_n}, \quad d_n = \omega'\left(1 - \frac{1}{\omega_n{}^2}\right)^{1/2}, \quad \omega' = \left(\omega^2 - 1\right)^{1/2} \text{ and } \quad n = 1, \ldots, N.$$

Since $P_N(\omega)$ is the numerator of $S_{21}(\omega)$, $P_N(\omega)$ has zeros at the frequency of all the transmission zeros. Therefore

$$P_N(\omega) = \prod_{n=1}^{N} (1 - \frac{\omega}{\omega_n}). \tag{2.13}$$

The value of ε is now obtained from the characteristic of the equal ripple at the cut-off frequency of the low-pass prototype

$$\varepsilon = \left(10^{RL/10} - 1\right)^{-0.5} \cdot \left.\frac{P_N(\omega)}{F_N(\omega)}\right|_{\omega=1}. \tag{2.14}$$

The value of ε_R is determined by:

$$\varepsilon_{\mathrm{R}} = \begin{cases} \varepsilon \Big/ \sqrt{\varepsilon^2 - 1} & \text{for Canonicalfilter } (n = N) \\ 1 & \text{for non Canonical filter } (n < N) \end{cases}. \tag{2.15}$$

Finally, the common part of the denominator of S_{21} and S_{22} are found with

$$\left|S_{21}(\omega)\right|^2 = S_{21}(\omega) \cdot S_{21}{}^{*}(\omega) = \frac{1}{\left(1 + j\varepsilon C_N(\omega)\right) \cdot \left(1 - j\varepsilon C_N(\omega)\right)}, \tag{2.16}$$

where

$$C_N(\omega) = \frac{F_N(\omega)}{P_N(\omega)}. \tag{2.17}$$

2.3.2 Generating Coupling Matrix from Filter Polynomials

Once the Chebychev polynomials of the filter are obtained, the driving point impedance Z_{in} of a terminated network in Figure 2.2 can be expressed in the forms of its open circuit parameters z_{11}, z_{12}, z_{21}, and z_{22}

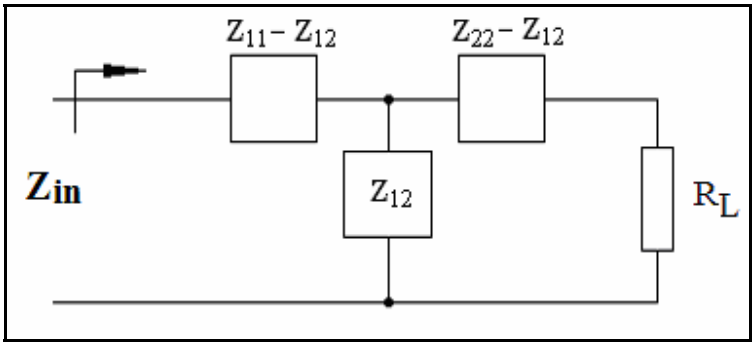

Figure 2.2 Terminated impedance network

Consequently,

$$Z_{in} = \frac{1-S_{11}(p)}{1+S_{11}(p)} = (z_{11}-z_{12}) + \left[\left((z_{22}-z_{12})+R_L\right) \| \, z_{12}\right] \tag{2.18}$$

$$= \left. \frac{z_{11}\left[(1/y_{22})+1\right]}{z_{22}+1} \right|_{\substack{z_{12}=z_{21} \\ R_L=1}}$$

If real and imaginary parts of the numerator are expressed by m_1, n_1 respectively, then those of denominator are expressed by m_2, n_2 . The driving point impedance Z_{in} can thus be expressed as

$$Z_{in} = \frac{m_1+n_1}{m_2+n_2} = \frac{n_1\left[\frac{m_1}{n_1}+1\right]}{m_2+n_2} \quad \text{(even ordered case)} \tag{2.19}$$

and

$$Z_{in} = \frac{m_1+n_1}{m_2+n_2} = \frac{m_1\left[\frac{n_1}{m_1}+1\right]}{m_2+n_2} \quad \text{(odd ordered case)} \tag{2.20}$$

Then, y_{22} of the circuit is represented by

$$y_{22} = \frac{n_1}{m_1} \quad (\text{even ordered case}) \tag{2.21}$$

and

$$y_{22} = \frac{m_1}{n_1} \, (\text{odd ordered case}). \tag{2.22}$$

For y_{21}, by knowing that its numerator has the same transmission zeros as $S_{21}(s)\big|_{s=j\omega}$, and its denominator is the same as that of y_{22}, y_{21} is now expressed as

$$y_{21} = \frac{j \cdot (P_N(\omega)/\varepsilon)}{m_1} \, (\text{even ordered case}) \tag{2.23}$$

and

$$y_{21} = \frac{P_N(\omega)/\varepsilon}{n_1} \, (\text{odd ordered case}). \tag{2.24}$$

From (2.4), the following is obtained:

$$[A][i] = [e] \rightarrow [R + sI - jM][i_1, i_2, ...i_n]^t = [e_1, e_2, ...e_n]^t \tag{2.25}$$

where R is a $n \times n$ matrix with all zero entries, except $R_{11} = R_S$ and $R_{nn} = R_L$.

The short-circuit admittance, $y_{21}(\omega)$, $y_{21}(\omega)$, can be determined as follows:

$$y_{21}(\omega) = \frac{i_N}{e_1} = -j[M - \omega I]^{-1}_{N1} = -j\left[T \cdot \Lambda \cdot T^t - \omega I\right]^{-1}_{N1} = -j\sum_{k=1}^{N} \frac{T_{Nk} T_{1k}}{\omega - \lambda_k} \tag{2.26}$$

and

$$y_{22}(\omega) = \frac{i_N}{e_1} = -j[M - \omega I]^{-1}_{NN} = -j\left[T \cdot \Lambda \cdot T^t - \omega I\right]^{-1}_{NN} = -j\sum_{k=1}^{N} \frac{T_{Nk}^2}{\omega - \lambda_k}. \tag{2.27}$$

By expanding $j \cdot y_{21}(\omega)$ and $j \cdot y_{22}(\omega)$, $\sum_{k=1}^{N} \frac{T_{Nk} T_{1k}}{\omega - \lambda_k}$ and $\sum_{k=1}^{N} \frac{T_{Nk}^2}{\omega - \lambda_k}$ are obtained.

Based on the method introduced in [4] , the N+2 coupling matrix, which includes the couplings to source and load, is obtained as in(2.28).

$$\begin{bmatrix} 0 & T_{11} & T_{12} & \cdots & T_{1N} & M_{SL} \\ T_{11} & \lambda_1 & 0 & & 0 & T_{N1} \\ T_{12} & 0 & \lambda_2 & & 0 & T_{N2} \\ \cdot & \cdot & \cdot & \cdots & \cdot & \cdot \\ \cdot & \cdot & \cdot & \cdots & \cdot & \cdot \\ \cdot & \cdot & \cdot & \cdots & \cdot & \cdot \\ T_{1N} & 0 & 0 & & \lambda_N & T_{NN} \\ M_{LS} & T_{N1} & T_{N2} & \cdots & T_{NN} & 0 \end{bmatrix}, \tag{2.28}$$

where $M_{SL} = M_{LS} = y_{21}\big|_{s \to j\infty}$.

Finally, a realizable filter topology can be obtained with a series of similarity transformation (rotation) performed on the matrix in (2.28).

2.4 Design Example of Cross-Coupled Waveguide Filter

In this section, a design case is illustrated for a filter with prescribed transmission zeros realized by cross coupled resonators with a folding back topology. The coupling matrix of the filter is synthesized according to the given specifications. Then the filter is realized with waveguide cavities with special effort on minimizing the usage of the EM simulator for the optimization.

The filter specification is given as follow:

- centre frequency: $f_0 = 6GHz$
- bandwidth: $BW = 210MHz$ (or fractional band width: $FBW = 3.5\%$)
- return loss in pass band: $RL = 30dB$
- degree of the filter: $N = 6$
- prescribed transmission zero(s): $\omega_1 = 1.96,\ \omega_2 = -1.96$

Following the procedure, described in Section 2.3, the original N+2 coupling matrix of this filter is computed

$$\begin{bmatrix} 0 & 0.3951 & -0.3951 & -0.5300 & 0.5300 & 0.5260 & -0.5260 & 0 \\ 0.3951 & -1.3728 & 0 & 0 & 0 & 0 & 0 & 0.3951 \\ -0.3951 & 0 & 1.3728 & 0 & 0 & 0 & 0 & 0.3951 \\ -0.5300 & 0 & 0 & -1.2161 & 0 & 0 & 0 & 0.5300 \\ 0.5300 & 0 & 0 & 0 & 1.2161 & 0 & 0 & 0.5300 \\ 0.5260 & 0 & 0 & 0 & 0 & -0.4599 & 0 & 0.5260 \\ -0.5260 & 0 & 0 & 0 & 0 & 0 & 0.4599 & 0.5260 \\ 0 & 0.3951 & 0.3951 & 0.5300 & 0.5300 & 0.5260 & 0.5260 & 0 \end{bmatrix} \quad .(2.29)$$

After a series of similarity transformations (rotations) applied to (2.29), the following coupling matrix is obtained:

$$\begin{bmatrix} 0 & 1.1947 & 0 & 0 & 0 & 0 & 0 & 0 \\ 1.1947 & 0 & 1.0374 & 0 & 0 & 0 & 0 & 0 \\ 0 & 1.0374 & 0 & 0.6724 & 0 & -0.0968 & 0 & 0 \\ 0 & 0 & 0.6724 & 0 & 0.7133 & 0 & 0 & 0 \\ 0 & 0 & 0 & 0.7133 & 0 & 0.6724 & 0 & 0 \\ 0 & 0 & -0.0968 & 0 & 0.6724 & 0 & 1.0374 & 0 \\ 0 & 0 & 0 & 0 & 0 & 1.0374 & 0 & 1.1947 \\ 0 & 0 & 0 & 0 & 0 & 0 & 1.1947 & 0 \end{bmatrix} \quad (2.30)$$

The coupling matrix in (2.30) represents a realizable topology with cross coupled resonators, as signified in Figure 2.3, where M_{ij} indicates the coupling coefficients between different resonators..

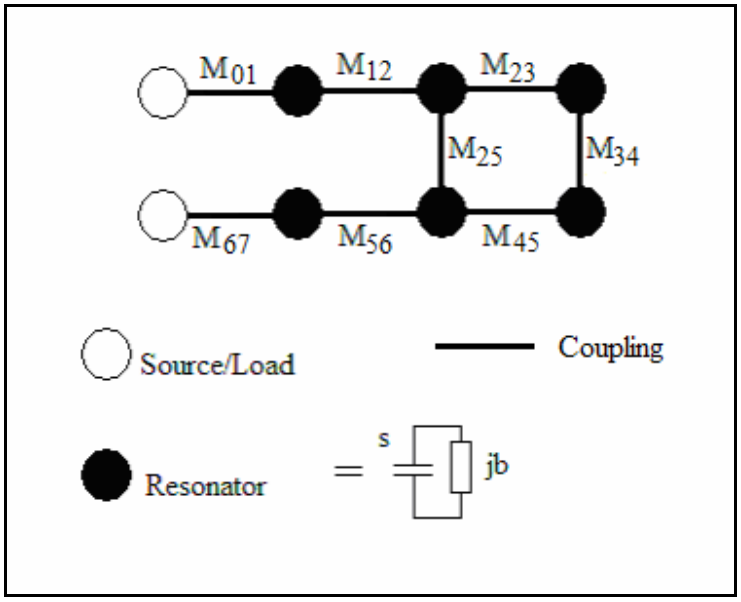

Figure 2.3 Topology of 6-pole fold back cross coupled filter

The differently signed couplings are realized with inductive and capacitive [10] and [11]. The waveguide filter, corresponding to above topology, is shown in Figure 2.4. which is realized in the HFSS EM simulator [12].

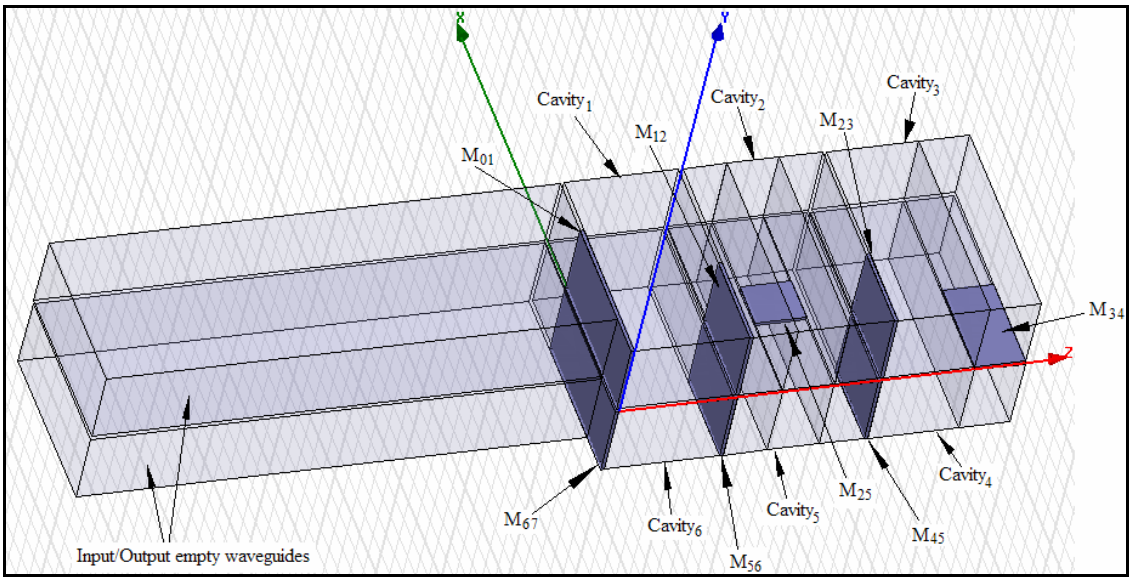

Figure 2.4 6-pole cross coupled waveguide filter

Designing procedure is adapted from the literature [13], which can be divided into following sub-steps.

a) Determine the Width of the Irises for Direct Coupling $M_{01/67}$, $M_{12/56}$ and $M_{23/45}$

For the first and last nodes, the inverter value K can be calculated with:

$$K_{01} = M_{01} \cdot \sqrt{\frac{\pi}{2} \cdot FBW} \cdot \frac{\lambda_g}{\lambda}. \tag{2.31}$$

For the remaining nodes in the filter, the inverter value is calculated by

$$K_{ij} = M_{ij} \cdot \frac{\pi}{2} \cdot FBW \cdot \left(\frac{\lambda_g}{\lambda} \right)^2. \tag{2.32}$$

It is known that the impedance inverter of value K represents a two-port network with an ABCD matrix as

$$ABCD = \begin{bmatrix} 0 & \pm jK \\ \mp \dfrac{1}{jK} & 0 \end{bmatrix}. \tag{2.33}$$

Consequently, the S parameters of the inverters are calculated from the ABCD matrix with formulas given in the literature [12]. In this example, following parameters are calculated:

$$M_{01} = 1.1947 \Rightarrow K_{01} = M_{01} \cdot \sqrt{\frac{\pi}{2} \cdot FBW} \cdot \frac{\lambda_g}{\lambda_0} = 0.3432 \Rightarrow S_{21} = -4.235 dB,$$

$$M_{12} = 1.0374 \Rightarrow K_{12} = M_{12} \cdot \frac{\pi}{2} \cdot FBW \cdot \left(\frac{\lambda_g}{\lambda_0} \right)^2 = 0.0856 \Rightarrow S_{21} = -15.39 dB, \tag{2.34}$$

and

$$M_{23} = 0.6724 \Rightarrow K_{23} = M_{23} \cdot \frac{\pi}{2} \cdot FBW \cdot \left(\frac{\lambda_g}{\lambda_0} \right)^2 = 0.0555 \Rightarrow S_{21} = -19.117 dB.$$

The structure used in HFSS for M_{01} is shown in Figure 2.5. For the other couplings, the same structure is used except that the waveguide on both sides of the iris have the same width.

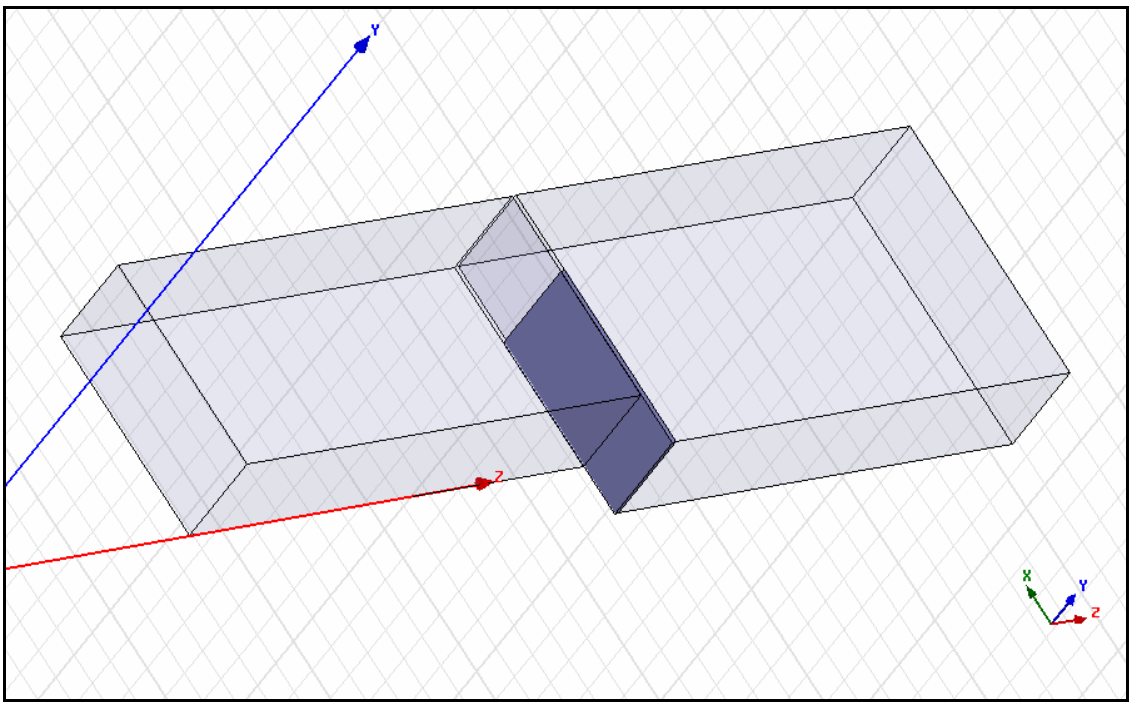

Figure 2.5 HFSS model for direct coupling

The initial value of the iris width can be calculated with some experimental formulas [15], or simply run a parameter sweep in HFSS to find out the width corresponding to the attenuation calculated in(2.34).

b) Adjust the Resonating Frequency of Resonator 1

The circuit model of the inverter has a negative transmission length on both sides of the inverter, which is absorbed by the actual length of the cavity; therefore, the actual cavity length will be slightly shorter than half wavelength. The length of cavity is calculated with the formula,

$$l_j = \frac{\theta_j}{\beta} = \frac{\lambda_g}{2\pi}\left[\pi - \frac{1}{2}\left(\arctan\left(2\cdot X_{j-1,j}\right) + \arctan\left(2\cdot X_{j,j+1}\right)\right)\right] \tag{2.35}$$

$$(\text{for } j = 1,2,...,6),$$

where

$$X_{j,j+1} = \frac{K_{j,j+1}}{1-K_{j,j+1}^2}. \tag{2.36}$$

Then, the length can be fine tuned in HFSS with the structure in Figure 2.6 in order to yield the exact resonating frequency.

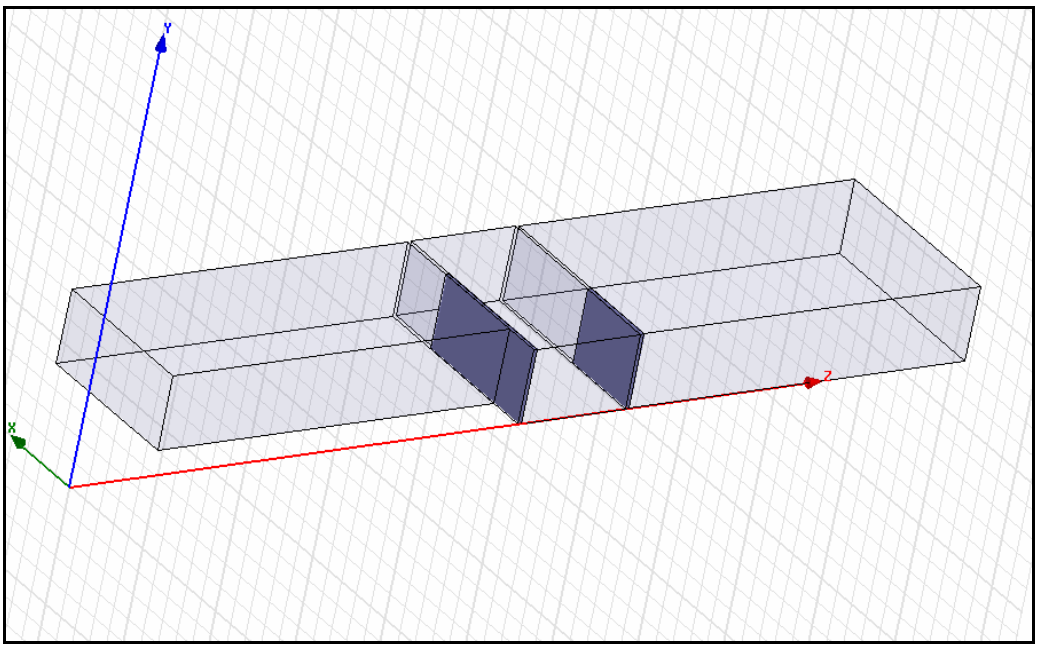

Figure 2.6 Structure for tuning cavity 1

After tuning, frequency response in Figure 2.7 is obtained

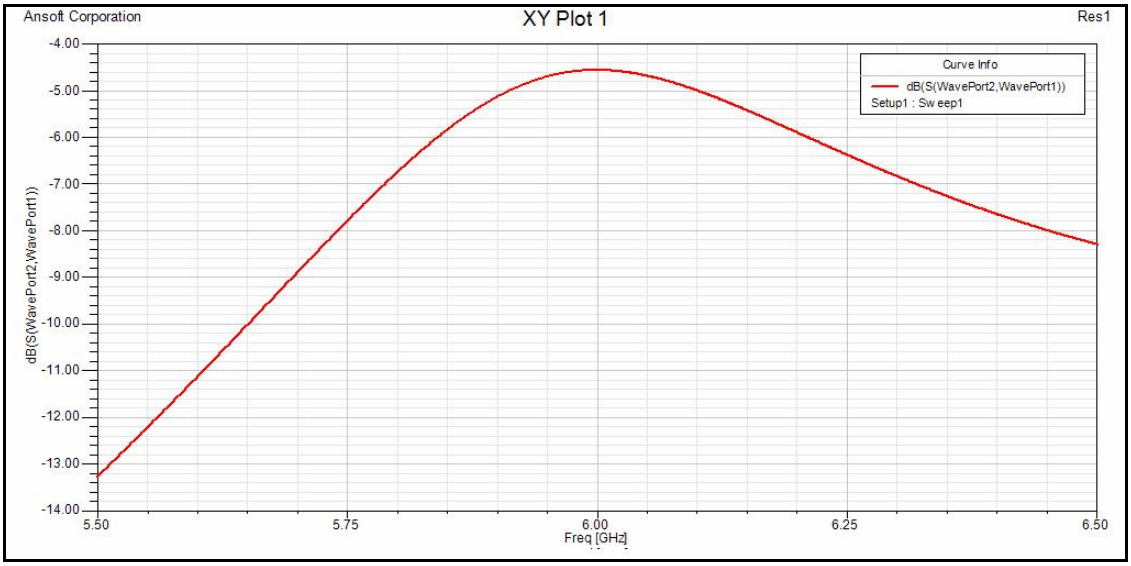

Figure 2.7 Frequency response of cavity 1

c) Determine the cross coupling M_{25}

The transfer function of cross coupling can be calculated in the same way as in a):

$$M_{25} = -0.0968 \Rightarrow K_{25} = M_{25} \cdot \frac{\pi}{2} \cdot FBW \cdot \left(\frac{\lambda_g}{\lambda_0} \right)^2 = -0.0555 \Rightarrow S_{21} = -35.9dB \quad (2.37)$$

The structure used in this step is shown in Figure2.8.

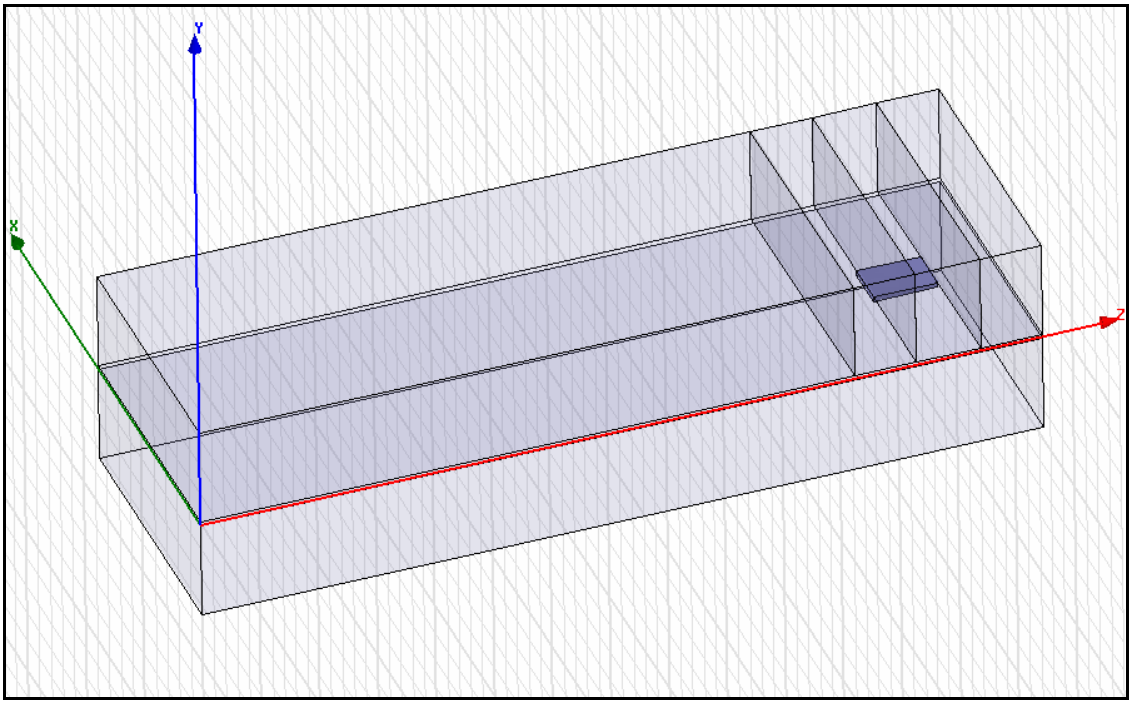

Figure 2.8 Structure to determine cross coupling M_{25}

d) Adjust the resonating frequency of cavity 2

In this step, the length of the cavity 2 is adjusted to exhibit a frequency response peak at exactly 6GHz. The structure, with coupling irises of M_{12} and M_{25} on each side of the cavity, is shown in Figure 2.9, and the frequency response is plotted in Figure 2.10.

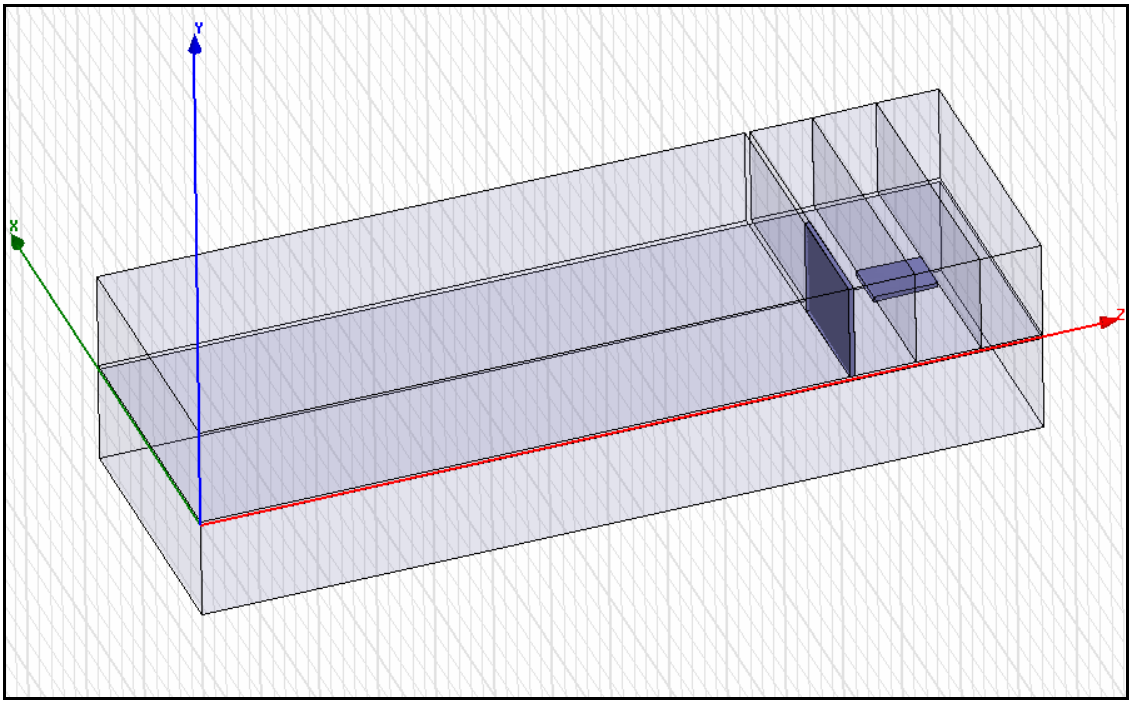

Figure 2.9 Structure for adjust resonating frequency of cavity 2

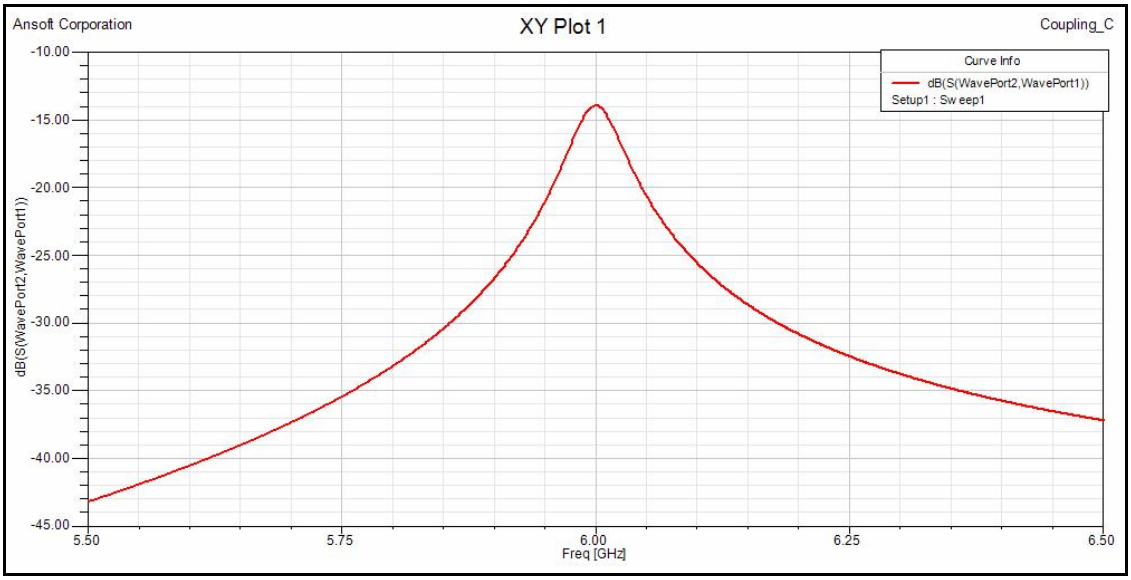

Figure 2.10 Frequency response of cavity 2 with merely coupling M_{12} and M_{25}

e) Re-adjusting the Cross Coupling M_{25}

Since the empty waveguide is used to determine cross coupling M_{25}, once the iris M_{12}, which can be considered as a new discontinuity, is added, the effective coupling of the

iris M_{25} will be affected, therefore cross coupling iris has to be re-adjusted. In order to do so, a reduced filter is built with merely cavity 2, 5, coupling irises M_{12}, M_{56} and cross coupling M_{25}, as shown in Figure 2.11, the coupling matrix of this module can be reduced from the original coupling matrix by multiplying M_{12} by $\sqrt{\frac{\pi}{2}FBW}\cdot\frac{\lambda_g}{\lambda_0}$ such that

$$\begin{bmatrix} 0 & 0.2980 & 0 & 0 \\ 0.2980 & 0 & -0.0968 & 0 \\ 0 & -0.0968 & 0 & 0.2980 \\ 0 & 0 & 0.2980 & 0 \end{bmatrix}. \tag{2.38}$$

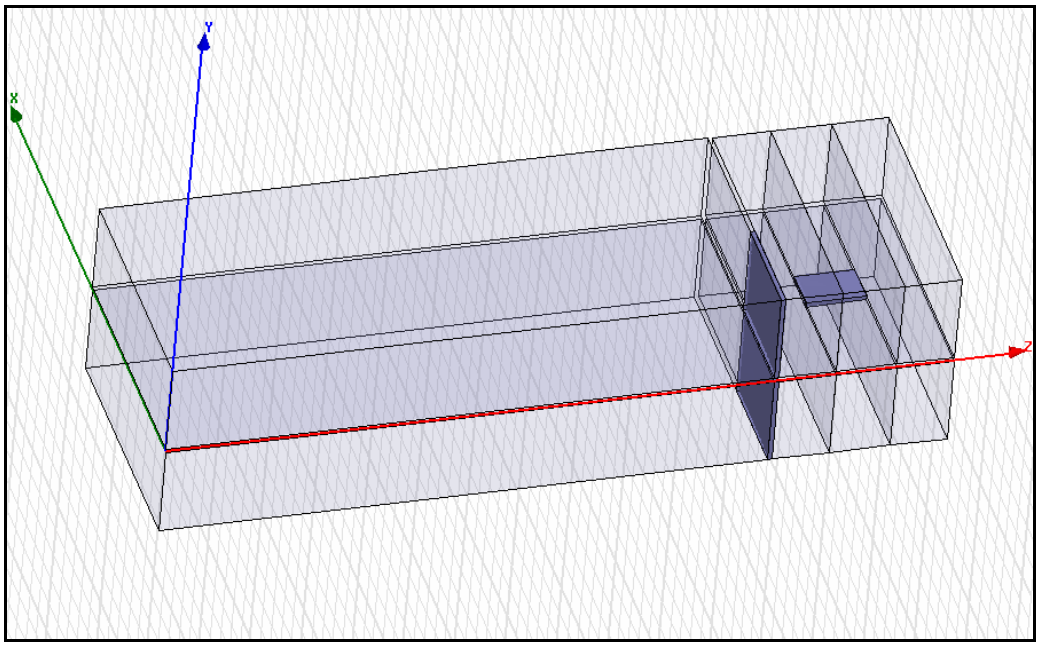

Figure 2.11 Reduced filter with coupling matrix 2.38

The iris for the cross coupling is adjusted till the frequency response from the EM simulation travels very close to that of the coupling matrix (2.38), as shown in Figure 2.12.

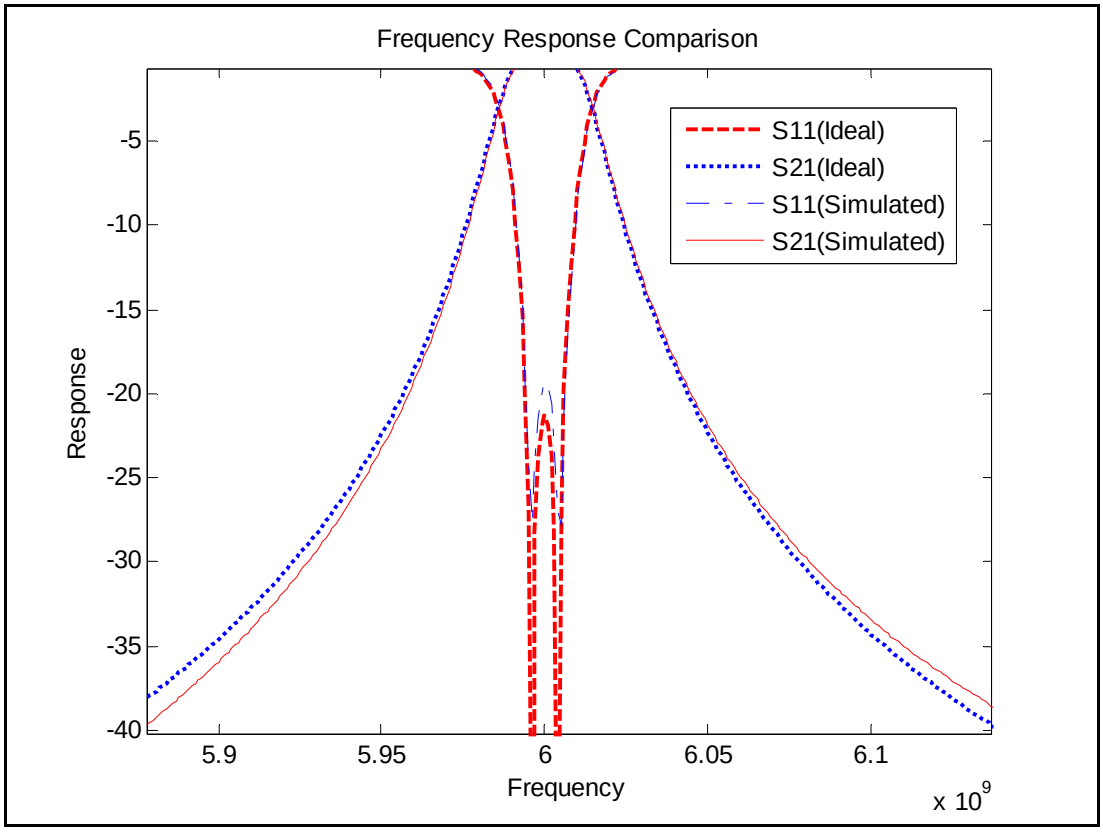

Figure 2.12 Frequency response comparison of EM simulation and coupling matrix

f) Re-adjusting the resonating frequency of cavity 2

In this step, coupling M_{23} is added to cavity 2, which affects again the effective length of cavity 2. As a result, the length of cavity must be re-adjusted. The structure, in Figure 2.13, yields the frequency response in Figure 2.14.

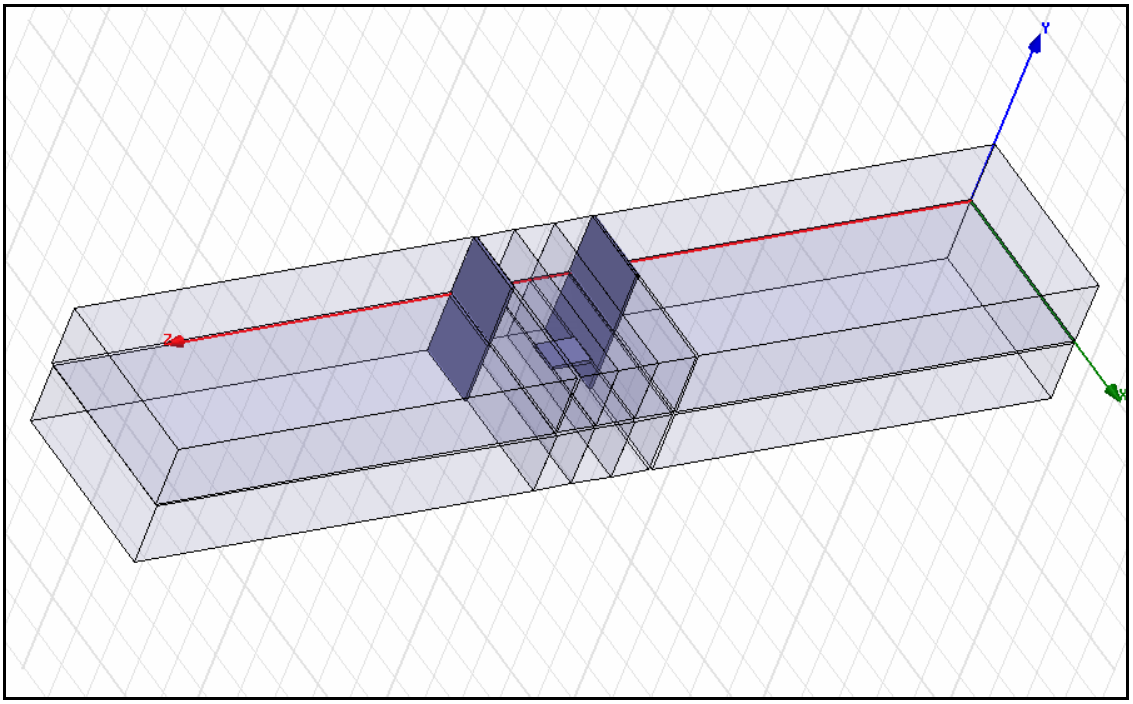

Figure 2.13 Re-adjust resonating frequency of resonator 2

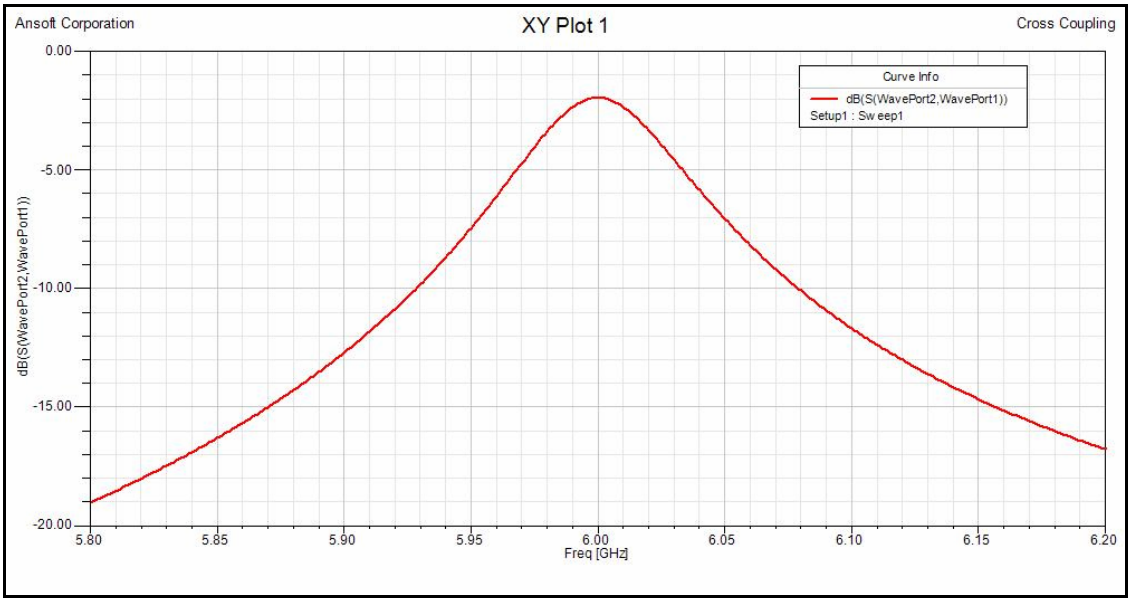

Figure 2.14 Frequency response of the structure in Figure 2.13

g) Determine the coupling M_{34} (Part1)

S parameters of M_{34} is calculated with

$$M_{34} = 0.7133 \Rightarrow K_{34} = M_{34} \cdot \frac{\pi}{2} \cdot FBW \cdot \left(\frac{\lambda_g}{\lambda_0}\right)^2 = 0.08257 \Rightarrow S_{21} = -15.7dB\,. \quad (2.39)$$

The same as in the previous step for cross coupling, the iris is firstly simulated with an empty waveguide on both sides of the coupling iris with the structure shown in Figure 2.15. The width of the iris is adjusted to attain the desired S parameter.

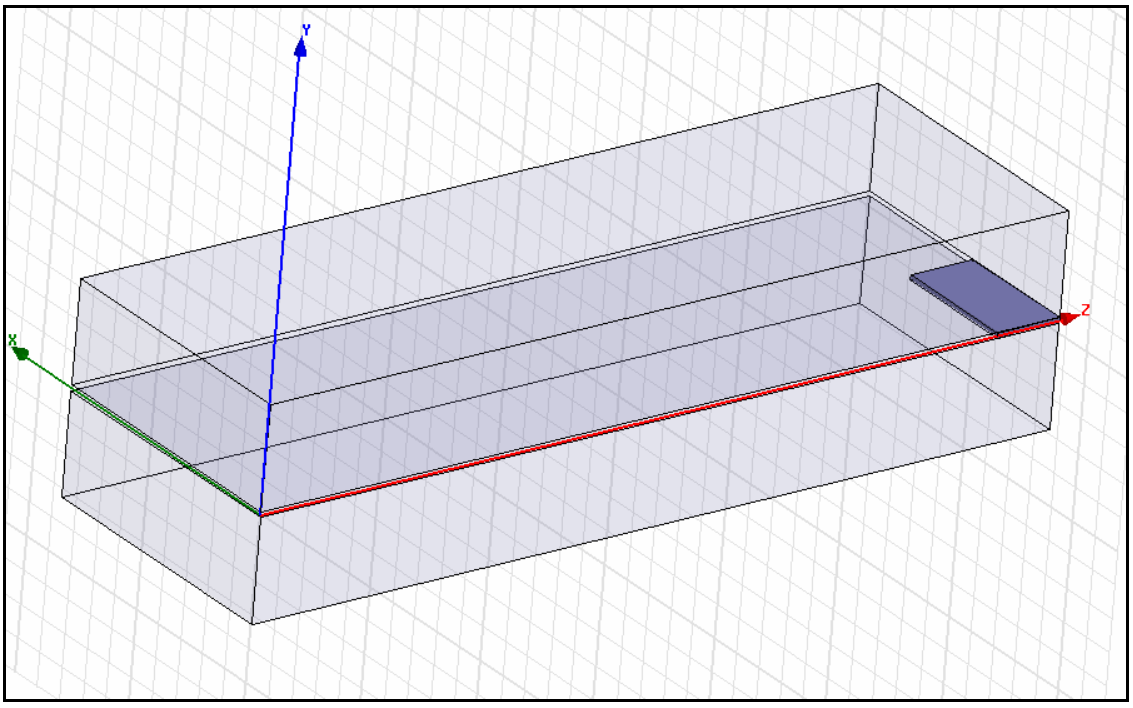

Figure 2.15 Structure for simulating the coupling M34

h) Adjust the Resonating Frequency of resonator 3 and Re-adjust the coupling M_{34}

The structure used in this step is shown in Figure 2.16, with a reduced coupling matrix,

$$\begin{bmatrix} 0 & 0.1937 & 0 & 0 \\ 0.1937 & 0 & 0.7133 & 0 \\ 0 & 0.7133 & 0 & 0.1937 \\ 0 & 0 & 0.1937 & 0 \end{bmatrix} \quad (2.40)$$

In this step, an iterative approach is performed as follows

Adjust length of cavity 3 $\rightleftarrows$ Adjust coupling M_{34}

until the frequency response of the EM simulation matches that of coupling matrix, as depicted in Figure 2.17.

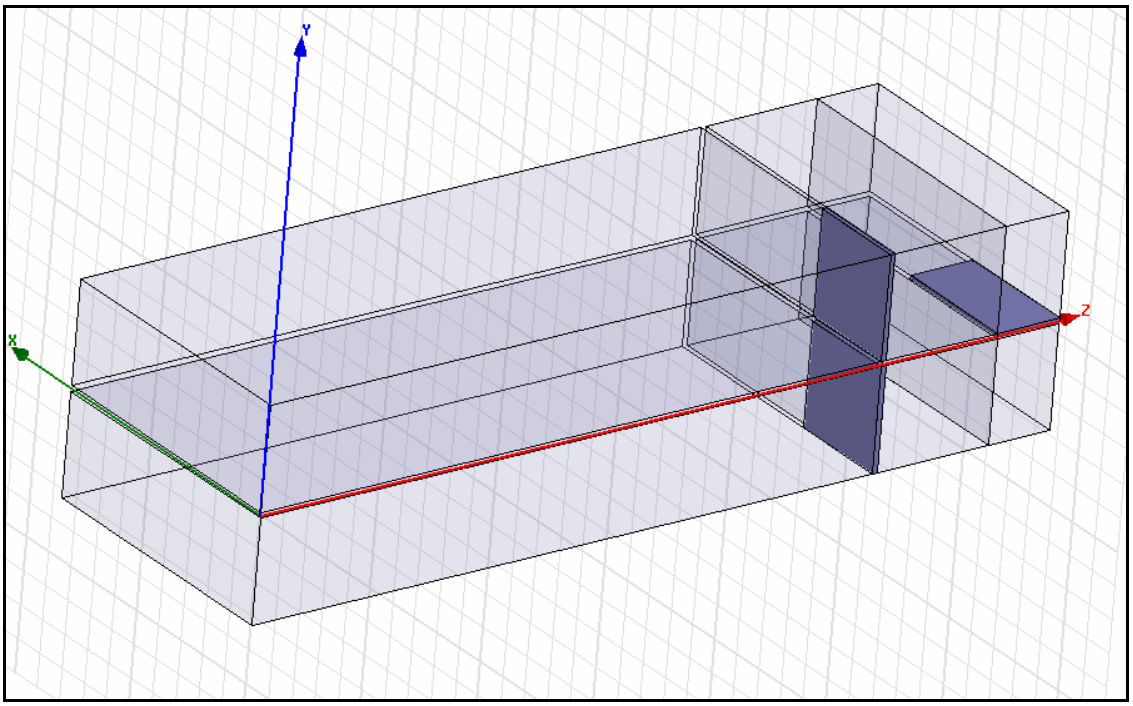

Figure 2.16 Structure to adjust length of cavity 3 and fine tune coupling M_{34}

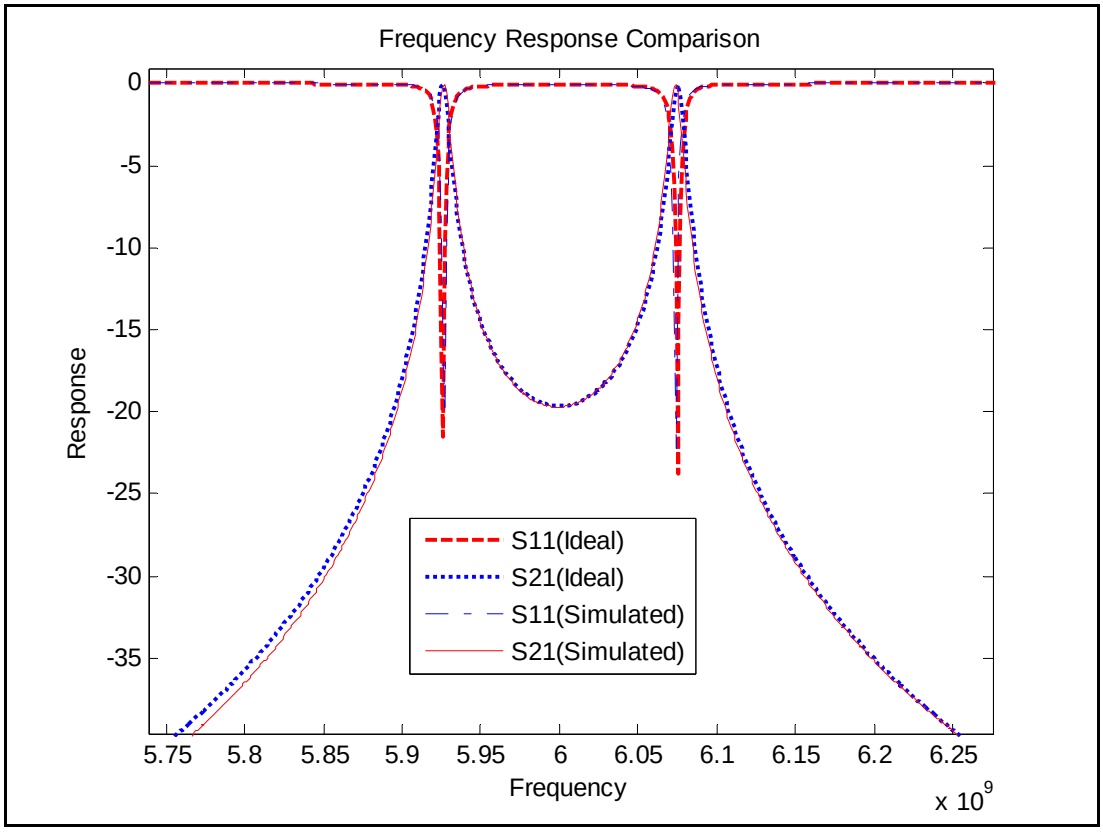

Figure 2.17 Frequency responses of previous structure with that of coupling matrix

Once all the modules are combined, the resulting frequency response in Figure 2.18 is obtained. It can be seen that without any global optimization, a return loss of about 22dB is achieved.

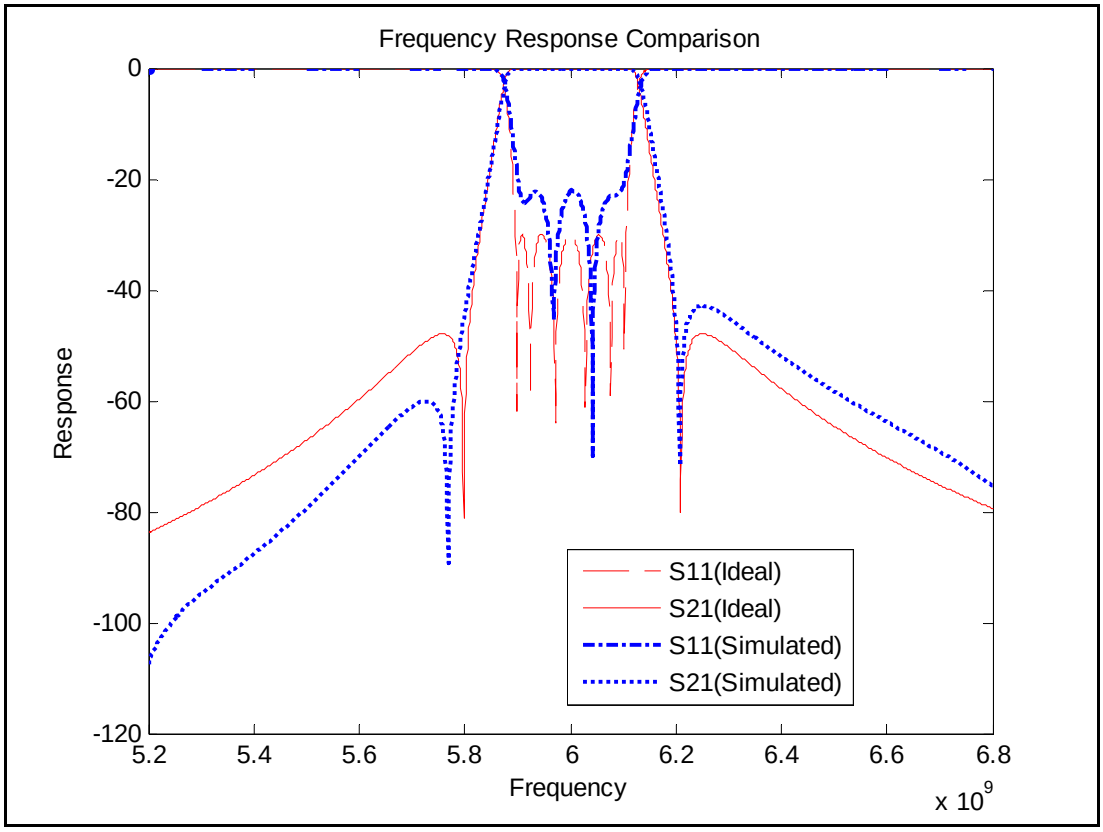

Figure 2.18 Frequency response of filter

2.5 Conclusions

This chapter reviews the method in the literature of synthesizing the coupling matrix of a filter with the prototype of N ordered coupled resonator transversal array. This method is highly efficient with the capability to synthesize an N ordered filter with up to N finite transmission zeros.

However, there are still certain limitations. First of all, the coupling matrix obtained from this method is only one of the possible solutions [16], at least two different coupling matrices whose entries differ in both signs and magnitude can be extracted from the same filter polynomials. Furthermore, this method does not work with the filter with NRNs.

Also, a design procedure is denoted with an effort made to minimize the usage of EM simulation in the optimization loops. The result is relatively good, regarding that it is obtained without any global optimization.

Nevertheless, the filter designed with this procedure has transmission zeros that are somewhat inaccurate. It is difficult to fine tune those transmission zeros on this filter without performing a global optimization, since there is no parameter explicitly related to these transmission zeros. Moreover, the accuracy and effectiveness of this procedure worsens for the wider bandwidth application. Figure 2.19 reflects the result of another design, the specification and design procedure of this filter are exactly the same except this filter has a wider bandwidth of 350MHz ($FBW = 5.83\%$). It is evident that the position of the transmission zeros and return loss performance are much worse than those of previous design.

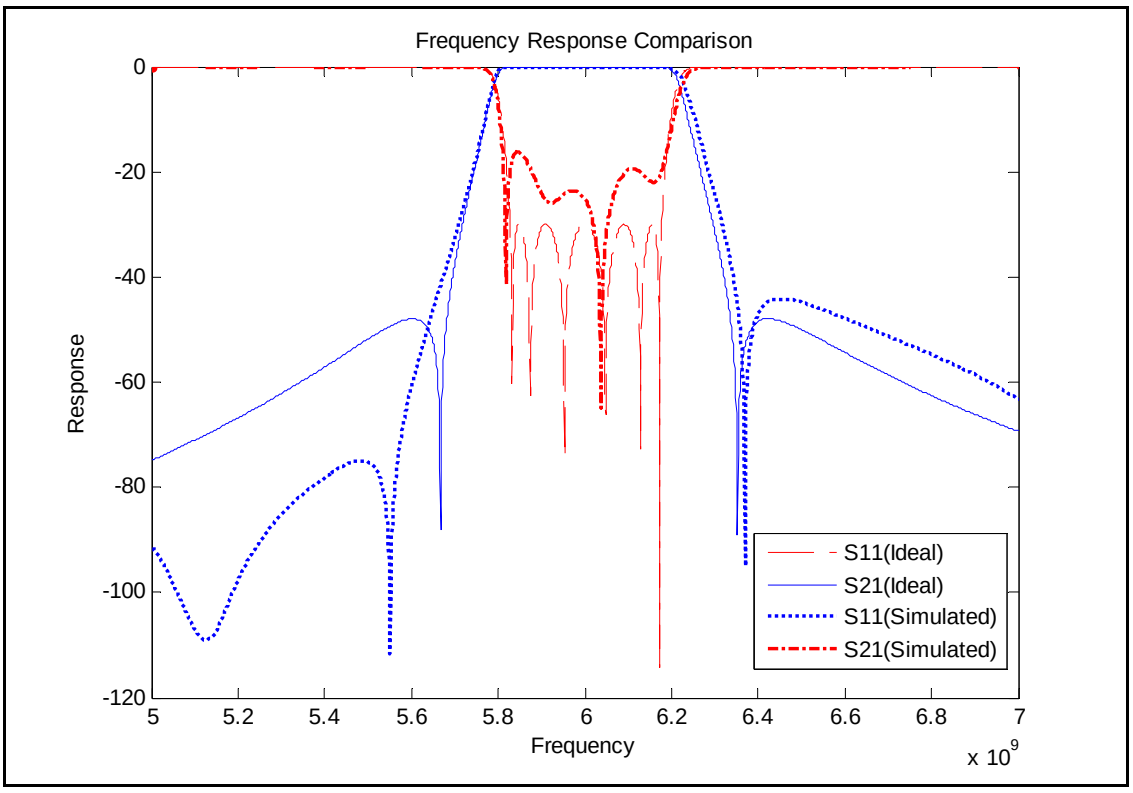

Figure 2.19 Frequency response of filter with 350MHz bandwidth

3. Filter with Non-Resonating Nodes

3.1 Introduction

Another class of filters which can provide prescribed transmission zeros are filters NRNs. The transmission zeros are determined independently by dedicated resonators coupled to non-resonating nodes [20].

In this section, a survey is carried out on the existing designs in the literature [16] - [22]. The procedure to synthesize the filter with NRNs based on extracted-pole technique is reviewed. After a trial design, the result is analyzed in order to find the limitations of the current design procedures.

3.2 Survey on Designs on Publications

With the literature [16]-[22], the specifications of several designs of filters, realized with NRNs, are listed in Table 3.1.

Table 3.1 Survey of existing design examples of filter with non-resonating nodes

#	Reference	Order of Filter	Center Frequency	Bandwidth	Fractional Bandwidth	Return Loss (dB)	Filter Structure
1	[18]	4	12 GHz	100MHz	0.83%	20	Waveguide
2	[18]	3	11.1 GHz	100MHz	0.9%	25	Waveguide
3	[21]	3	11 GHz	100 MHz	0.9%	22	Triple-mode Waveguide
4	[19]	4	27.4 GHz	800MHz	2.9%	22	Waveguide
5	[21]	6	22.3GHz	600MHz	2.7%	23	Triple-mode Waveguide
6	[22]	8	12 GHz	500MHz	4.17%	20	Waveguide
7	[19]	2	2.5 GHz	200MHz	8%	22	Microstrip
8	[20]	5	836 MHz	26 MHz	3.1%	20	Cylindrical rods in combline configuration

Filters #1 to #6 are realized by waveguide cavities. #1, #2 and #3 have very narrow bandwidth. #4 and #5 have a relatively wider bandwidth. But #4 conveys a steep spike close to the band of interest. Since #5 has a narrow display window for the frequency response, it is impossible to verify the spikes in wider range.

Filter #6 has a relatively wide bandwidth and a wider spurious free window, which is achieved by using the stepped waveguide width and the global optimizations. The different waveguide widths and unsymmetrical structure of the filter leave a great number of parameters to be optimized, which is very time consuming.

3.3 Synthesis of Filter with Non-Resonating Nodes (NRNs)

The filter polynomials are obtained with the same recursive method described in the literature [3], and the S parameters and input/output admittance of the filter are expressed as following:

$$S_{11}(s) = \frac{M(s)}{D(s)} \cdot e^{j\phi_{11}}, \tag{3.1}$$

$$S_{22}(s) = \frac{M(s)}{D(s)} \cdot e^{j\phi_{22}}, \tag{3.2}$$

$$y_{in}(s) = \frac{1 - S_{11}(s)}{1 + S_{11}(s)} = \frac{D(s) - M(s) \cdot e^{j\phi_{11}}}{D(s) + M(s) \cdot e^{j\phi_{11}}} \tag{3.3}$$

and

$$y_{out}(s) = \frac{1 - S_{22}(s)}{1 + S_{22}(s)} = \frac{D(s) - M(s) \cdot e^{j\phi_{22}}}{D(s) + M(s) \cdot e^{j\phi_{22}}} \tag{3.4}$$

As stated by S. Amari and G. Macchiarella in [20], a phase term is added to the S parameters to guarantee the satisfaction of unitary condition. The value of the angle in this phase term is determined by different configurations of the first node at input and output respectively.

If the first node from input is a resonator, ϕ is determined with the following:

$$e^{j\phi_{11}} = \left.\frac{D(s)}{M(s)}\right|_{s\to\infty} = 1 \Rightarrow \phi_{11} = 0\,. \tag{3.5}$$

If the first node from input is non-resonating node, ϕ is obtained with the following:

$$e^{j\phi_{11}} = \left.\frac{D(s)}{M(s)}\right|_{s\to j\omega_z} \Rightarrow \phi_{11} = \angle\left(\left.\frac{D(s)}{M(s)}\right|_{s\to j\omega_z}\right), \tag{3.6}$$

where ω_Z is the frequency on which there is a transmission zero generated by the resonator coupled to that non-resonating node.

Once the topology of the filter is determined, each component of the filter is extracted from the expression of input and output admittance which is calculated by (3.3) and (3.4).

There are two distinct cases in the extraction:

1) Resonator coupled through an admittance inverter, as in Figure 3.1.
2) NRN, to which a resonator is coupled to generate a transmission zero, coupled through an admittance inverter, as in Figure 3.2.

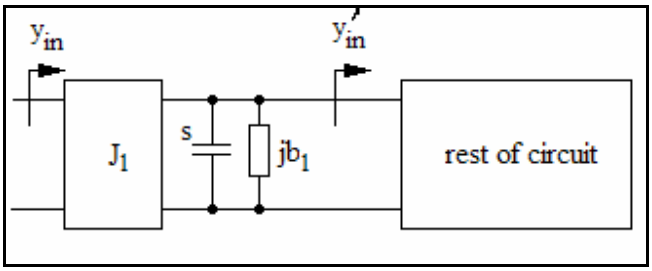

Figure 3.1 Extracting a resonator from circuit

In the first case, the input admittance of the circuit can be expressed as

$$y_{in} = \frac{J_1^2}{(s + jb_1) + y'_{in}}\,. \tag{3.7}$$

Therefore, the inverter value J_1 is calculated as

$$J_1 = \sqrt{\lim_{s\to\infty}(s \cdot y_{in})}\,. \tag{3.8}$$

The value of b_1 depends on the rest of the circuit with an input admittance of y'_{in}. If the first node in the rest of circuit is a resonator, coupled through another inverter, then

$$\lim_{s\to\infty}\left(y'_{in}\right)=0\text{'} \tag{3.9}$$

Therefore, the shun susceptance b_1 is found by calculating

$$b_1=\lim_{s\to\infty}\left(\frac{J^2}{y_{in}}-s\right)=\lim_{s\to\infty}\left(\frac{J^2-s\cdot y_{in}}{y_{in}}\right). \tag{3.10}$$

Otherwise, if the first node in the rest of circuit is a non-resonating node, which generates a transmission zero at frequency ω_Z, the following can be found:

$$\lim_{s\to j\omega_Z}\left(y'_{in}\right)=0 \tag{3.11}$$

and

$$b_1=\lim_{s\to j\omega_Z}\left(\frac{J^2}{y_{in}}-s\right)=\lim_{s\to j\omega_Z}\left(\frac{J^2-s\cdot y_{in}}{y_{in}}\right). \tag{3.12}$$

After extraction, the input admittance of the remaining circuit is

$$y'_{in}=\frac{J_1^2}{y_{in}}-\left(s+jb_1\right). \tag{3.13}$$

In the second case, as shown in Figure 3.2, the input admittance of the circuit is expressed as

$$y_{in}=\frac{J_1^2}{jB+\dfrac{J_2^2}{s-jb_Z}+y'_{in}}. \tag{3.14}$$

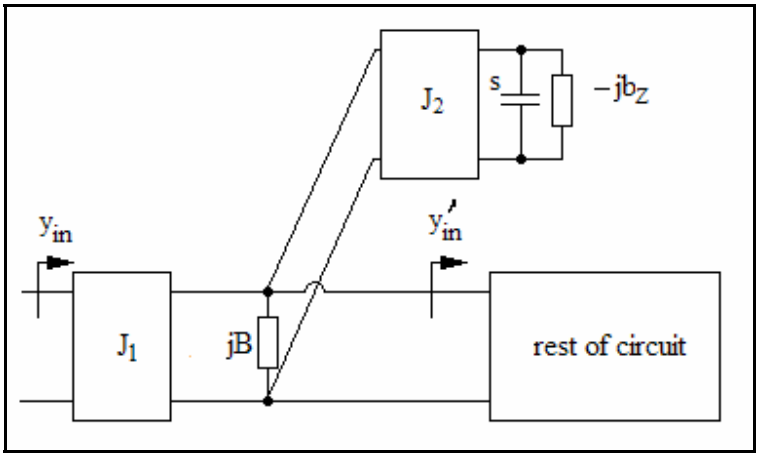

Figure 3.2 Extracting an NRN

By re-arranging the terms in (3.14),

$$\frac{1}{y_{in}} = \frac{J_2^2}{J_1^2}\frac{1}{s - jb_Z} + \frac{jB + y'_{in}}{J_1^2}. \tag{3.15}$$

Therefore, the value of $\frac{J_2^2}{J_1^2}$ is found by taking the residue of $\frac{1}{y_{in}}$ at $s = jb_Z$. There is an infinite combination of the individual value of J_1 and J_2 as long as following is satisfied.

$$\frac{J_2^2}{J_1^2} = \text{Residue}\left(\frac{1}{y_{in}}\right)\Big|_{s=jb_Z}. \tag{3.16}$$

Let $J = \sqrt{\text{Residue}\left(\frac{1}{y_{in}}\right)\Big|_{s=jb_Z}}$, then $J_1 = \alpha$, $J_2 = \alpha J$, and

$$y'_{in} = \frac{J_1^2}{y_{in}} - \frac{J_2^2}{s - jb_Z} - jB. \tag{3.17}$$

To determine value B of the NRN, the first node in the rest of the circuit, of which the input admittance is y'_{in}, must be considered. If the first node in the rest of circuit is a resonator coupled through an inverter, then admittance y'_{in} attains zero at infinitely high frequency, such that

$$\lim_{s\to\infty}\left(y'_{in}\right)=0. \tag{3.18}$$

By combining (3.17) and (3.18), the shunt susceptance B of NRN can be found by computing

$$B=\lim_{s\to\infty}\left(\frac{J_1^2}{y_{in}}-\frac{J_2^2}{s-jb_Z}\right)=\alpha^2\cdot\lim_{s\to\infty}\left(\frac{1}{y_{in}}-\frac{J^2}{s-jb_Z}\right). \tag{3.19}$$

Otherwise, if the first node in the rest of the circuit is another NRN, to which a resonator is coupled to generate another transmission zero at ω'_Z, admittance y'_{in} possesses a zero at ω'_Z such that

$$\lim_{s\to j\omega'_Z}\left(y'_{in}\right)=0. \tag{3.20}$$

Shunt susceptance B is found by combining (3.17) and (3.20),

$$B=\lim_{s\to j\omega'_Z}\left(\frac{J_1^2}{y_{in}}-\frac{J_2^2}{s-jb_Z}\right)=\alpha^2\cdot\lim_{s\to j\omega'_Z}\left(\frac{1}{y_{in}}-\frac{J^2}{s-jb_Z}\right) \tag{3.21}$$

After the extraction, the input admittance of the remaining circuit is

$$y'_{in}=\alpha^2\left\{\frac{1}{y_{in}}-\frac{J^2}{s-jb_Z}-j\left[\lim_{s\to j\omega'_Z}\left(\frac{1}{y_{in}}-\frac{J^2}{s-jb_Z}\right)\right]\right\} \tag{3.22}$$

Equations (3.13) and (3.22) yield the input admittance with which the next step of the extraction is started. Furthermore, from (3.16), (3.19), and (3.22), it can be seen that the inverters connected to NRN can be scaled by an arbitrary coefficient, α, which does not affect the circuit response, as long as the NRN value is scaled by α^2.

3.4 Design of NRN Waveguide Filter with Intermediate Bandwidth

In this section, a trial design of the filter with NRN of an intermediate bandwidth is performed in order to verify the effectiveness of the current designing approach in the literatures. The specification of the filter will be the same as the example in 2.4 with a topology shown in Figure 3.3.

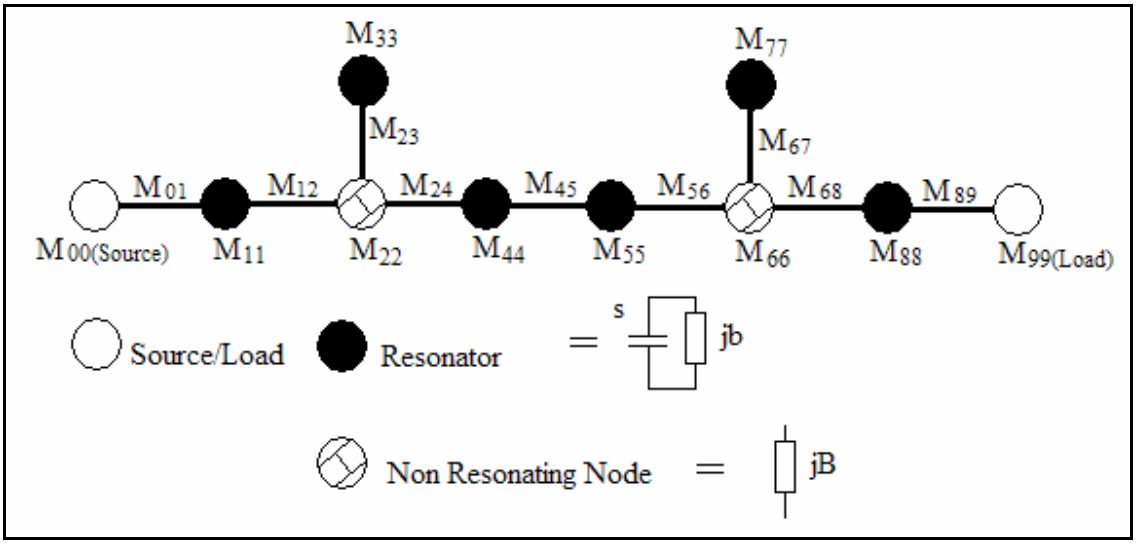

Figure 3.3 Topology of 6-pole waveguide filter with two NRNs

With the procedures described in previous section, the coupling matrix of this filter can be calculated by

$$\begin{bmatrix} 0 & 1.1947 & 0 & 0 & 0 & 0 & 0 & 0 & 0 & 0 \\ 1.1947 & 0.63525 & 1 & 0 & 0 & 0 & 0 & 0 & 0 & 0 \\ 0 & 1 & 1.57417 & 1.5052 & 0.6334 & 0 & 0 & 0 & 0 & 0 \\ 0 & 0 & 1.5052 & 1.96 & 0 & 0 & 0 & 0 & 0 & 0 \\ 0 & 0 & 0.6334 & 0 & 0.19261 & 0.64322 & 0 & 0 & 0 & 0 \\ 0 & 0 & 0 & 0 & 0.64322 & -0.19261 & 0 & 0.6334 & 0 & 0 \\ 0 & 0 & 0 & 0 & 0 & 0.82827 & -1.96 & 1.5052 & 0 & 0 \\ 0 & 0 & 0 & 0 & 0 & 0 & 1.5052 & 1.57417 & 1 & 0 \\ 0 & 0 & 0 & 0 & 0 & 0 & 0 & 1 & 0.63525 & 1.1947 \\ 0 & 0 & 0 & 0 & 0 & 0 & 0 & 0 & 1.1947 & 0 \end{bmatrix} \quad .(3.23)$$

To avoid excessive global optimization, the entire filter is decomposed into several individual modules. Each module is tuned by comparing the responses of the EM simulation and those of the circuit model.

The first module to be designed is NRN 1, with the reduced circuit topology and EM structure shown in Figure 3.4

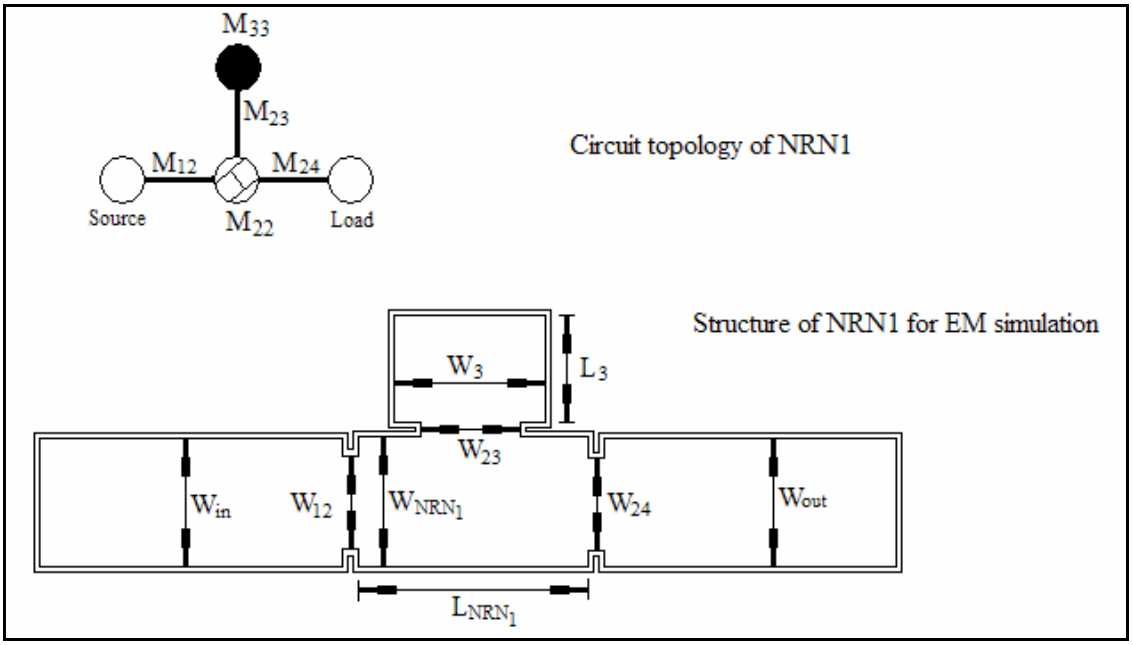

Figure 3.4 Module of NRN1 (circuit topology and EM structure)

When adjusting the parameters in the structure, the frequency response of the EM simulation is compared with that from an ideal circuit model until they are very close to each other in the pass band, as signified in Figure 3.5.

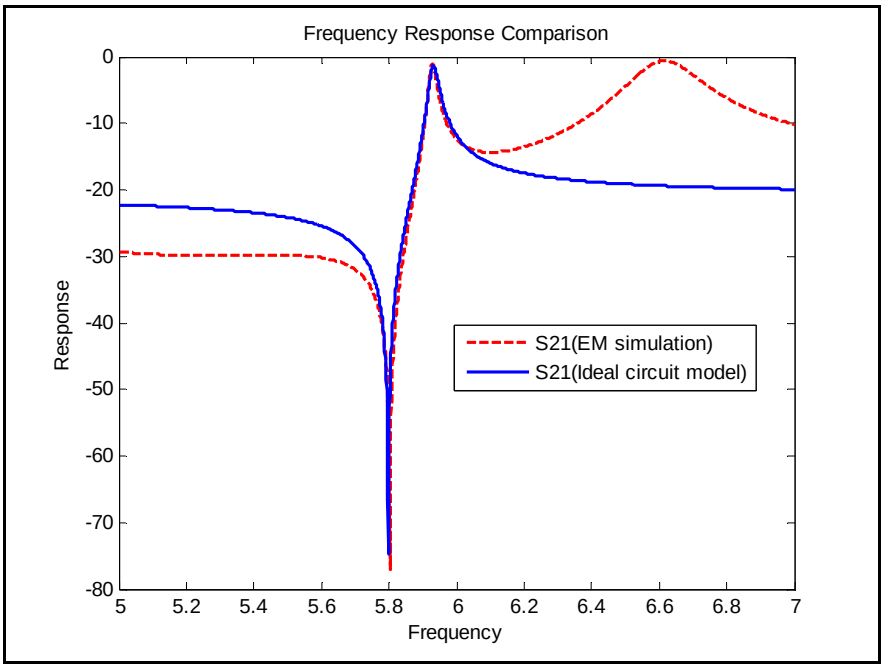

Figure 3.5 Frequency response comparison of NRN1

NRN 2 is designed in the same way which yields the frequency response in Figure 3.6.

For the remaining parts of the filter, the same method as that in section 2.4 is used to determine the widths of all the irises and the lengths of all the cavities. Once all components are combined, the overall filter performance is obtained, as evident in Figure 3.7.

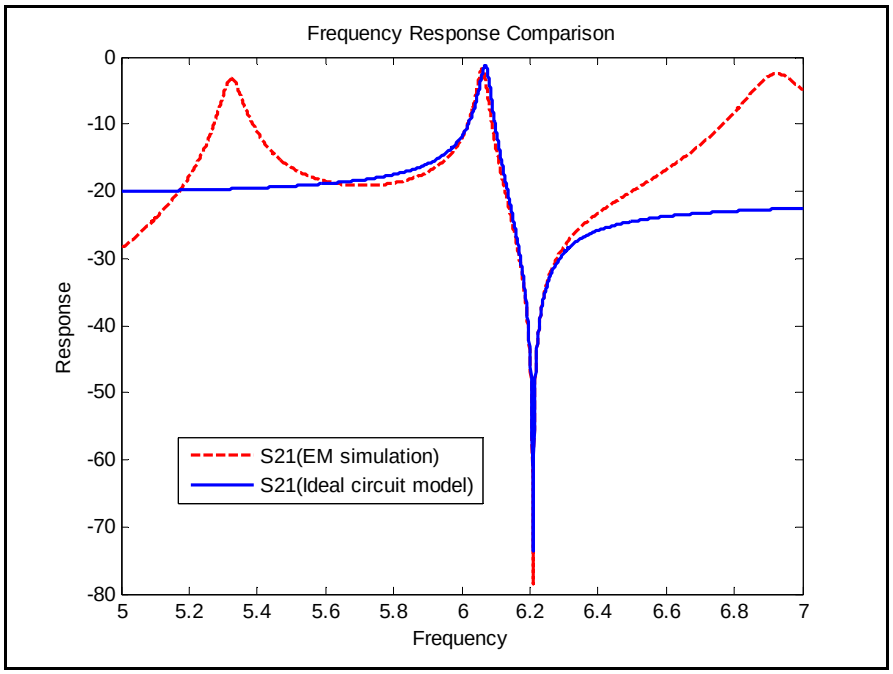

Figure 3.6 Frequency response comparison of NRN 2

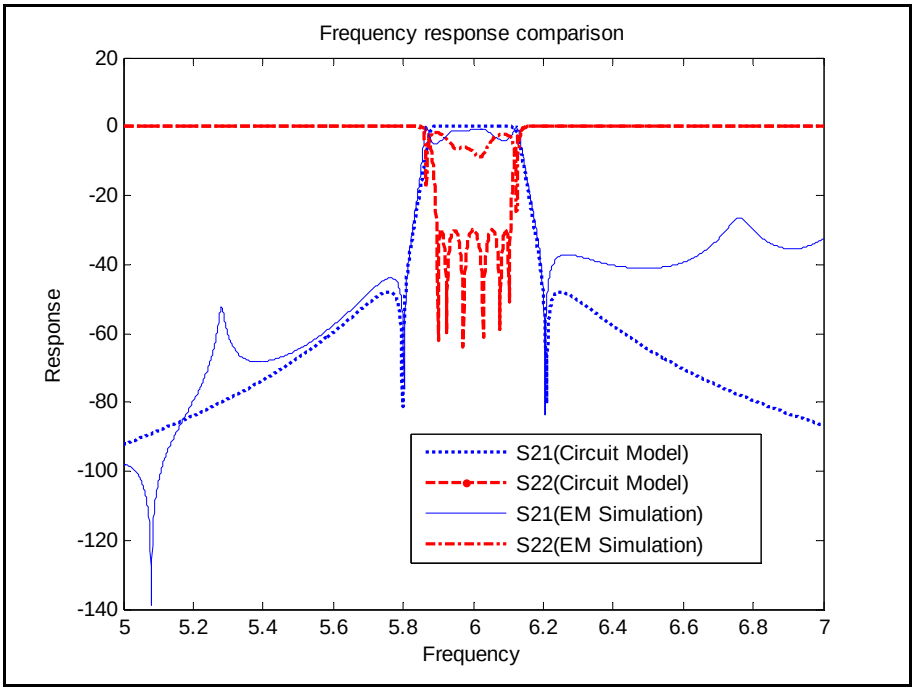

Figure 3.7 Frequency response comparison of the entire filter

This design approach is inappropriate, possibly due to the following:

1) The spikes in the frequency response, which is caused by the unwanted resonance in the NRNs can not be attenuated sufficiently. The E-Field of NRN 1 in Figure 3.8 E-Field distribution of NRN1 at 6.75 GHz shows clearly that NRN 1 is resonating at 6.75GHz where there is a spike on frequency response of entire filter. To resolve this problem, special attention must be paid in choosing the empty waveguide for realizing the NRNs.

2) The circuit model does not accurately represent the waveguide structure behavior in the EM simulation, especially the frequency dependence of the coupling iries. Therefore, the method of tuning the individual module is not effective. It yields only an initial solution with which an intensive overall optimization must be performed. To avoid this trouble, a new circuit model is needed in order to better approximate the frequency dependence of coupling irises.

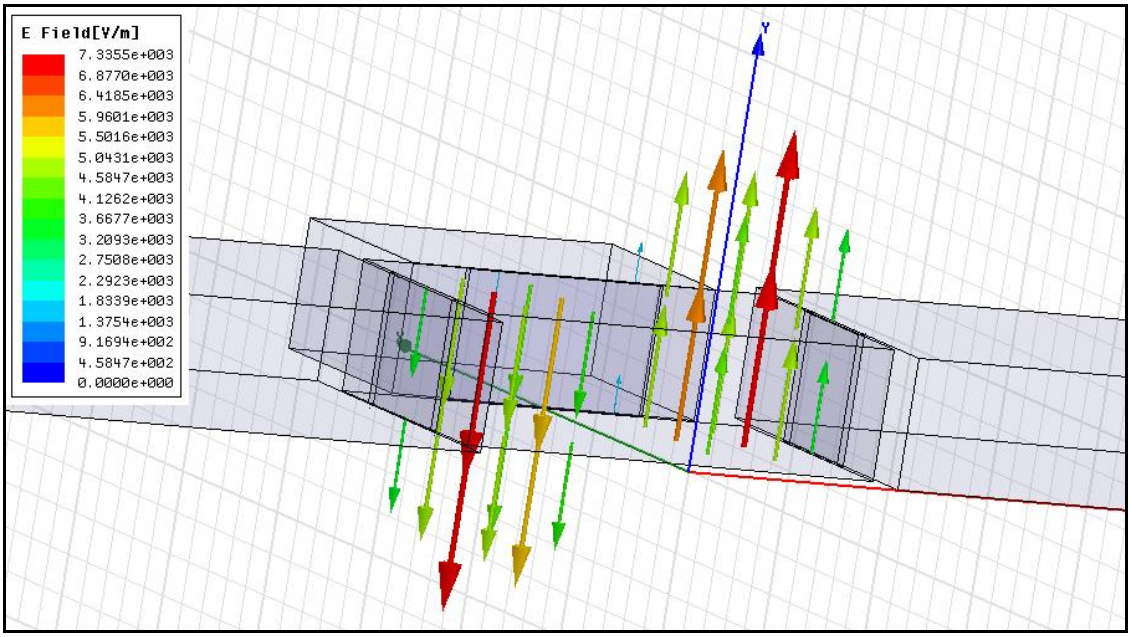

Figure 3.8 E-Field distribution of NRN1 at 6.75 GHz

3.5 Conclusions

This chapter reviews the method of synthesis of the filters with NRNs with the extracted pole method. For this class of filters, the transmission zeros are determined by dedicated resonators. Therefore, it is easier to tune the transmission zeros to the desired frequency. However, an unsuccessful preliminary design shows that further effort is needed to design this class of filter efficiently.

In the following chapter, the goal is to work out a new circuit model for the coupling iris which can predict precisely the frequency dependence of the coupling iris in the waveguide filters.

4. A Novel Circuit Model of Coupling Irises

4.1 Introduction

The frequency dependence of the coupling iris is the primary reason of degradation in frequency response of the band-pass filter, especially in the wide bandwidth application. Improved iris models have been provided in recent research [23] and [24], which took into consideration the frequency dependence of the coupling iris in waveguide filters. However, the design procedures based on those models are all developed for the pure Chebychev filters. The feasibility of utilizing such models to design waveguide filter with the NRNs is unknown.

In this chapter, a novel circuit model, of which the frequency response matches that of the EM simulation on both magnitude and phase, is developed. This novel circuit model can be easily realized with a simple π network comprising L and C. Also the parameters of the circuit can be extracted directly from the coupling matrix without using full-wave simulations.

Some simple structures are simulated in this chapter to demonstrate the soundness of the proposed circuit model.

4.2 Circuit Model for Coupling Iris

A numerical investigation is conducted to realize a coupling iris with a coupling coefficient of 1.34161, for a filter with the fractional bandwidth 3.5%. Inverter value K is calculated by

$$K = \sqrt{\frac{\pi}{2} \cdot FBW} \cdot \frac{\lambda_g}{\lambda_0} \cdot M \Big|_{f=6GHz} = \sqrt{\frac{\pi}{2} \cdot 0.035} \cdot \frac{61.25976}{50} \cdot 1.34161 = 0.3854,$$

which corresponds an S21 value of -3.46dB.

The corresponding structure for the EM simulation is shown in Figure 4.1.

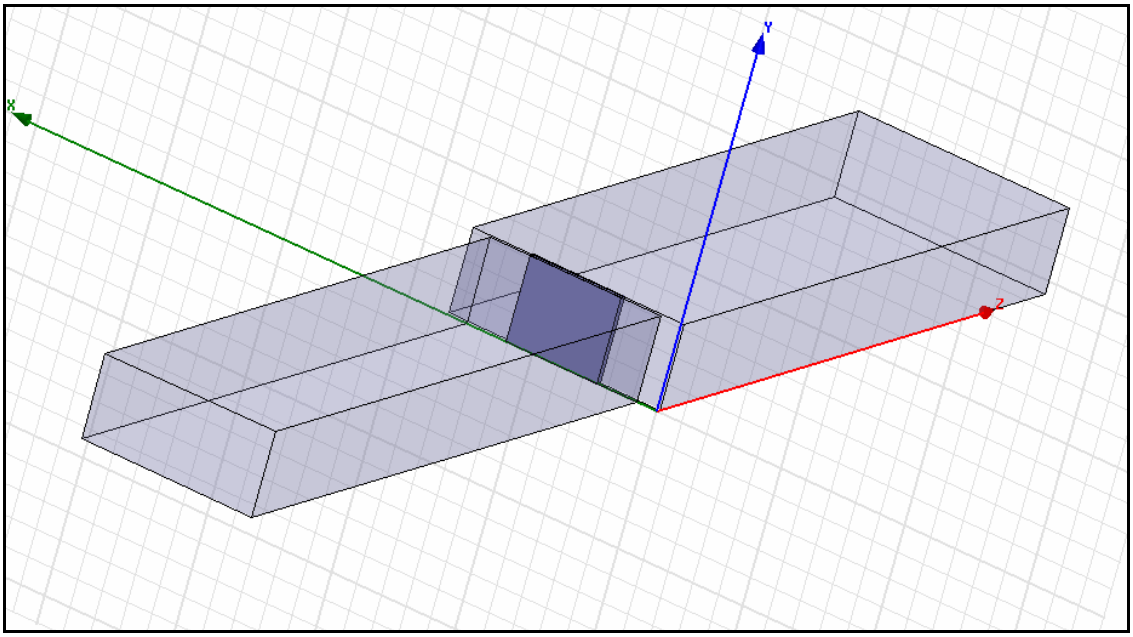

Figure 4.1 Coupling iris between two empty waveguides

The width of the iris can be adjusted to achieve the exact attenuation on S21. The iris size in this case is 0.733187 inch. The structure in Figure 4.1 generates a frequency response in Figure 4.2 for the EM simulation.

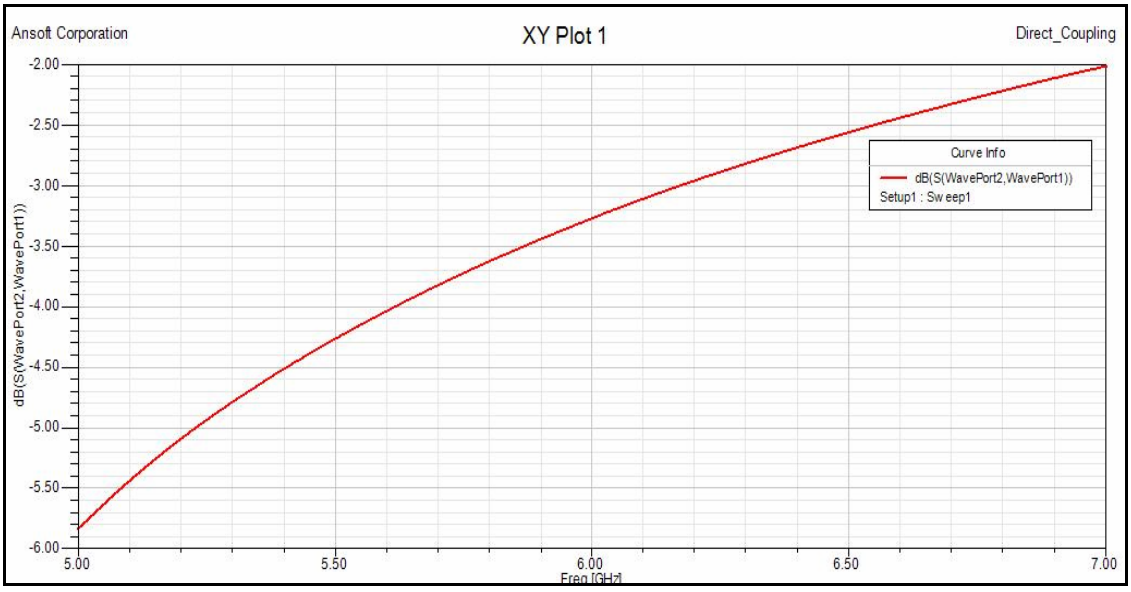

Figure 4.2 Amplitude of S21 of waveguide iris

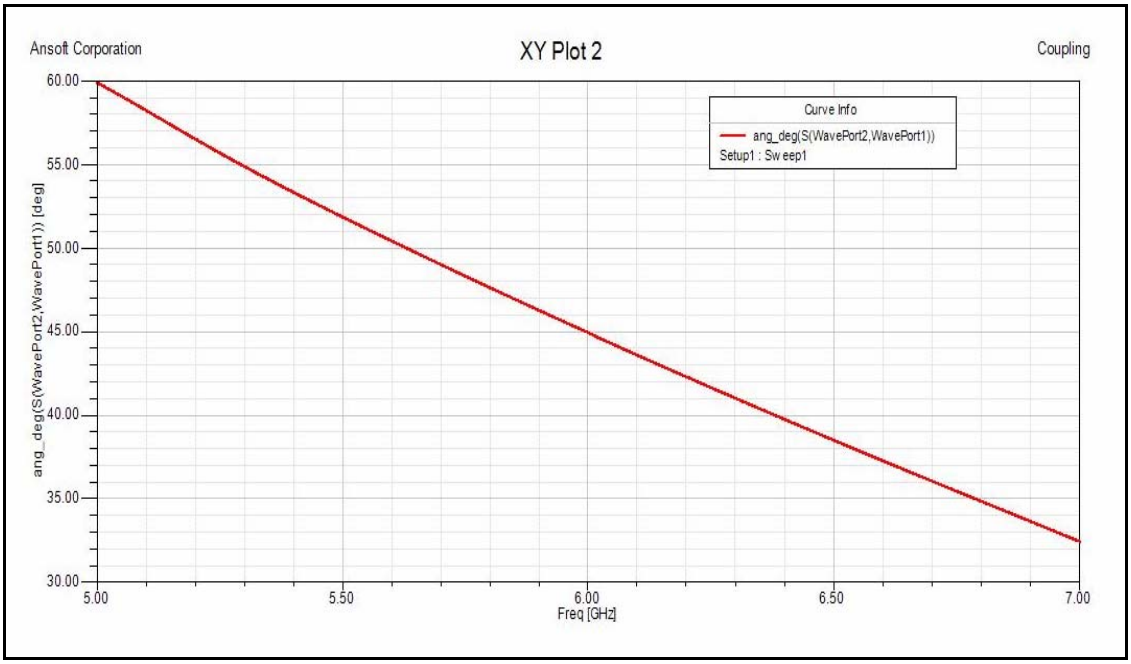

Figure 4.3 Phase of S21 of waveguide iris

Traditionally, an admittance inverter represents a π admittance matrix, as shown in Figure 4.4.

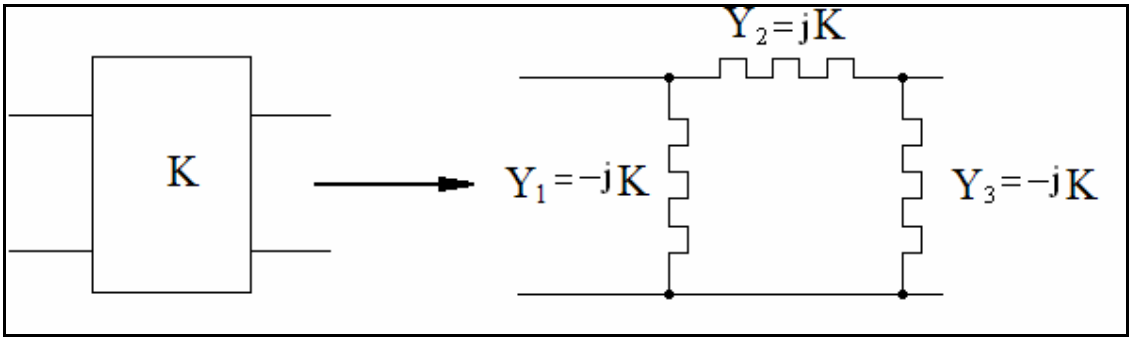

Figure 4.4 Admittance inverter prototype

By replacing the ideal susceptance components with real reactive components, and keeping in mind that the resulting circuit must have a high-pass response, the circuit n Figure 4.5 is obtained.

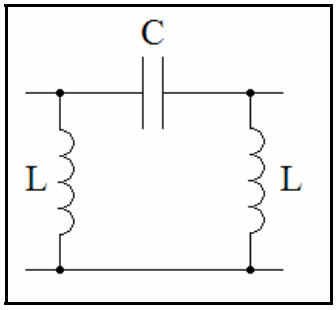

Figure 4.5 Modified circuit model of inverter

By choosing $C = \frac{K}{2\pi f_0}$, $L = \frac{1}{2\pi K f_0}$ at the centre frequency, the admittance of the components can be calculated as:

$$Y_C = j2\pi f_0 \cdot C = jK \tag{4.1}$$

and

$$Y_L = \frac{1}{j2\pi f_0 \cdot L} = -jK\,. \tag{4.2}$$

The combination of these components forms, indeed, an admittance inverter at the centre frequency. At the same time, this circuit is a third order high pass filter.

By comparing frequency response of above circuit with that of coupling iris in the HFSS model, it is evident that the HFSS structure has stronger frequency dependence. This is caused by waveguide dispersion which is not taken into consideration in the circuit model.

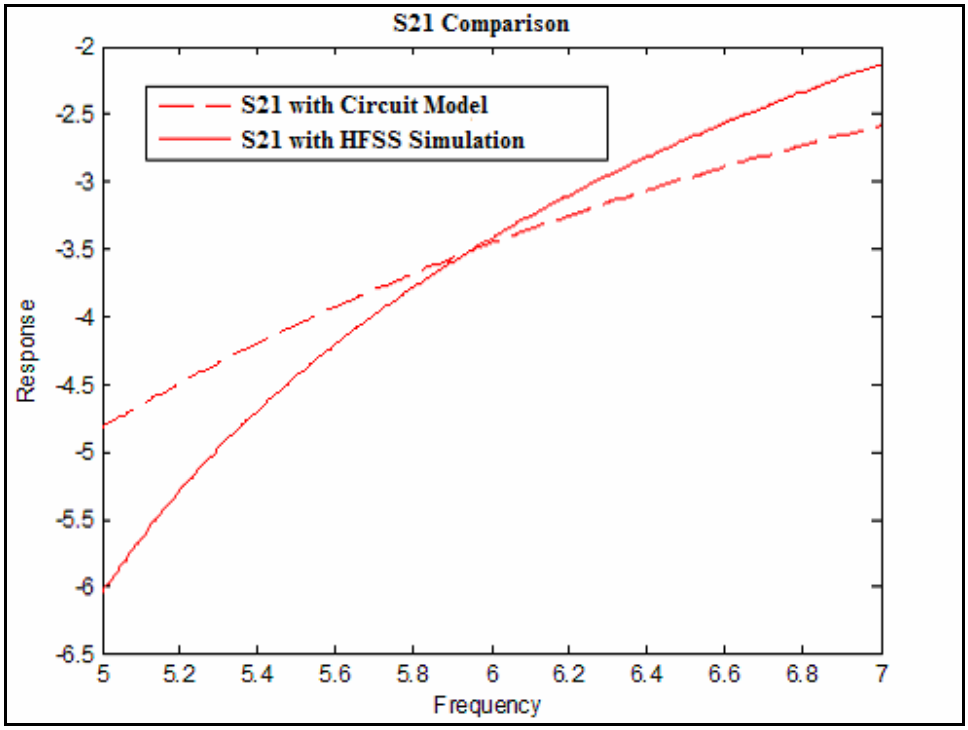

Figure 4.6 Frequency response comparison of circuit model vs. HFSS

The coupling coefficient needs to be modified with a frequency depending coefficient. Setting $K = \sqrt{\frac{\pi}{2} \cdot FBW} \cdot \frac{\lambda_g}{\lambda_0} \cdot M \cdot \left(\frac{f}{f_0}\right)^P$. Here $\left(\frac{f}{f_0}\right)^P$ is a frequency dependent. Since the waveguide dispersion depends on the width of waveguide, the value of P must be determined based on the width of waveguide. In this case, where the width of the waveguide is 1.7 inches, the value of P can be found by an optimization which gives P=0.5.

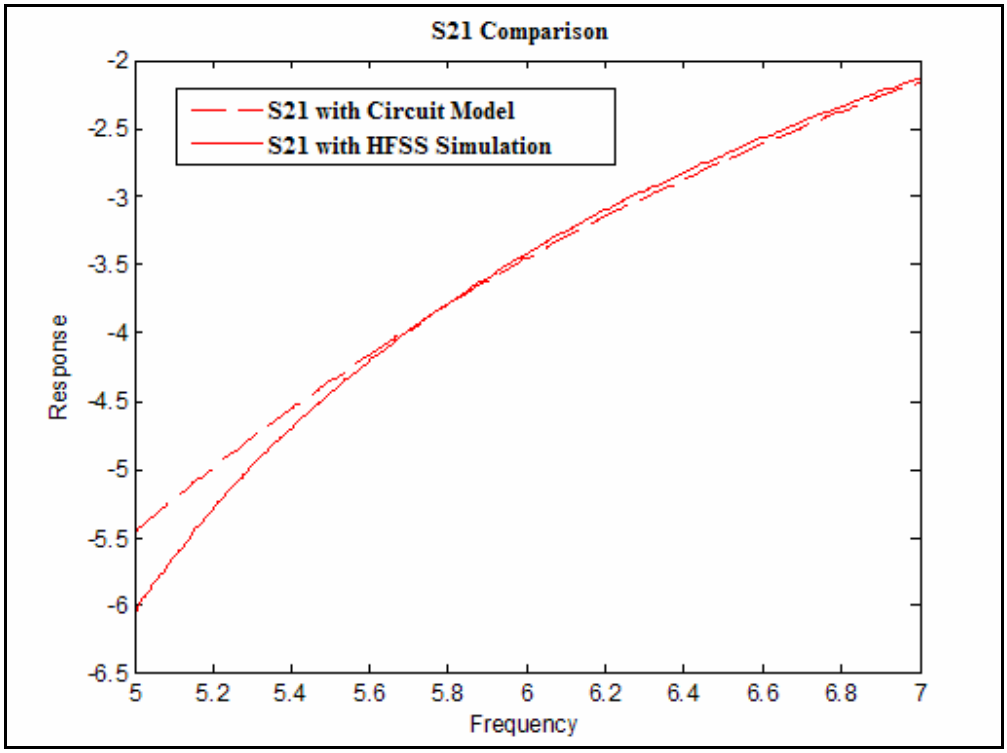

Figure 4.7 Amplitude of S21 (modified circuit model vs. HFSS)

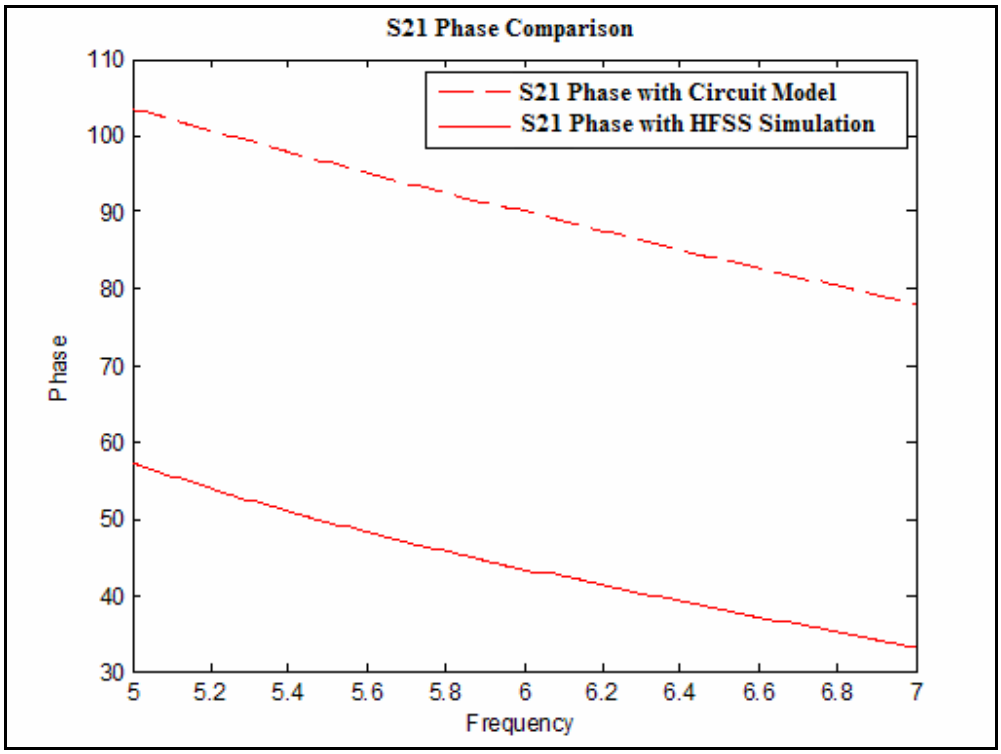

Figure 4.8 Phase of S21 (modified circuit model vs. HFSS)

The phase of the modified circuit model has same frequency dependency as the EM simulation. The difference in phase can be explained by the negative phase length caused by coupling iris, whose value can be calculated as follow:

$$X = \frac{K}{1-K^2}. \tag{4.3}$$

With $K = 0.3854$,

$$\theta = \arctan\left(2X\right) \approx 42°. \tag{4.4}$$

4.3 Finding the Equivalent Coupling Coefficient of the Modified Circuit Model

As illustrated in Figure 4.9, the modified circuit model of an iris is considered as a lumped element inverter with the additional Ls and Cs at a frequency different than that of f_0. These extra capacitances and inductances change the frequency response of the resonator. Therefore, to render the modified circuit model comparable to the ideal lump element model, the coupling coefficient of the modified circuit model must be scaled to some new value.

Furthermore, if the resonator is not tuned at f_0, as in the case of asynchronously tuned filter, this extra inductances and capacitances shift the resonating frequency of the resonator connected to them.

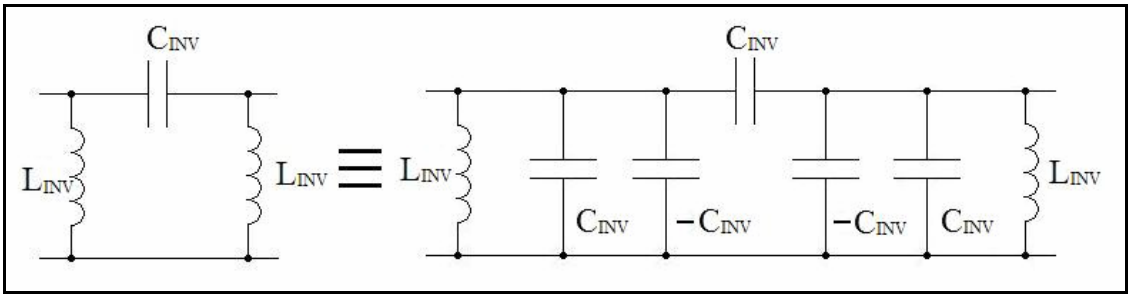

Figure 4.9 Equivalent circuit of modified circuit model of iris

4.3.1 Single Resonator with Coupling Irises on Both Sides

The equivalent circuit of the resonator is shown in Figure 4.10, with $C_{INV} = \frac{K}{2\pi f_0}$ and $L_{INV} = \frac{1}{2\pi K f_0}$.

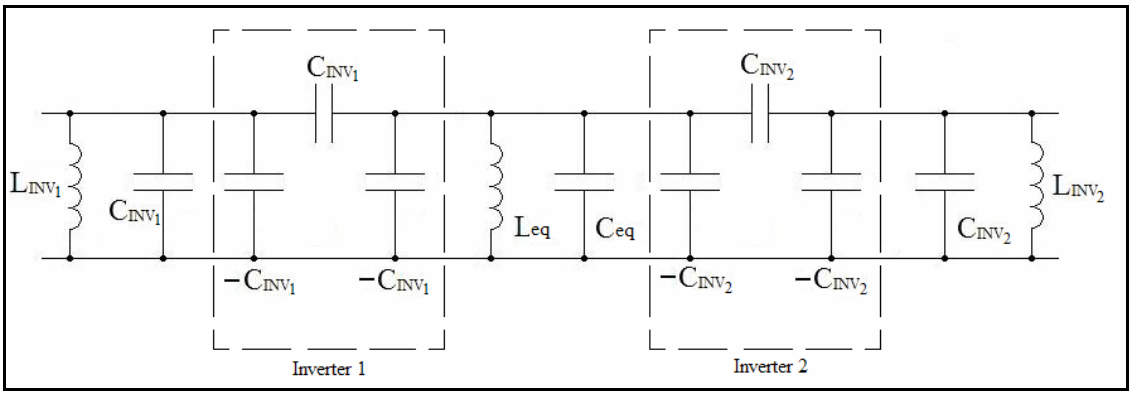

Figure 4.10 Equivalent circuit of resonator with iris on both sides

In the circuit in Figure 4.10, $C_{eq} = C_0 \| C_{INV1} \| C_{INV2}$, and $L_{eq} = L_0 \| L_{INV1} \| L_{INV2}$

C_0, and L_0 are original values of LC resonators in ideal lump element model, whose values are calculated by

$$C_0 = \frac{1}{2\pi f_0}(\text{Farad}), \text{and } L_0 = \frac{1}{2\pi f_0}(\text{Henry}). \tag{4.5}$$

. C_{eq} and L_{eq} in Figure 4.10 can be calculated as follow:

$$C_{eq} = C_0 + C_{INV1} + C_{INV2} = \frac{1}{2\pi f_0} + \frac{K_1}{2\pi f_0} + \frac{K_2}{2\pi f_0} = C_0\left(1 + K_1 + K_2\right) \tag{4.6}$$

$$L_{eq} = \left(\frac{1}{L_0} + \frac{1}{L_{INV1}} + \frac{1}{L_{INV2}}\right)^{-1} = \left(2\pi f_0 + 2\pi K_1 f_0 + 2\pi K_2 f_0\right)^{-1} = \frac{L_0}{\left(1 + K_1 + K_2\right)} \tag{4.7}$$

Total equivalent admittance of the resonator is:

$$Y_{eq} = Y_{Ceq} + Y_{Leq} = (1 + K_1 + K_2)\left(j\omega C_0 + \frac{1}{j\omega L_0} \right) \tag{4.8}$$

This novel circuit model and the ideal lumped element model, in Figure 4.11, without taking into consideration of frequency depending coefficient $\left(\frac{f}{f_0} \right)^P$, have the same frequency response when following conditions are satisfied:

$$K_1' = \frac{K_1}{\sqrt{1 + K_1 + K_2}} \tag{4.9}$$

and

$$K_2' = \frac{K_2}{\sqrt{1 + K_1 + K_2}} \tag{4.10}$$

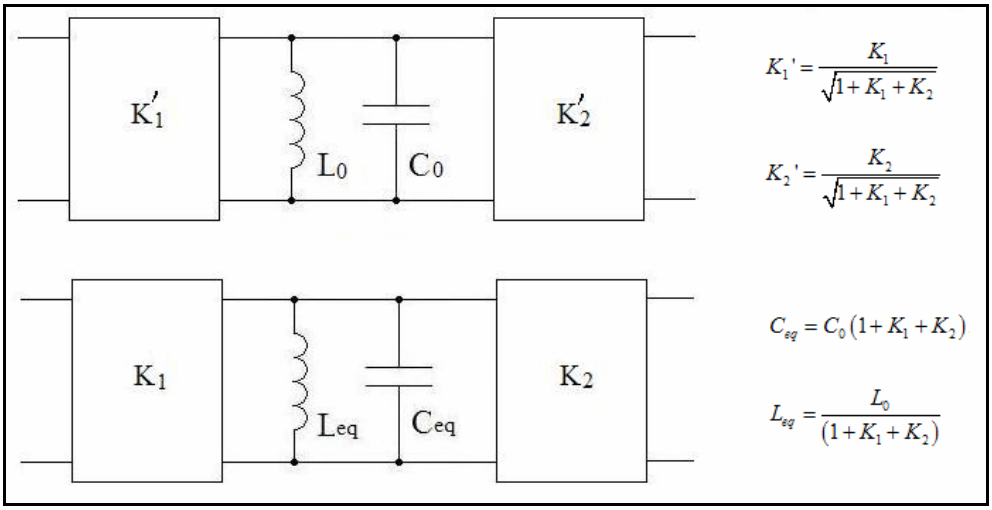

Figure 4.11 Scaling the coupling coefficient of two coupled resonator to yield same response

From (4.9) and (4.10), the following are obtained:

$$K_1 = \frac{K_1'}{K_2'} K_2 \tag{4.11}$$

and

$$K_1^2 = K_1'^2 \left[1 + K_1 \cdot \left(1 + \frac{K_2'}{K_1'} \right) \right]. \tag{4.12}$$

The solution of (4.11) and (4.12) are found as follows:

$$K_1 = \frac{K_1'^2 \cdot C_1 + \sqrt{\left(K_1'^2 \cdot C_1\right)^2 + 4K_1'^2}}{2}, K_2 = \frac{K_2'^2 \cdot C_2 + \sqrt{\left(K_2'^2 \cdot C_2\right)^2 + 4K_2'^2}}{2}, \tag{4.13}$$

where $C_1 = 1 + \frac{K_2'}{K_1'};\ C_2 = 1 + \frac{K_1'}{K_2'}.$

Furthermore, L_{eq} and L_0, C_{eq} and C_0 have the same value only at the center frequency. When the resonator is asynchronously tuned, the resonating frequency of the original resonator will be shifted once the inverters are replaced by the modified circuit model. Therefore, an extra susceptance must be added to bring back the resonating frequency, the value of the susceptance is

$$Y_{extra} = Y_{L_{INV1}} + Y_{L_{INV2}} = -j\left(K_1 + K_2\right)\left(\frac{f}{f_0} - \frac{f_0}{f}\right)\Bigg|_{f=f_{res}}, \tag{4.14}$$

where f_{res} is the resonating frequency of the resonator which is different from f_0.

By taking a numerical design case with $K_1' = K_2' = 1.34161$, $f_0 = 6GHz$, $f_{0b} = 6.1GHz$ and $FBW = 3.5\%$, the frequency responses of both lumped circuit model and modified circuit model are compared with that of the EM simulation.

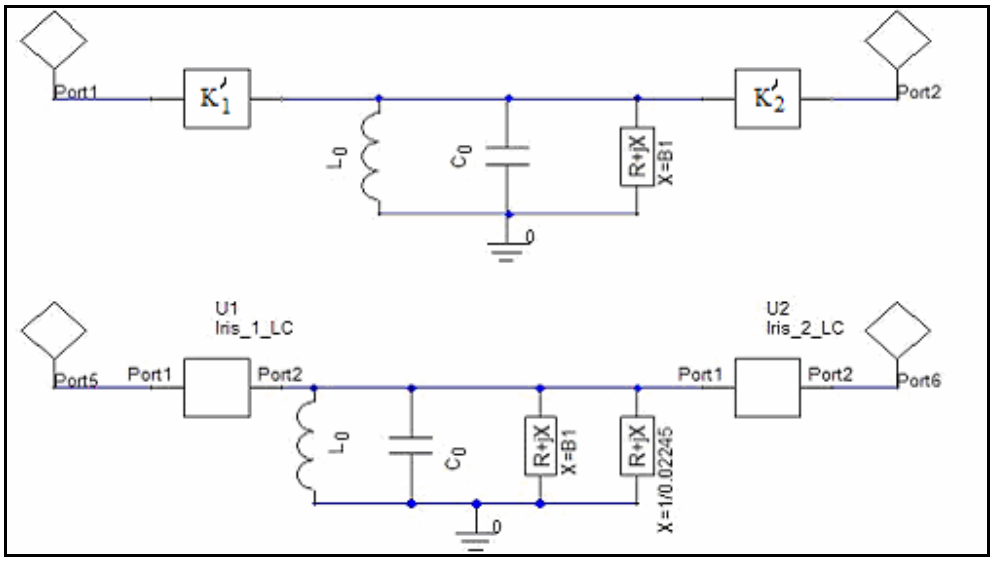

Figure 4.12 Circuit models used to represent a coupled waveguide resonator

In the circuit of Figure 4.12, an ideal circuit model of the coupled resonators is on the top, and the corresponding modified circuit model is on the lower portion; and L_0 and C_0 are inductor and capacitor which form a resonator resonating at f_0; and shunt susceptance B_1 is responsible to bring the resonating frequency to f_{0b}. The extra susceptance of the modified circuit is calculated by (4.14) with a value of 0.02245.

The frequency responses are shown in Figure 4.13.

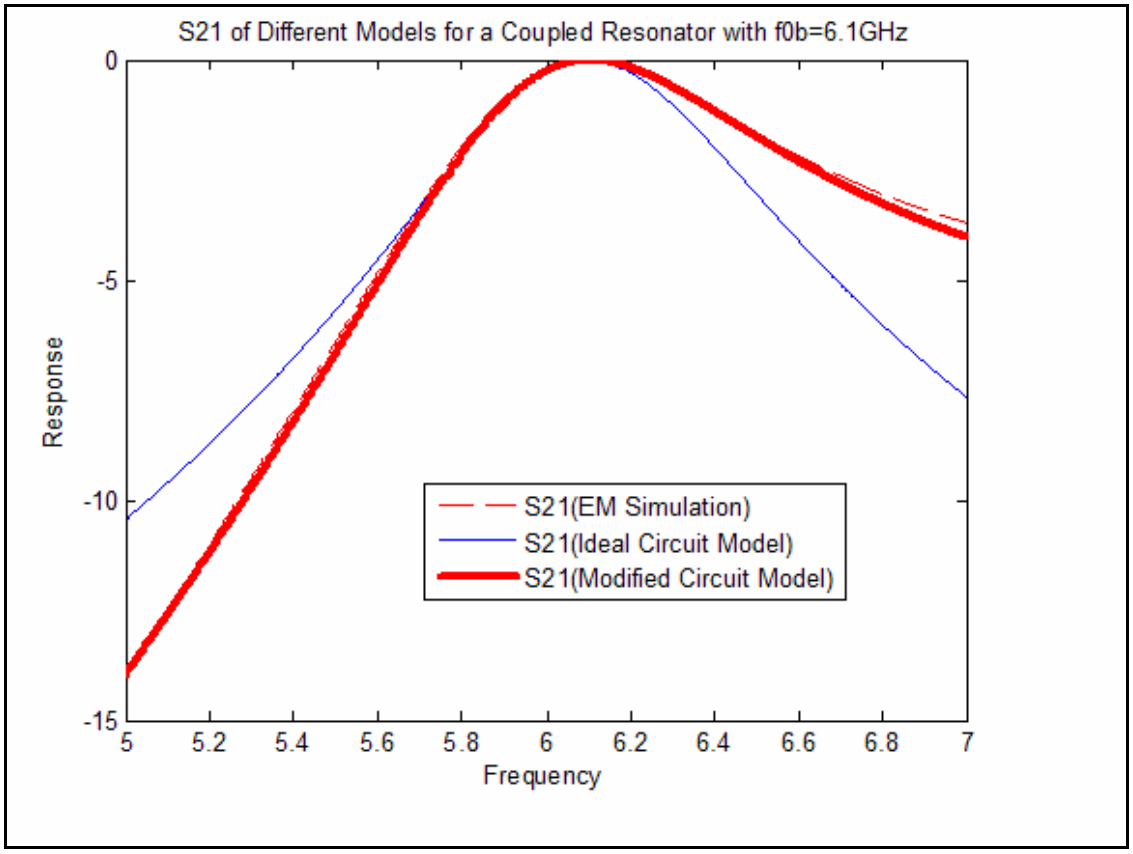

Figure 4.13 Frequency response comparison of circuit models vs. EM simulation

It is evident that the frequency response of the modified circuit model approximates much better that of the EM simulation.

4.3.2 Resonating Cavities in Series

The circuit models the structure are illustrated as follow:

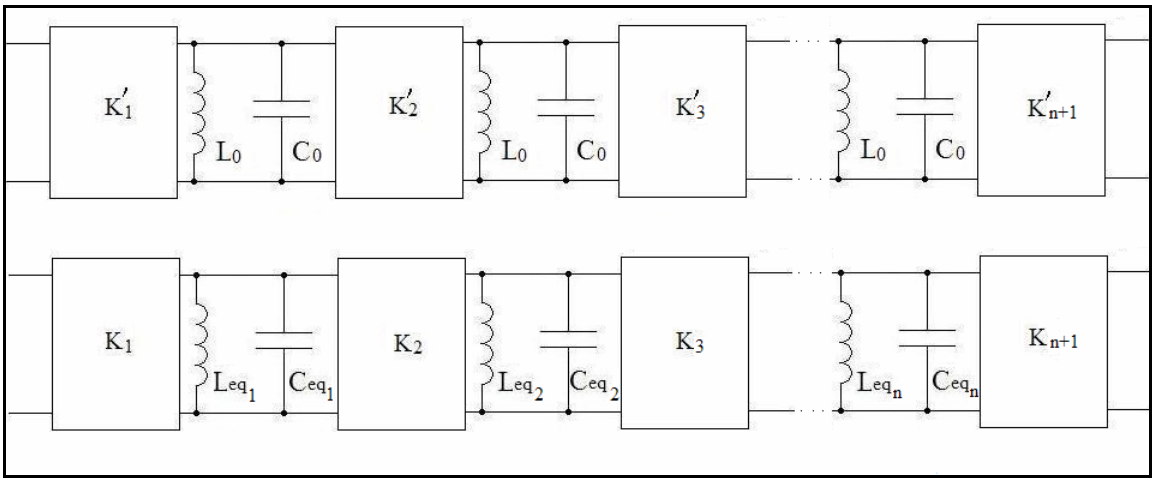

Figure 4.14 Circuit models for the structure with N resonators in series

Blocks K_1', $K_2' \ldots K_{n+1}'$ represent ideal lumped element inverters; K_1, $K_2 \ldots$ K_{n+1} represent modified circuit model of the coupling irises. The equivalent capacitance and inductance are calculated by

$$C_{eq1} = C_0\left(1+K_1+K_2\right);\ L_{eq1} = \frac{L_0}{\left(1+K_1+K_2\right)},$$

$$C_{eq2} = C_0\left(1+K_2+K_3\right);\ L_{eq2} = \frac{L_0}{\left(1+K_2+K_3\right)}, \ldots, \tag{4.15}$$

$$C_{eqn} = C_0\left(1+K_n+K_{n+1}\right);\ L_{eqn} = \frac{L_0}{\left(1+K_n+K_{n+1}\right)}.$$

To obtain the same frequency response from both networks in Figure 4.14, the following must be satisfied:

$$
\begin{aligned}
K_1' &= \frac{K_1}{\sqrt{1+K_1+K_2}}, \\
K_2' &= \frac{K_2}{\sqrt{1+K_1+K_2}\sqrt{1+K_2+K_3}}, \ \cdots, \\
K_n' &= \frac{K_n}{\sqrt{1+K_{n-1}+K_n}\sqrt{1+K_n+K_{n+1}}}, \\
K_{n+1}' &= \frac{K_{n+1}}{\sqrt{1+K_n+K_{n+1}}}.
\end{aligned}
\tag{4.16}
$$

Given the numerical value of K_1', $K_2' \ldots K_{n+1}'$, the values for K_1, $K_2 \ldots K_{n+1}$ are found by solving the n+1 equations.

By taking a numerical example with: n=2, $K_1' = K_3' = 1.34161$, $K_2' = 0.70885$, $f_0 = 6GHz$, $f_{b1} = 5.9GHz$, $f_{b2} = 6.1GHz$ and $FBW = 3.5\%$, the frequency response of the circuit models can be compared to that of the EM simulation.

From (4.16), the following can be obtained:

$$
\begin{cases}
K_1' = \dfrac{K_1}{\sqrt{1+K_2+K_3}} \\
K_2' = \dfrac{K_2}{\sqrt{1+K_1+K_2}\sqrt{1+K_2+K_3}} \\
K_3' = \dfrac{K_3}{\sqrt{1+K_2+K_3}}
\end{cases}
\tag{4.17}
$$

Since K_1' and K_3' have same value, so do K_1 and K_3, such that

$$\left.\begin{aligned} K_1' &= \frac{K_1}{\sqrt{1+K_1+K_2}} \Rightarrow K_1^2 = K_1'^2\left(1+K_1+K_2\right) \\ K_2' &= \frac{K_2}{1+K_1+K_2} \Rightarrow K_2 = K_2'\left(1+K_1+K_2\right) \end{aligned}\right\} \Rightarrow \frac{K_1^2}{K_2} = \frac{K_1'^2}{K_2'} \tag{4.18}$$

$$\Rightarrow K_1^2 = K_1'^2\left(1+K_1+\frac{K_1^2}{K_1'^2}K_2'\right) \Rightarrow \left(1-K_2'\right)K_1^2 - K_1'^2\cdot K_1 - K_1'^2 .$$

By resolving (4.18), the following are obtained:

$$K_1 = \frac{K_1'^2+\sqrt{K_1'^4+4\left(1-K_2'\right)K_1'^2}}{2\cdot\left(1-K_2'\right)},$$

$$K_2 = \frac{K_1\cdot K_3}{K_1' K_3'}K_2' \tag{4.19}$$

and

$$K_3 = \frac{K_3'^2+\sqrt{K_3'^4+4\left(1-K_2'\right)K_3'^2}}{2\cdot\left(1-K_2'\right)}.$$

The circuits in Figure 4.15 represent two coupled resonators with the corresponding modified circuit model and ideal circuit model, respectively.

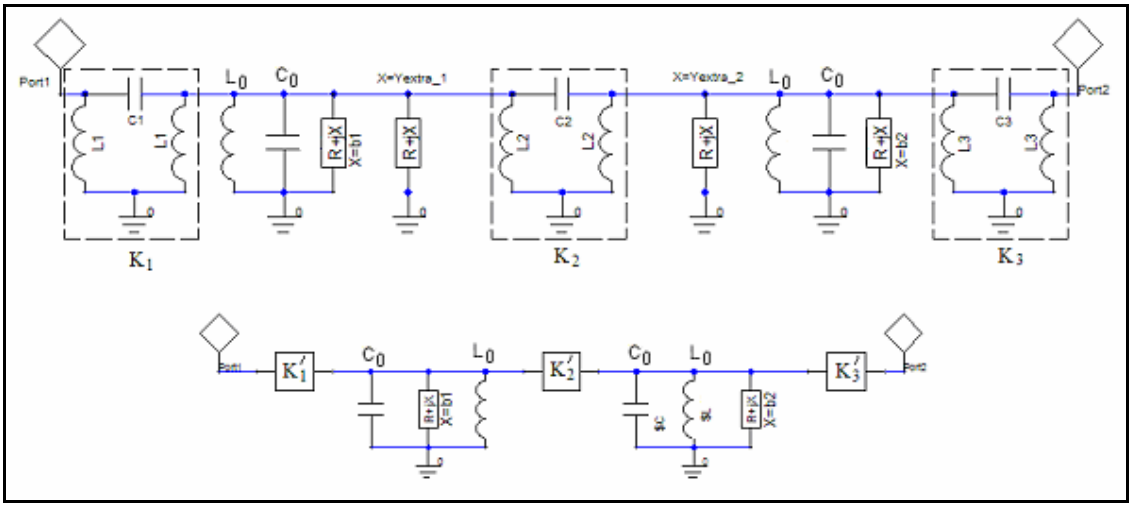

Figure 4.15 Circuit models for two coupling resonators in series

The extra susceptance, introduced by modified circuit models at f_{b1} and f_{b2}, are calculated by

$$Y\_Extra_1 = -j\left(K_1 + K_2\right)\cdot\left(\frac{f}{f_{b1}} - \frac{f_{b1}}{f}\right) \tag{4.20}$$

and

$$Y\_Extra_2 = -j\left(K_2 + K_3\right)\cdot\left(\frac{f}{f_{b2}} - \frac{f_{b2}}{f}\right). \tag{4.21}$$

Figure 4.16 shows corresponding structure used in HFSS simulation.

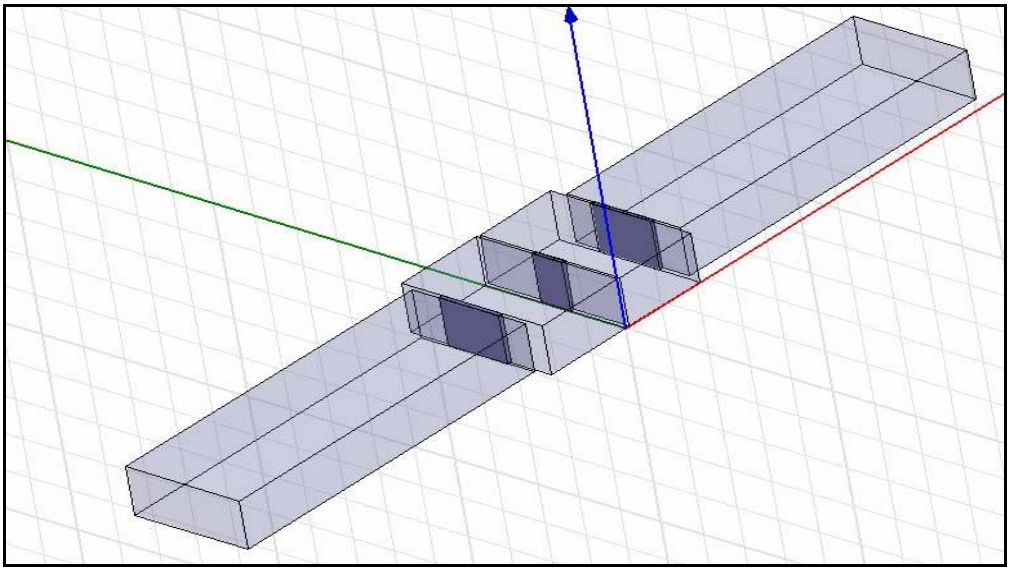

Figure 4.16 Structure with two resonators in series

The frequency responses are shown in Figure 4.17, indicating that the modified circuit model approximates better the EM simulation.

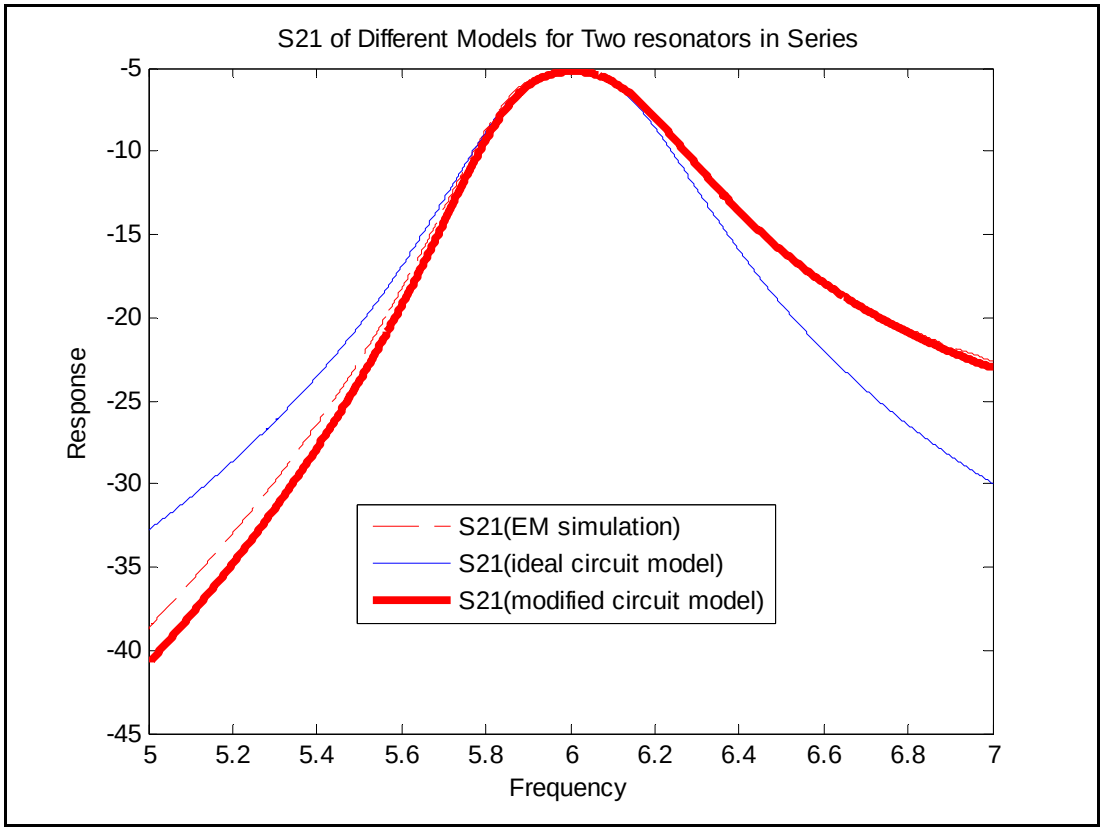

Figure 4.17 Frequency responses of different models of two resonators in series

5. Novel Design Approach of Waveguide Filters with NRNs

5.1 Introduction

In this chapter, two filters are designed with the procedure based on the novel circuit model described in Chapter 4. The first one has intermediate fractional bandwidth of 3.5%, which is wider than most of the design example in the literatures [16]-[21]. The other one has relatively wide fractional bandwidth of 8.333%, which illustrate approximately the upper limit of the design approach.

Both filters are realized with individually fine tuned modules. Thus the usage of EM simulation in optimization is minimized. Moreover, to improve the spurious free window of the filter, new criteria are proposed for determining the width of the empty waveguide which is used as NRNs.

The procedure, with which both filters with NRNs are designed successfully, is summarized in the last section of this chapter, which can be used as a general design approach of the waveguide filter with NRNs.

5.2 Design Example with Intermediate Bandwidth

In this section, the filter, which is poorly designed in Section 3.4, is redesigned. The specifications of the filter are listed as follow:

- 6 Pole Chebychev band-pass filter with a pair of normalized transmission zeros at $\pm 1.96\, j$
- Center Frequency $f_0 = 6GHz$, and bandwidth $BW = 210MHz$
- Return loss $RL = 30dB$

5.2.1 Circuit Model Optimization

The coupling matrix of this filter is the same as that in (3.23), with elements M_{22} (b_2)=1.57417, M_{66}(b_6)=-1.57417 representing two non resonating nodes respectively.

As shown Figure 5.1, the filter is decomposed into five individual blocks so as to fine tune each of the blocks by simply using the associated parameters. This avoids optimizing a large number of the parameters at the same time, which usually takes numerous iterations to converge.

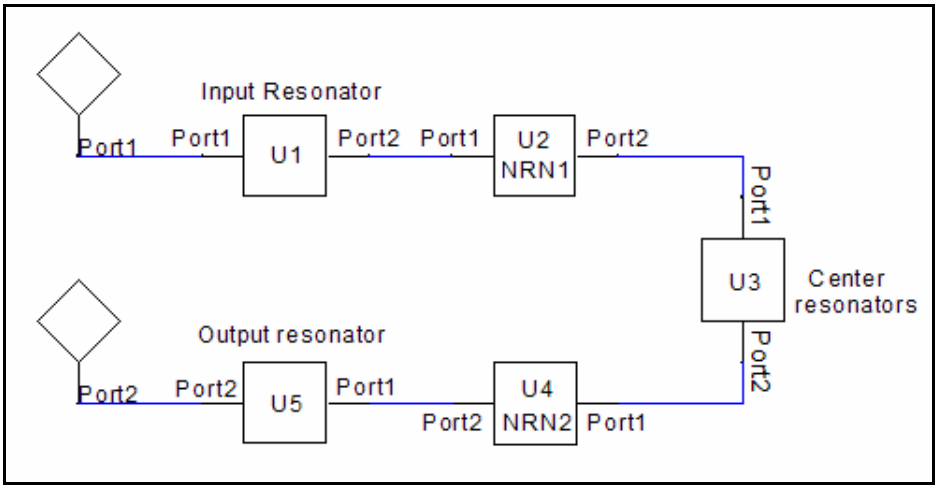

Figure 5.1 Block diagram of circuit model

If modified circuit model is built on the ideal coupling values, the resulting filter performance is poor, as depicted in Figure 5.2.

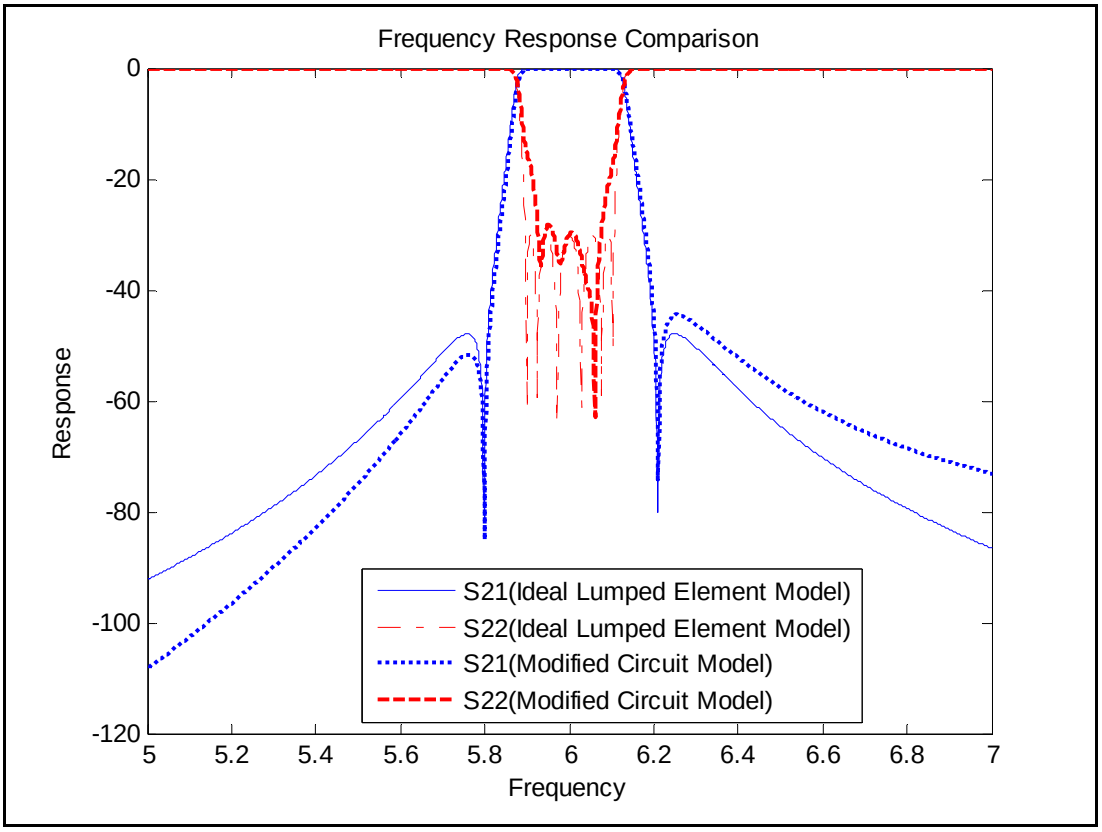

Figure 5.2 Frequency response of circuit model with original values from coupling matrix

Therefore, some optimization on the coupling matrix is needed in order to yield the desired filter performance with modified circuit model. The modification can be done in any circuit model optimizer such as Ansoft Designer [25]. The modified N+2 coupling matrix is

$$\begin{bmatrix}
0 & 1.16917 & 0 & 0 & 0 & 0 & 0 & 0 & 0 & 0 \\
1.16917 & 0.56327 & 1.22985 & 0 & 0 & 0 & 0 & 0 & 0 & 0 \\
0 & 1.22985 & 2.69188 & 2.0010 & 0.79557 & 0 & 0 & 0 & 0 & 0 \\
0 & 0 & 2.0010 & 1.9600 & 0 & 0 & 0 & 0 & 0 & 0 \\
0 & 0 & 0.79557 & 0 & 0.204576 & 0.638426 & 0 & 0 & 0 & 0 \\
0 & 0 & 0 & 0 & 0.638426 & -0.171634 & 0.864121 & 0 & 0 & 0 \\
0 & 0 & 0 & 0 & 0 & 0.864121 & -2.69188 & 1.94495 & 1.35344 & 0 \\
0 & 0 & 0 & 0 & 0 & 0 & 1.94495 & -1.9600 & 0 & 0 \\
0 & 0 & 0 & 0 & 0 & 0 & 1.35344 & 0 & -0.62515 & 1.18258 \\
0 & 0 & 0 & 0 & 0 & 0 & 0 & 0 & 1.18258 & 0
\end{bmatrix} \quad (4.22)$$

The frequency response of the circuit model and the ideal response are shown in Figure 5.3.

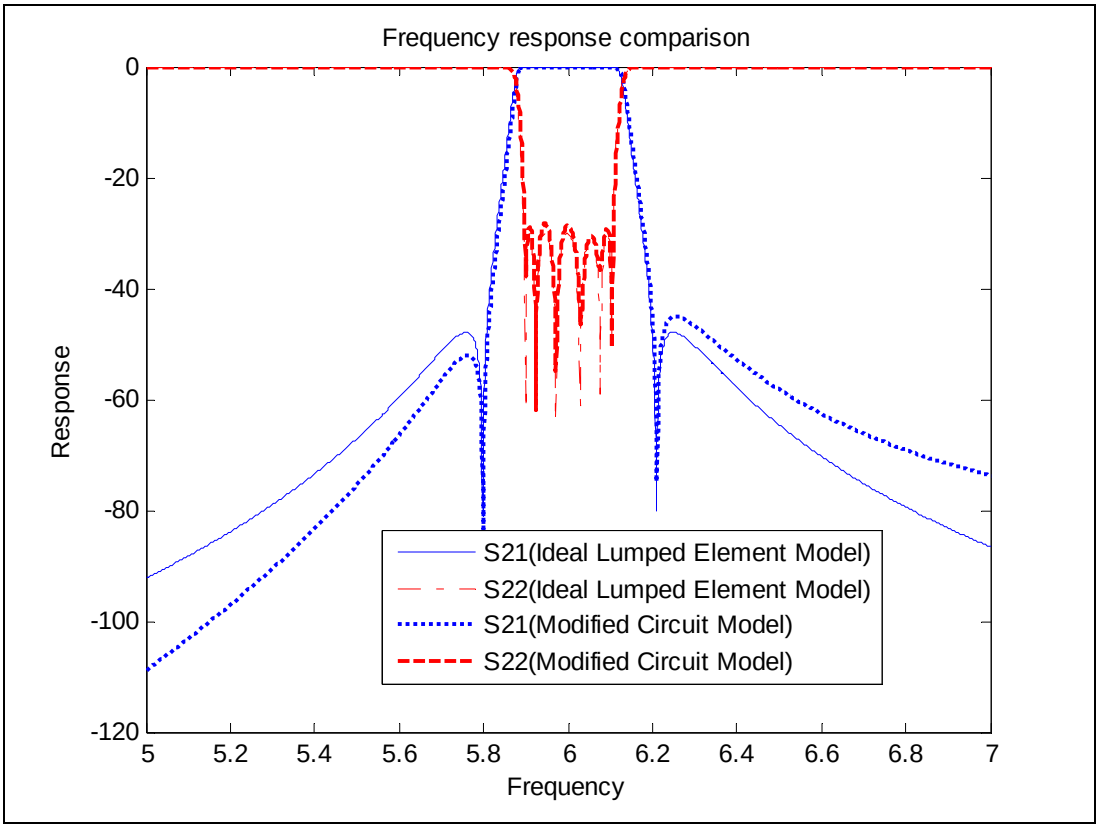

Figure 5.3 Optimized circuit model response

5.2.2 Realize NRN 1

NRNs are realized by a highly detuned waveguide resonator. The first NRN has a capacitive susceptance of -2.69188. Usually, a waveguide with an electrical length between the TE102 mode and the TE103 mode can be chosen [22]. However, this configuration generates spikes caused by unwanted resonance on both the higher and the lower sides of pass-band. In this design, a waveguide of electrical length less than the TE101 mode is chosen. Moreover, the width of this waveguide is chosen so that the cut-off frequency is adjacent to the pass-band. This guarantees a spurious free response on the lower side of the pass-band and helps to attenuate the unwanted resonance generated by other NRNs. The width of the cavity is chosen to be 1.02inchs corresponding to a cut off frequency around 5.7GHz. The length of the cavity is 1 inch. The lowest resonating frequency is around 8.2GHz.

Since it is difficult to measure the equivalent susceptance of the cavity, individual iris size is difficult to determine. However, as being proven in Section 3.2, the susceptance value can be scaled with adjacent coupling coefficient to any realizable value. The design procedure is started with the arbitrary initial values as shown in Table 5.1, and then these parameters are optimized by a method similar to space mapping technique described in the literature [26]. The iterative steps to optimize NRN 1 are listed as follow:

1) Capture the frequency response of EM simulation with circuit model optimizer
2) Compare the optimized values and initial values, if the difference is small (<1%) then stop the optimization
3) Otherwise, modify the relevant sizes of the structure, and then restart the first step

Table 5.1 Arbitrary values for NRN1

Parameter	Arbitrary initial values
W_{12} (M_{12})	0.6 inch
W_{23} (M_{23})	0.7 inch
W_{24} (M_{24})	0.5 inch
L_{b3} (Side cavity length)	1 inch

The structure for the EM simulation is given in Figure 5.4. With the initial arbitrary values, it yields frequency response in Figure 5.5.

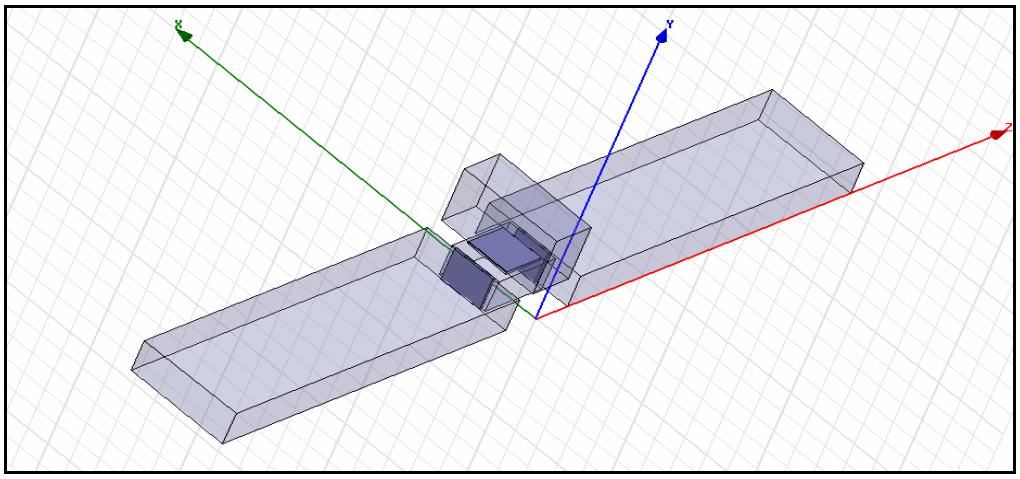

Figure 5.4 Structure used to realize NRN1

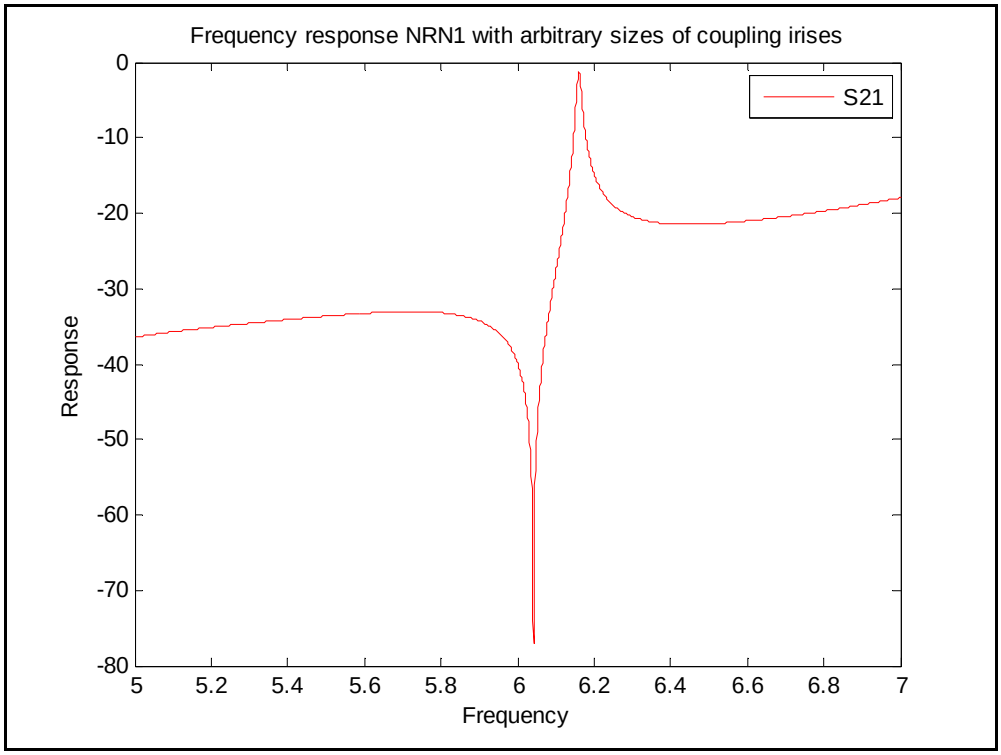

Figure 5.5 Frequency response of NRN with arbitrary values

In NRN 1, four parameters are optimized (3 irises and 1 cavity length). Equivalent circuit model of NRN1 is conveyed in Figure 5.6.

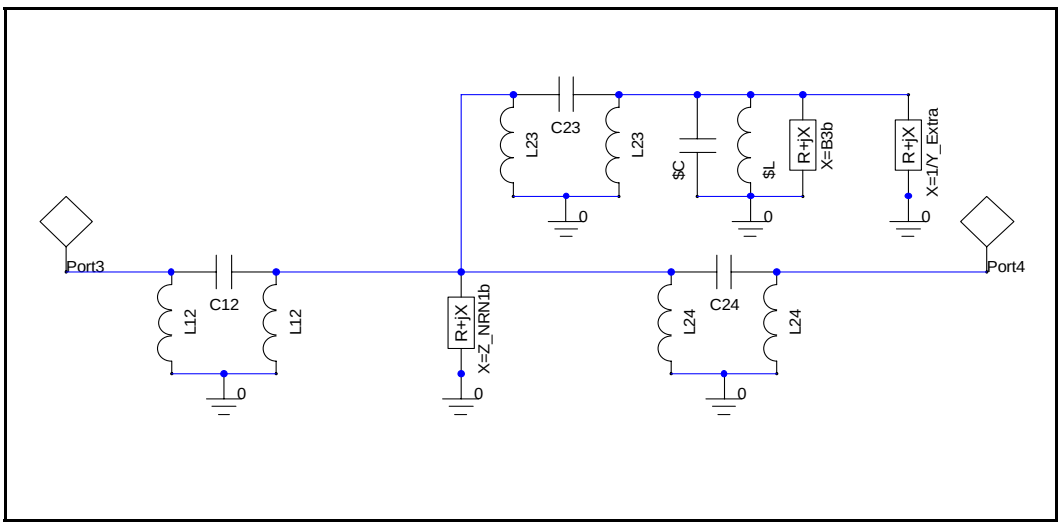

Figure 5.6 Circuit model of NRN1

The parameters of the circuit can be calculated referring previous chapter:

$$C_{12} = \frac{K_{12}}{2\pi f_0},\ L_{12} = \frac{1}{2\pi K_{12} f_0},$$
$$C_{24} = \frac{K_{24}}{2\pi f_0},\ L_{24} = \frac{1}{2\pi K_{24} f_0},$$

$$K_{12} = M_{12}\sqrt{\frac{\pi}{2}\cdot FBW}\cdot\frac{\lambda_g}{\lambda_0}\cdot\left(\frac{f}{f_0}\right)^{0.5},$$

$$C_{23} = \frac{K_{01}}{2\pi f_0},\ L_{23} = \frac{1}{2\pi K_{01} f_0},$$

$$K_{23} = \left(\frac{K_{23}{}'^2 + \sqrt{K_{23}{}'^4 + 4K_{23}{}'^2}}{2}\right)\cdot\left(\frac{f}{f_0}\right)^{0.5},$$

$K_{23}{}' = M_{23}\cdot\sqrt{FBW}$, $M_{23} = 2.001, M_{12} = 1.22985, M_{24} = 0.795571, FBW = 0.035$,

$Z\_NRN1b = -1/b_2$, $b_2 = 2.69188$, $X3b = -1/(b_3\cdot FBW)$, $b_3 = 1.96$ and

$$Y\_Extra = -jK_{23}\cdot\left(\frac{f}{f_{b3}} - \frac{f_{b3}}{f}\right).$$

Table 5.2 shows optimized sizes to attain NRN 1 frequency response in Figure 5.7.

Table 5.2 Optimized parameters for NRN1

Parameter	Optimized value
W_{12} (M_{12})	0.649 inch
W_{23} (M_{23})	0.758 inch
W_{24} (M_{24})	0.56 inch
L_{Z_LO} (Side cavity length)	1.0248 inch

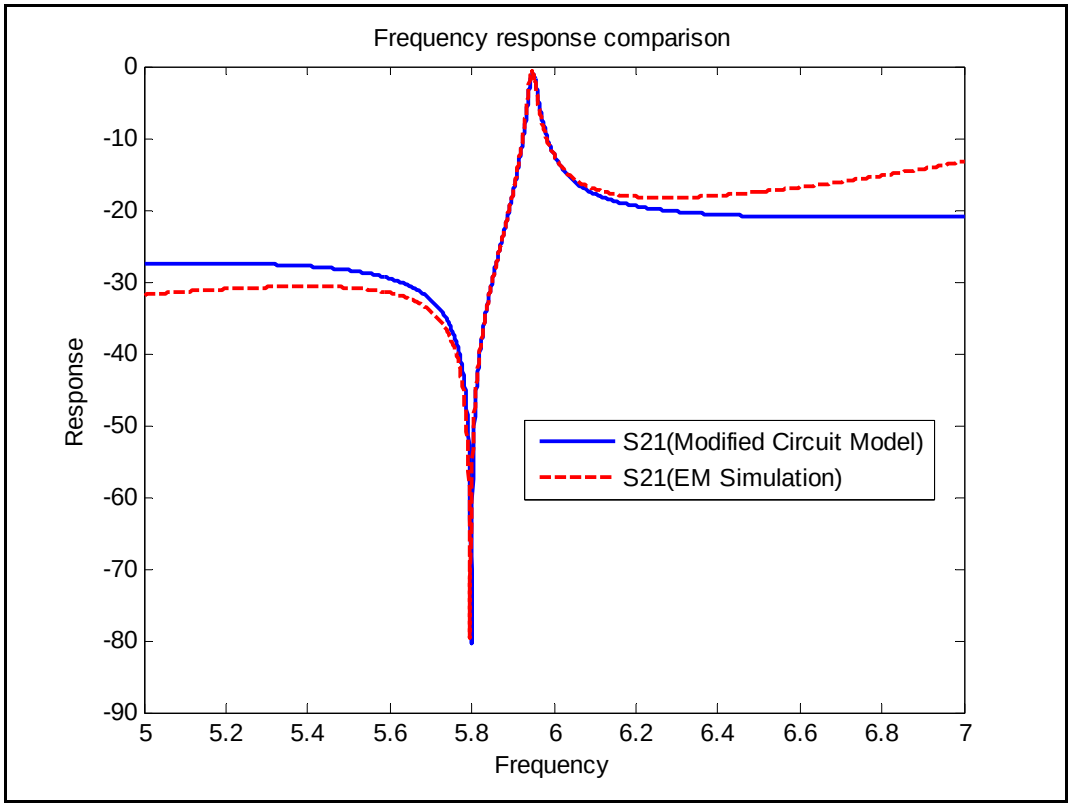

Figure 5.7 Frequency responses after manual optimization

5.2.3 Realize NRN 2

The cavity used as NRN2 is actually a resonator with an inductive susceptance. Therefore, the electrical length is chosen between the TE101 and the TE102 mode. To get a relatively large distance between two resonating frequency, the width of the cavity is chosen to be large, which reduces the waveguide dispersion to the frequency in the band of interest. Moreover, the length of the cavity is determined to have TE101 resonance lower than the cut-off frequency of NRN1.

Here, the width of the cavity is determined as 2.5inch, and the length is 1.4inch. The cavity has lowest resonating frequency of approximately 4.8 GHz (TE101) and second resonating frequency of around 8.4GHz. The design procedure of NRN 2 is the same as that of NRN 1.

Table 5.3 shows optimized sizes of NRN 2 which yield the frequency responses in Figure 5.9

Table 5.3 Optimized sizes of NRN 2

Parameter	Final Value
W_{68} (M_{68})	0.646 inch
W_{67} (M_{67})	0.755 inch
W_{56} (M_{56})	0.528 inch
L_{b7} (Side Cavity Length)	0.944inch

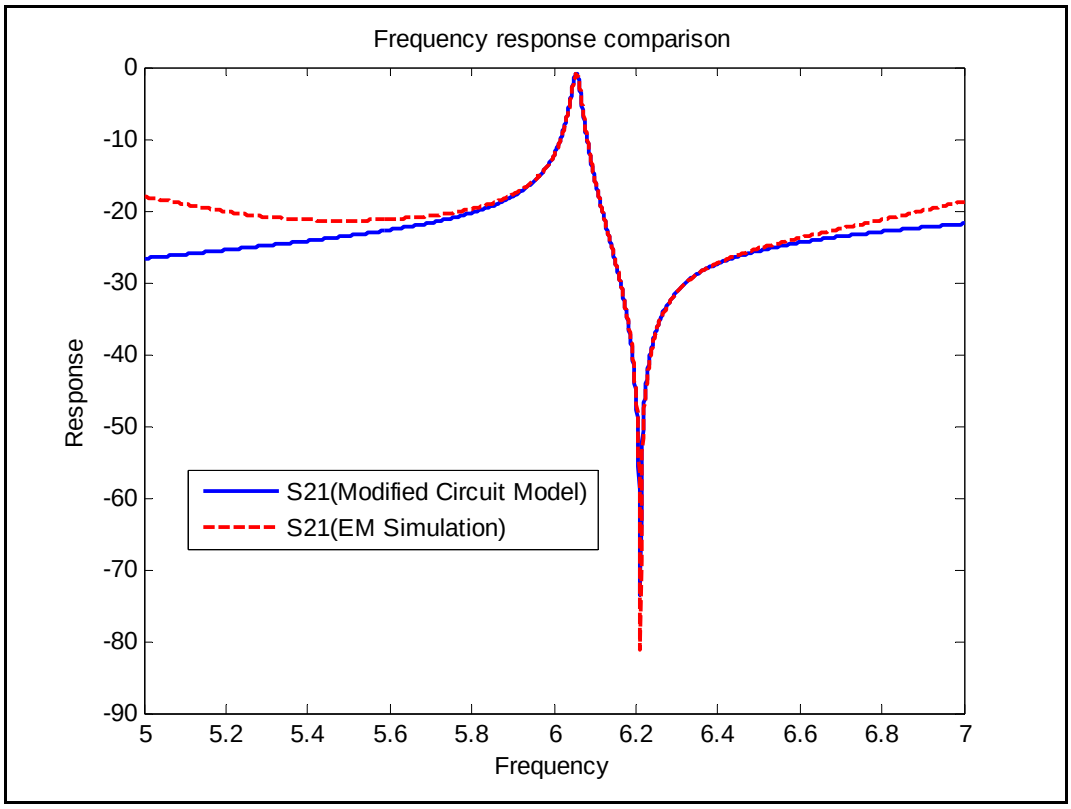

Figure 5.8 Frequency response of NRN2

5.2.4 Build 4-Pole Module

The 4-Pole module comprises of both NRNs and the two resonators between them. The size of the resonators and irises is obtained by the same method used in Section 2.3,

which are listed in Table 5.4 and Table 5.5. Figure 5.9 represents the frequency response of the 4-Pole module without optimization.

Table 5.4 Realizing coupling M45

Coupling value	K value	S21 Value	Iris Size	S21 of EM
M_{45}=0.638426	0.052687	-19.568 dB	0.353 inch	-19.54 dB

Table 5.5 Tuning resonator no.4 and 5

Normalized Frequency Offset	Resonating Frequency	Cavity Length
b4=0.209232	5.9781 GHz	$L_{\_b4}$=1.0912 inch
b5=-0.161598	6.017 GHz	$L_{\_b5}$=1.106 inch

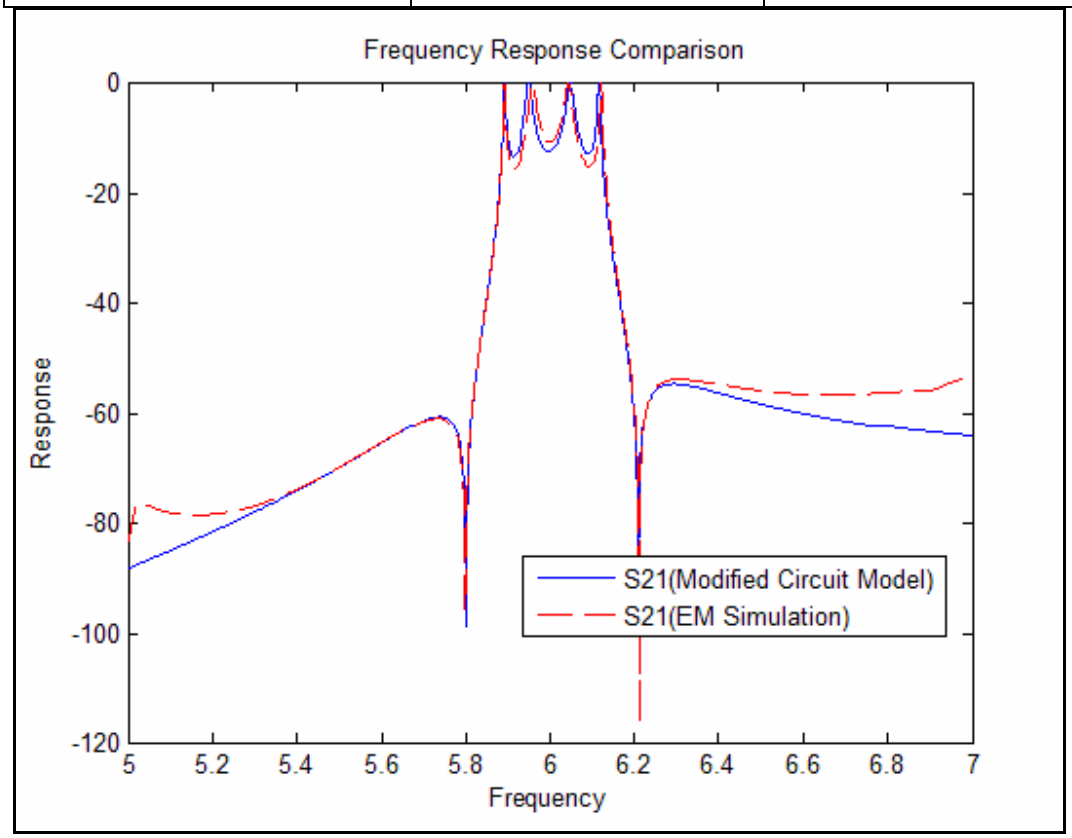

Figure 5.9 Frequency response of 4-Pole module before optmization

Since NRN1 and NRN2 are already tuned, the error in the frequency response is assumed to be caused by the width of the centre coupling iris W_{45} and cavity lengths $L_{\_b4}$ as well

as L_{b5}. Consequently, in the circuit model, only M_{45}, b4 and b5 are set as the optimizing variables to capture the EM response.

Table 5.6 shows optimized sizes, which yield a frequency response of the EM simulation almost superposed on that of circuit model as shown in Figure 5.10.

Table 5.6 Optimized sizes for 4-pole module

Size	Optimized Values
W_{45}	0.356 inch
L_{b4}	1.0862 inch
L_{b5}	1.1108inch

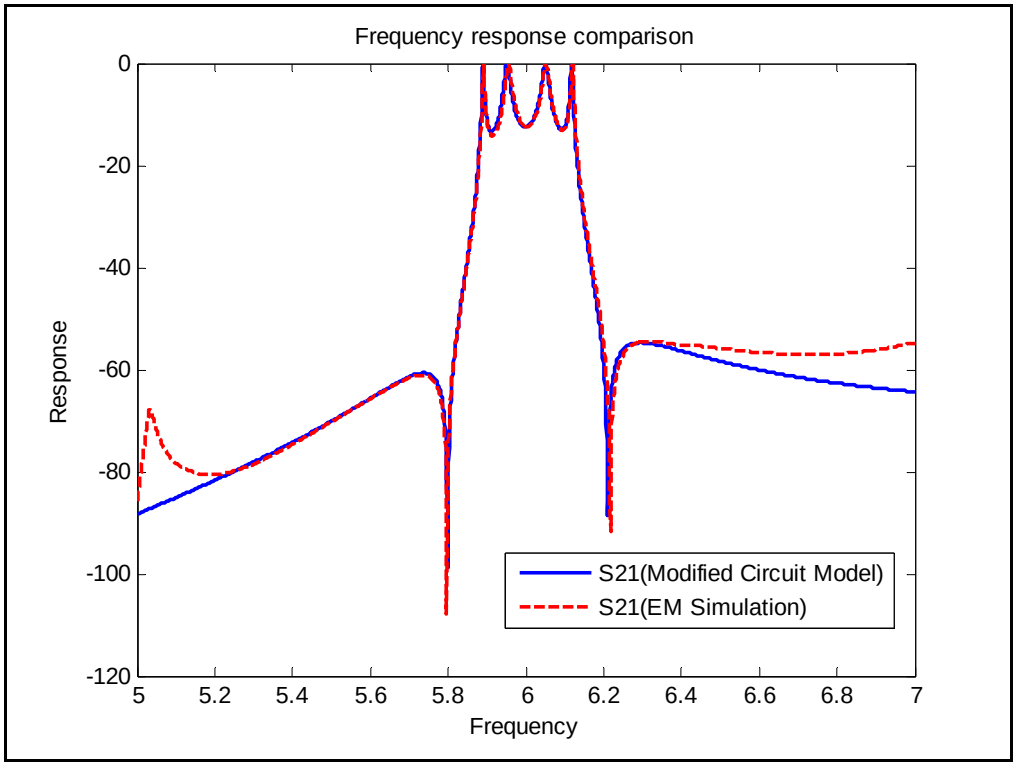

Figure 5.10 Frequency response of 4-pole module

5.2.5 Build Entire Filter

Calculate the remaining sizes of the filter, as in Table 5.7 and 5.8. Then the entire filter is built that yields the frequency response in Figure 5.11.

Table 5.7 Realizing coupling M01 and M89

Coupling Value	K Value	S21 Value	Iris Size	S21 of EM
M_{01}=1.16017	0.333289	-4.437 dB	0.6948 inch	-4.43326 dB
M_{89}=1.18258	0.339726	-4.3062 dB	0.6975 inch	-4.303 dB

Table 5.8 Tune resonator no.1 and 8

Normalized Frequency offset	Resonating Frequency	Cavity Length
b1=0.56327	5.9411 GHz	L_{b1}=0.9327 inch
b8=-0.625157	6.066 GHz	L_{b8}=0.956 inch

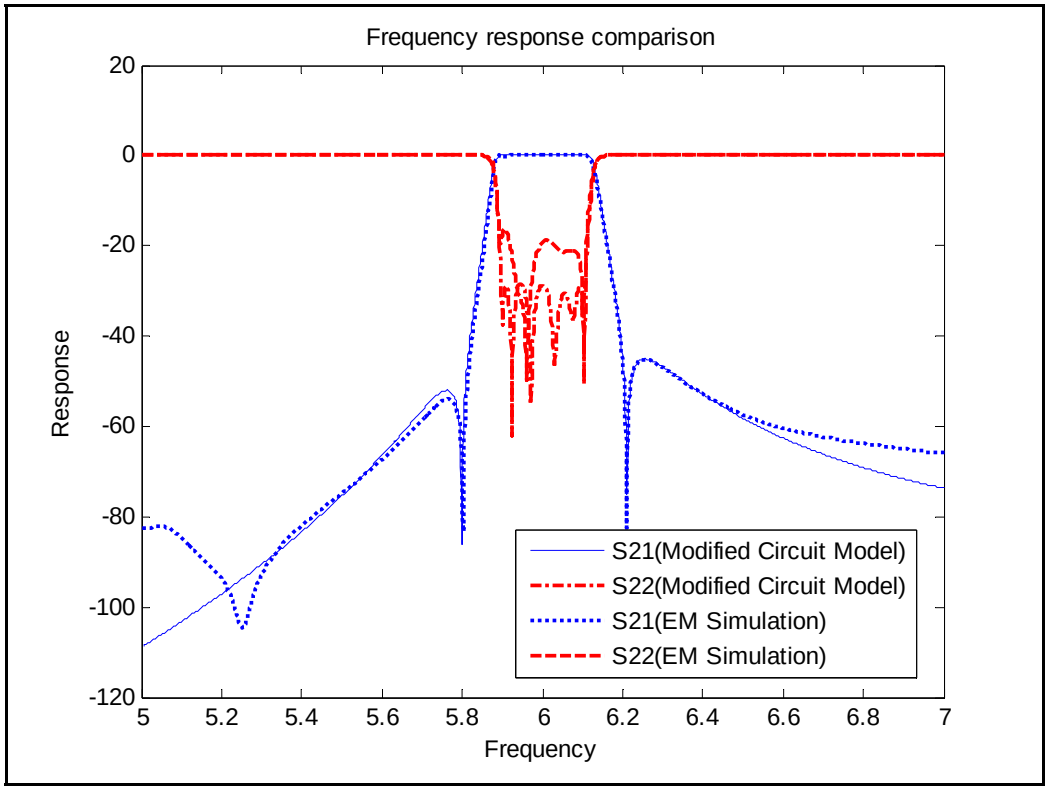

Figure 5.11 Compare of frequency responses of EM and circuit model

Here, the return loss is almost better than 20dB without any optimization. Optimizing only the input/output coupling irises and cavity lengths can further improve return loss performance to 22dB, as shown in Figure 5.12. Table 5.9 lists the relevant sizes optimized in this step.

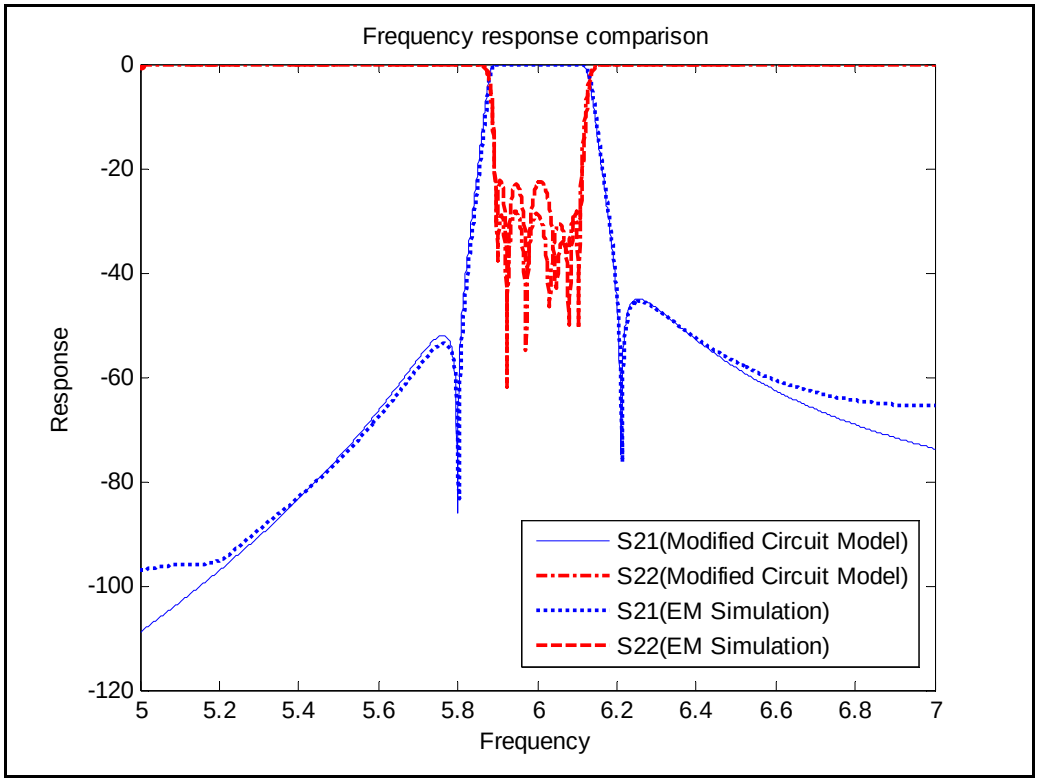

Figure 5.12 Frequency response of the filter after optimization

Table 5.9 Optimizing sizes of last step

Sizes	Values in individual tuning	Values after optimization
$W_{01}(M_{01})$	0.6948 inch	0.698 inch
$W_{12}(M_{12})$	0.649 inch	0.649 inch
$L_{\_b1}$	0.9327 inch	0.933 inch
$L_{\_b8}$	0.956 inch	0.964 inch

Finally, the filter performance is verified in HFSS with copper as the waveguide material. The response is denoted in Figure 5.13. and the insertion loss is less than 0.24dB.

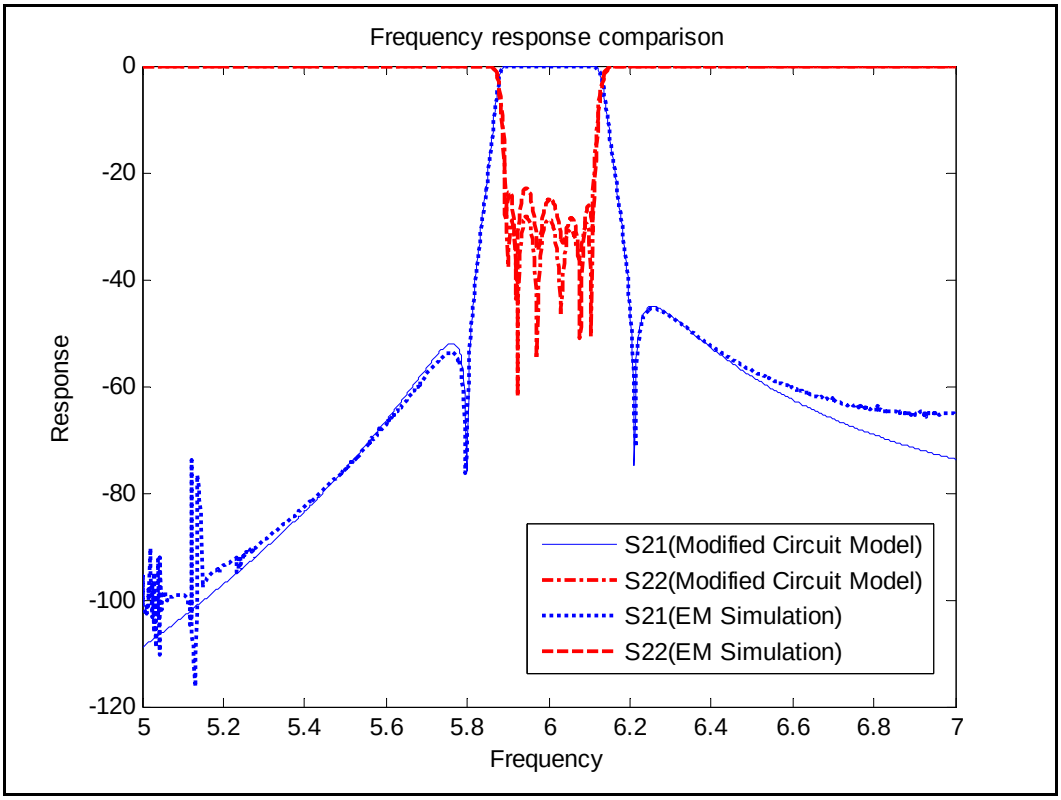

Figure 5.13 Frequency response of the filter with material of finite conductivity (copper)

5.3 Design NRN Filter with the Wide Bandwidth

In this section, a design example is given with a relatively wide bandwidth with BW=500MHz (FBW=8.33%). The other specifications of this filter remain the same as previous design example in Section 5.2.

5.3.1 Optimizing Parameters

Figure5.14 shows the frequency responses of both the ideal model and the modified circuit model with the original values.

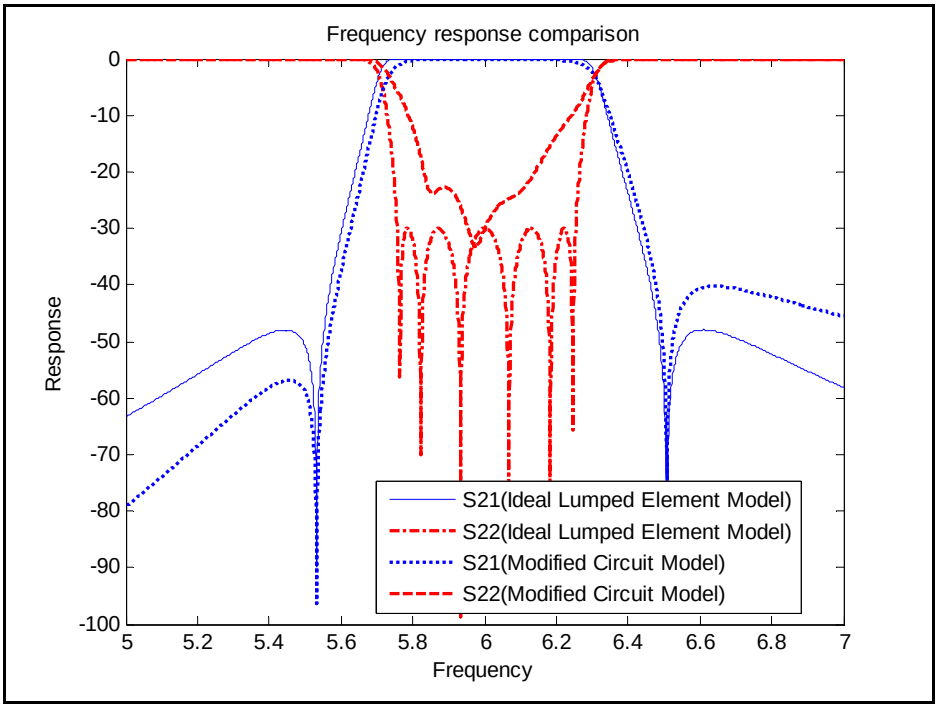

Figure 5.14 Frequency response of the filter with original values

The circuit model is then optimized to attain an acceptable frequency response as shown in Figure 5.15.

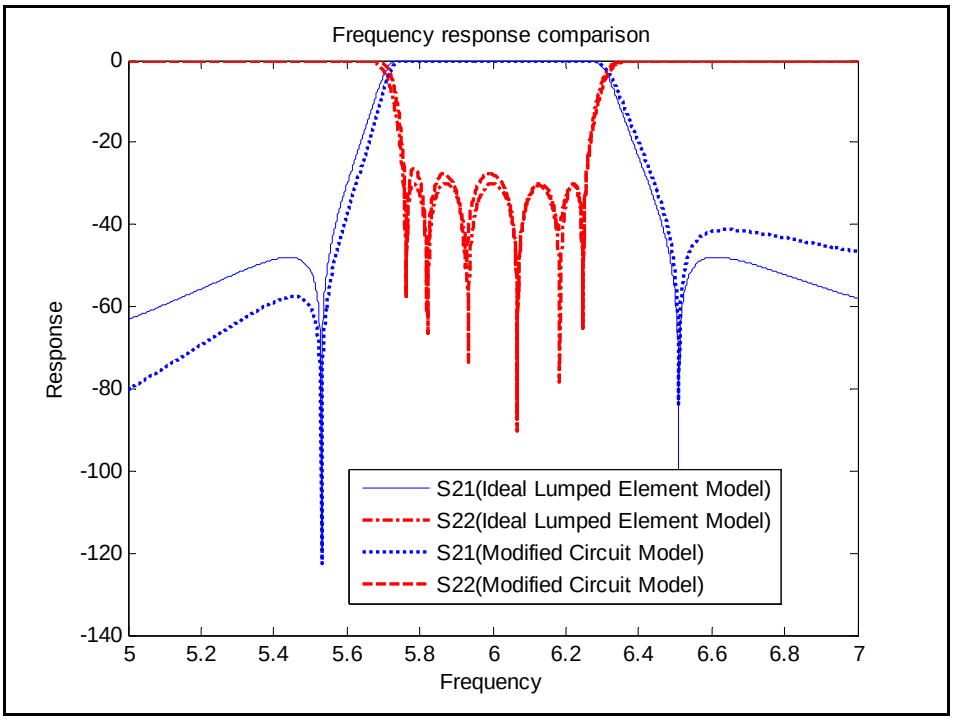

Figure 5.15 Frequency response of optimized filter with modified circuit model

The new parameters for the circuit model are summarized in Table 5.10.

Table 5.10 ideal and optimized value of the filter

Parameters	Ideal Values for Lumped Element Model	Optimized Values for Modified Circuit Model
M_{01}	1.19469	1.13065
M_{89}	1.19469	1.16395
M_{12}	1.30768	1.12738
M_{68}	1.30768	1.43722
M_{23}	1.96834	2.04833
M_{67}	1.96834	1.91036
M_{24}	0.82827	0.76044
M_{56}	0.82827	0.921174
M_{45}	0.64322	0.634436
b1	0.63525	0.470039
b8	-0.63525	-0.588563
b4	0.19261	0.233192
b5	-0.19261	-0.112289

With some trial simulations of NRN 1, it is found that the maximum realizable value for M_{23} is around 1.9 because of the limitation of the cavity width. Here, two options are available to resolve this problem:

1) The cavity width can be increased to accommodate a stronger coupling. This method might give a narrower spurious free window by bringing the resonating frequency closer to the interested band.
2) A fixed value for M23 can be selected, and the remaining parameters are optimized to yield an acceptable return loss. This method can compromise in the return loss performance.

In this design, the second approach is chosen; the maximum value of M23 is set to 1.9. Figure 5.16 shows some compromise in the return loss; however the overall performance is still considered to be good.

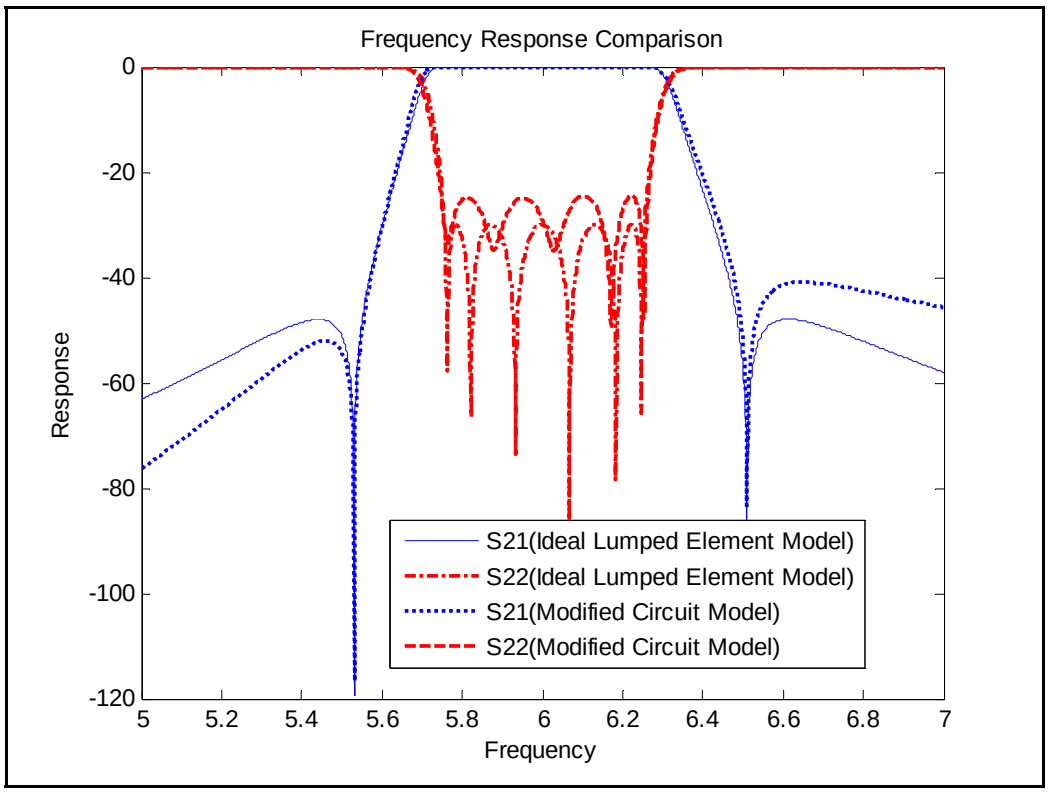

Figure 5.16 Optimized frequency response with M23 limited

The parameters used to attain the responses in Figure 5.16 are listed in Table 5.11.

Table 5.11 Parameters of coupling matrix

Parameters	Theoretical Values of Coupling Matrix	Optimized Value for Modified Circuit Model
M_{01}	1.19469	1.21248
M_{89}	1.19469	1.1024
M_{12}	1.30768	1.34104
M_{68}	1.30768	1.36586
M_{23}	1.96834	1.9
M_{67}	1.96834	1.94732
M_{24}	0.82827	0.830777
M_{56}	0.82827	0.928224
M_{45}	0.64322	0.660119
b1	0.63525	0.871662
b8	-0.63525	-0.486067
b4	0.19261	0.313446
b5	-0.19261	-0.0806057

5.3.2 Design Individual Modules

Following the same procedures as in Section 5.2, the filter is built with individually tuned modules.

Table 5.12 shows the sizes of NRN 1, which yields frequency responses in Figure 5.17.

Table 5.12 Relevant sizes of NRN1

Parameter	Initial Value	Final Value
W_{12} (M_{12})	0.8 inch	0.781 inch
W_{23} (M_{23})	0.9 inch	1.017 inch
W_{24} (M_{24})	0.7 inch	0.656 inch
AN_1 (Width of empty waveguide of NRN1)	1.1 inch	1.1 inch
LN_1 (length of empty cavity for NRN1)	0.65 inch	0.65 inch
L_{Z_LO} (Side cavity length)	1 inch ($\approx 0.5\lambda_g$)	0.892 inch

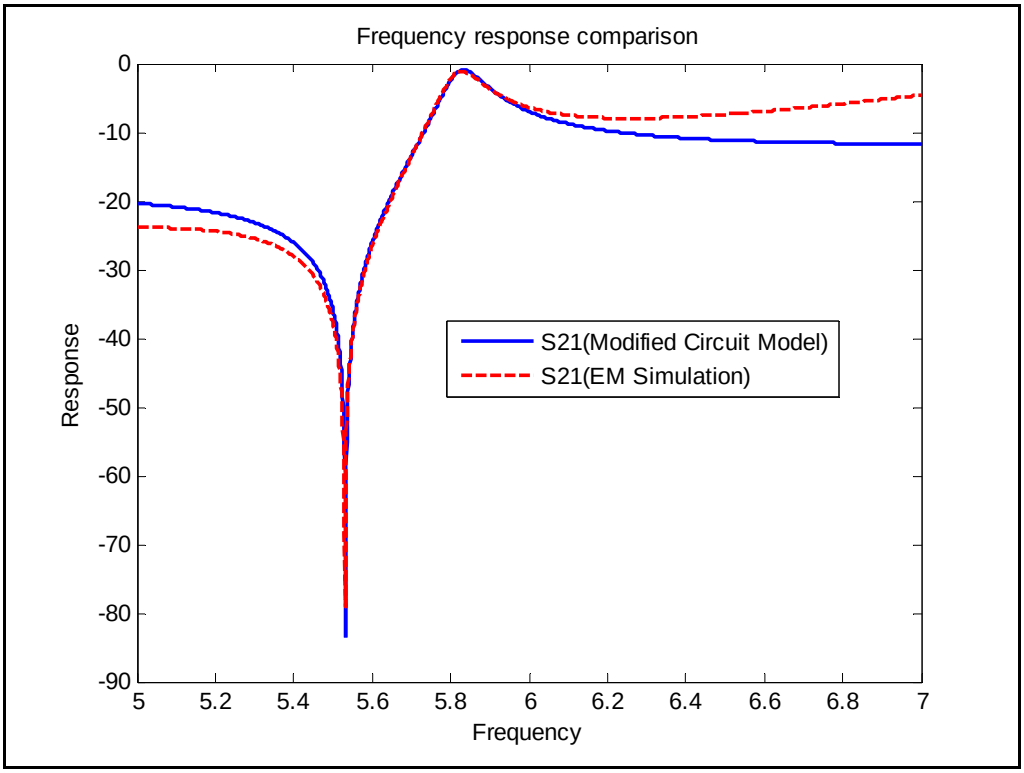

Figure 5.17 Frequency response of NRN 1

Table 5.13 and Figure 5.18 show the sizes and frequency responses of NRN 2.

Table 5.13 Relevant sizes of NRN2

Parameter	Initial value	Final value
W_{68} (M_{68})	0.8 inch	0.789 inch
W_{56} (M_{56})	0.6 inch	0.6436 inch
W_{67} (M_{67})	1 inch	0.848inch
AN_2 (Width of empty waveguide of NRN2)	2.5 inch	2.5 inch
LN_2 (length of empty cavity for NRN1)	1.4 inch	1.4 inch
L_{Z_HI} (Side cavity length)	1 inch ($\approx 0.5\lambda_g$)	0.7872inch

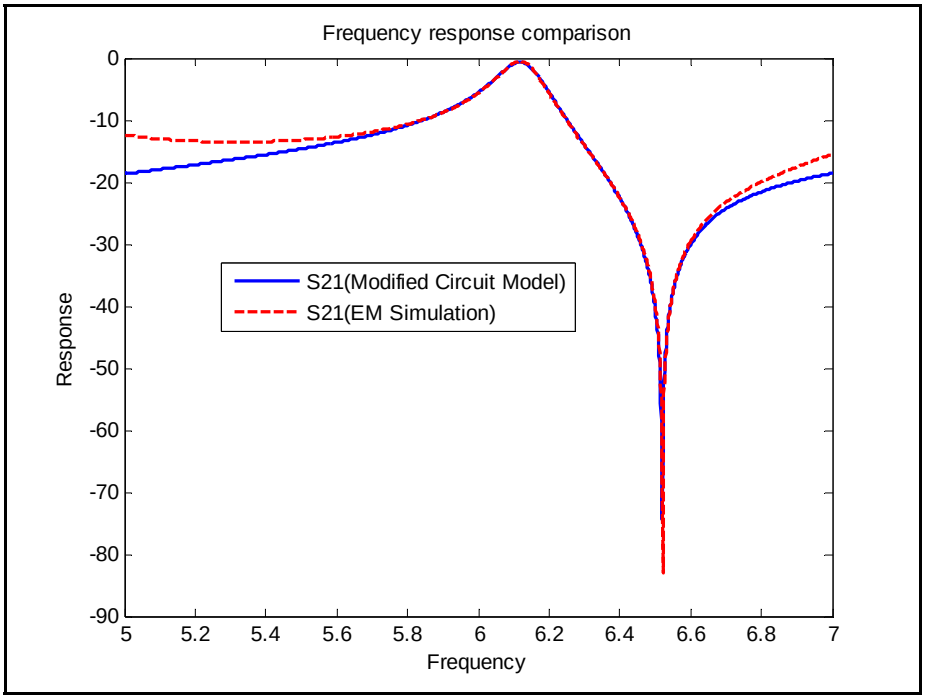

Figure 5.18 Frequency response of NRN2

When NRN 1 and NRN 2 are tuned, the 4-Pole module can be built with the frequency response displayed in Figure 5.19.

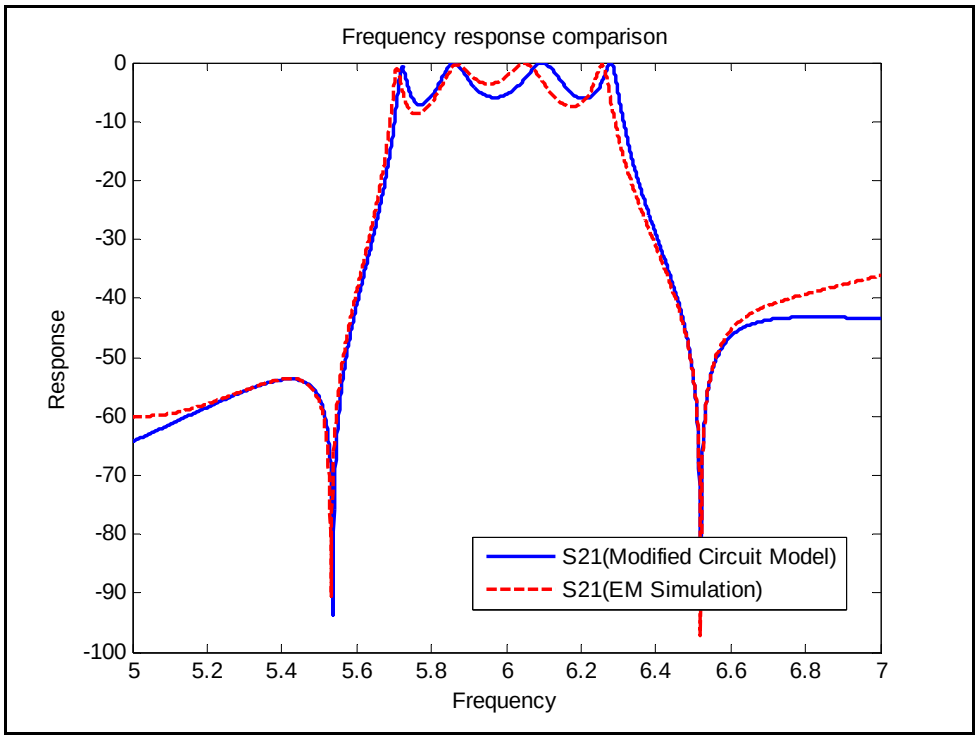

Figure 5.19 Initial Frequency response comparison of 4-pole EM structure and circuit model

Table 5.14 and Figure 5.2 show the relevant sizes and frequency response of the 4-Pole module.

Table 5.14 Relevant sizes of 4-Pole Module

Size	Initial Values	Final Values
W_{45}	0.491 inch	0.509 inch
$L_{\_b4}$	1.032 inch	1.001 inch
$L_{\_b5}$	1.044 inch	1.041 inch

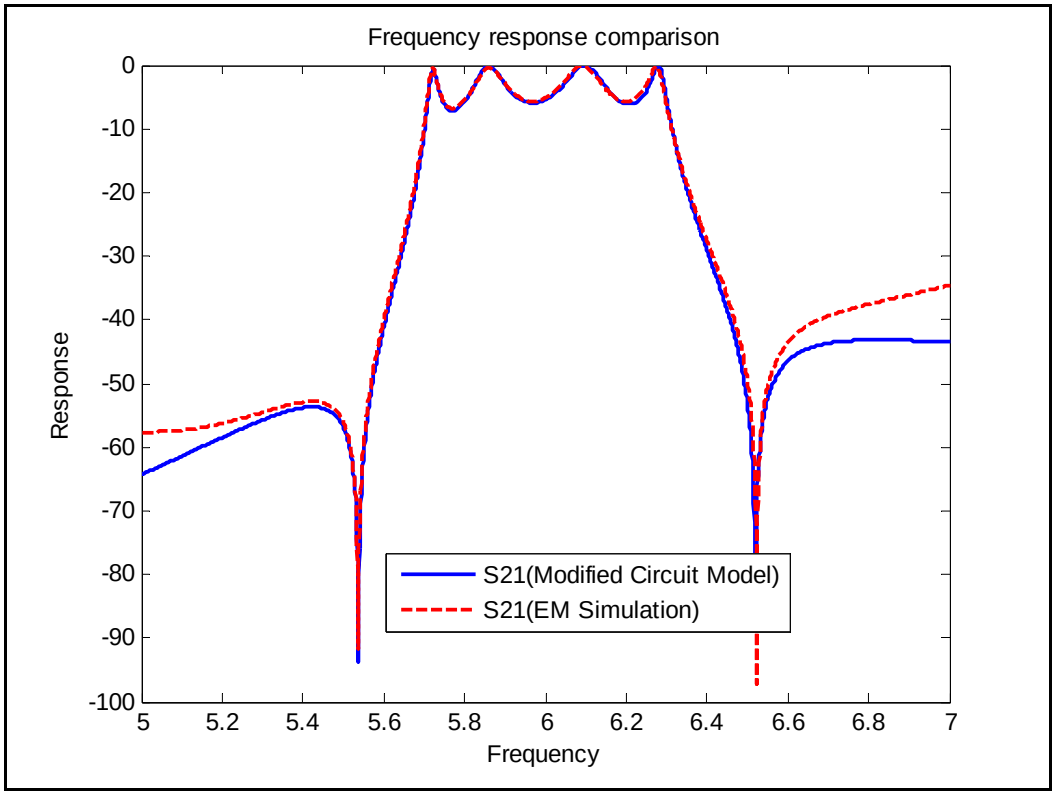

Figure 5.20 Frequency response comparison of 4-pole module after fine tuning

The rest of the parameters contain two coupling irises and two resonating frequencies with the relevant sizes, as shown in Table 5.15.

Table 5.15 Relevant sizes of the filter in last step

Size	Initial Values
W_{01}	0.865 inch
W_{89}	0.812 inch
$L_{\_b1}$	0.7892 inch
$L_{\_b8}$	0.865 inch

5.3.3 Entire Filter Response and Optimization

Once all parts are designed, the entire filter has the frequency response shown in Figure 5.21.

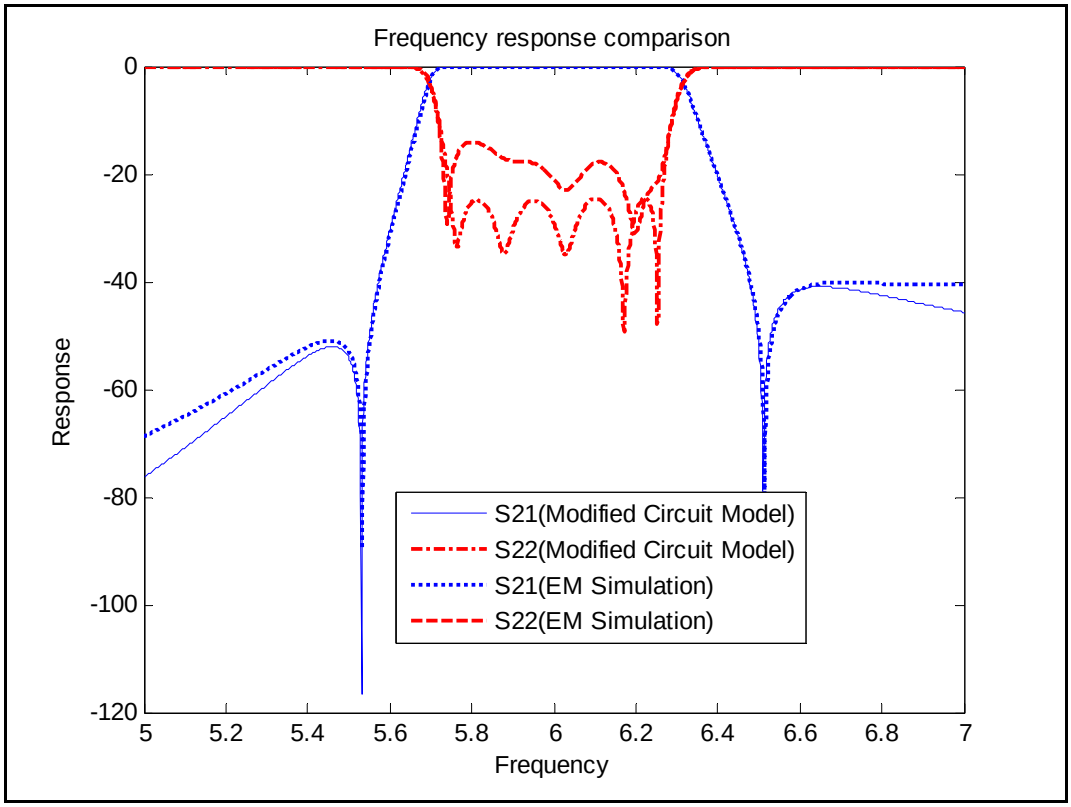

Figure 5.21 Frequency response after individual tuning

In this case, optimizing only the newly added parameters does not help much to improve the filter performance. This is probably due to the wider bandwidth of this filter. To further improve the return loss, a global optimization is needed.

Nevertheless, the permitted variation of all the previously tuned parameters can be limited to a very narrow range to avoid any divergence. Table 5.16 shows the parameters before and after optimization. Except the four relevant parameters in the last step, the others have been changed very little. The frequency responses of optimized filter are portrayed in Figure 5.22.

Table 5.16 Filter sizes before and after global optimization

Sizes	Values in Individual Tuning	Values after Optimization
$W_{01}(M_{01})$	0.865 inch	0.879 inch
$W_{12}(M_{12})$	0.781 inch	0.777 inch
$W_{23}(M_{23})$	1.017 inch	1.017 inch
$W_{24}(M_{24})$	0.656 inch	0.659 inch
$W_{68}(M_{68})$	0.789 inch	0.796 inch
$W_{56}(M_{56})$	0.644 inch	0.648 inch
$W_{67}(M_{67})$	0.848 inch	0.848 inch
$W_{45}(M_{45})$	0.509 inch	0.505 inch
$W_{89}(M_{89})$	0.812 inch	0.813 inch
L_{b1}	0.7892 inch	0.7744 inch
L_{b8}	0.865 inch	0.854 inch
L_{b4}	1.001 inch	0.999 inch
L_{b5}	1.041 inch	1.042 inch

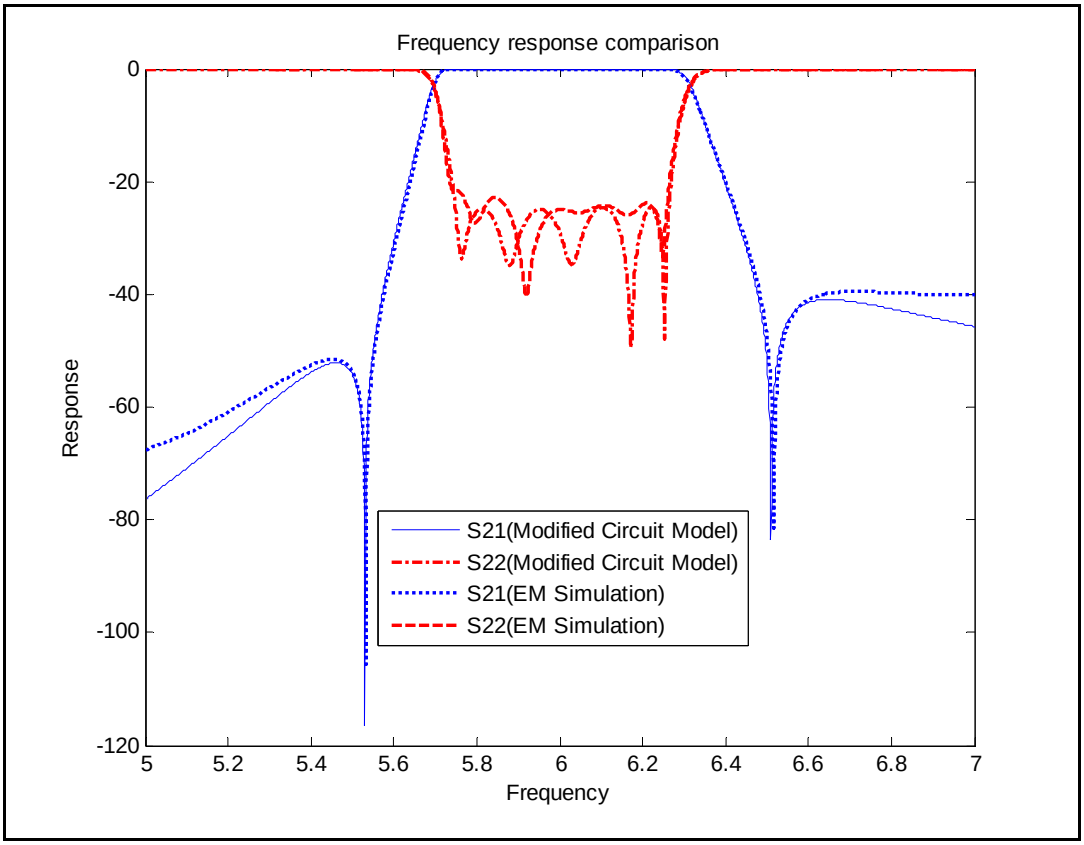

Figure 5.22 Frequency response of the filter after optimization

Figure 5.23 signifies the frequency response with finite conductivity, and Figure 5.23 shows the frequency response of the same filter with a wider band sweep. The insertion loss is less than 0.2dB.

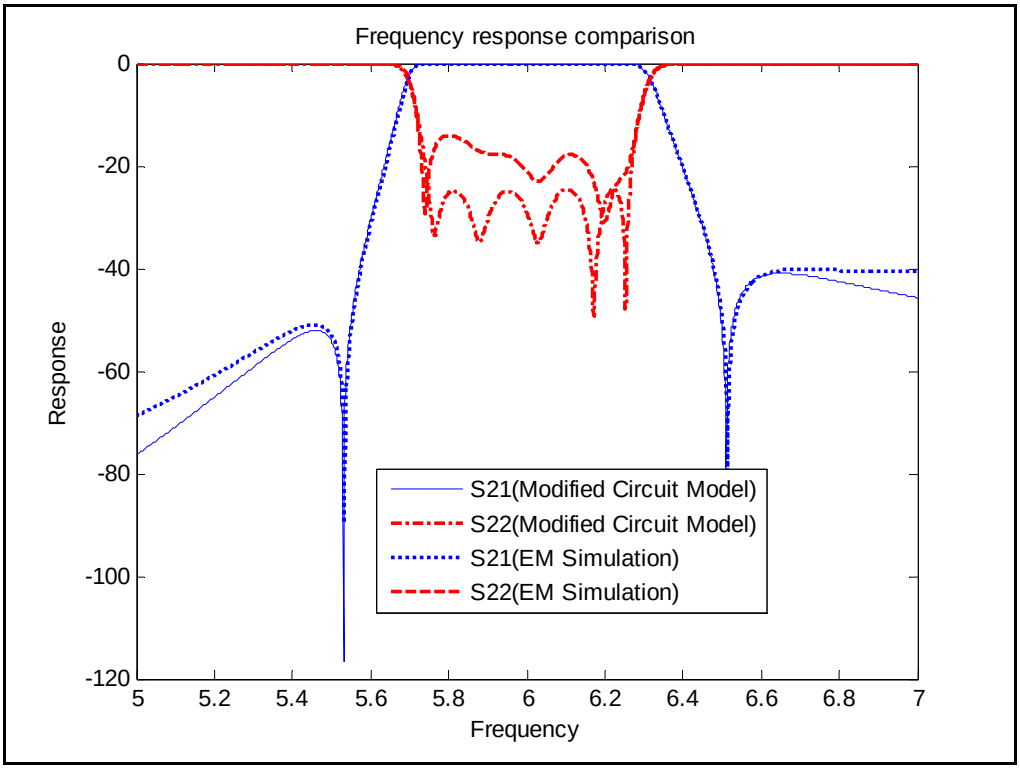

Figure 5.23 Frequency response of the filter with material of finite conductivity (copper)

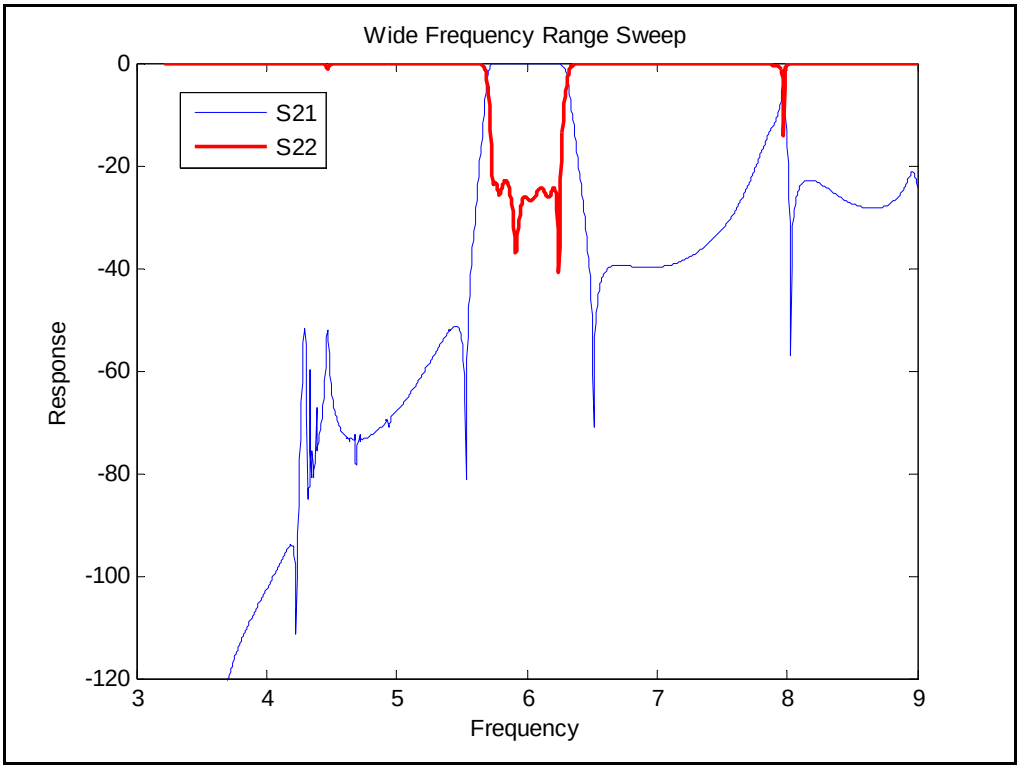

Figure 5.24 Wider frequency range sweep (filter with copper)

5.4 Summary of the Design Procedure

In this chapter, two waveguide filters with NRNs are designed with the same procedure the steps of which are summarized and listed as follow:

1) Calculate the filter parameters with the extracting pole method described in Section 3.2.
2) Build the novel circuit model described in Section 4, the values of all components are calculated from the ideal parameters obtained from the first step.
3) Optimize the values of the components in the novel circuit model in order to reach desired performance, as described in Section 5.2.1 and Section 5.3.1.
4) Build the individual module of NRNs based on the optimized values of the components in the novel circuit model; the module of the NRN comprises the NRN and side cavity coupled to it. The frequency responses of the individual modules are tuned by comparing it to those from the circuit model. This step is described in Section 5.2.2 and Section 5.2.3
5) Add the cavities and couplings between the NRNs, and then optimize the newly added parameters with the corresponding circuit model as described in Section 5.2.4.
6) Add the cavities and couplings between each NRN and input/output nodes, and then optimize the newly add parameters with the corresponding circuit model as described in Section 5.2.5. In wider bandwidth application, it might be necessary to perform global optimization; however a narrow variation range can be set for those parameters optimized in the previous steps in order to obtain a relatively faster convergence.

Moreover, when choosing the empty waveguide to function as the NRN, some criteria on determining the dimension of the waveguide are proposed to improve the spurious free window of the filter response.

1) To realize the NRN with the capacitive susceptance, as NRN 1 in the designs of Section 5, the electrical length of the waveguide is less than the TE101 mode, and

the width of the waveguide cavity is chosen to bring the cut-off frequency very close to the band of interest in order to guarantee a resonance free performance at a lower frequency as well as a higher frequency resonance far away from the band of interest.

2) To realize the NRN with the inductive susceptance, as NRN 2 in the designs of Section 5, the width and the length of the cavity must be optimized to generate the first resonating frequency (the TE101 mode) lower than the cut-off frequency of NRN 1, and the second resonating frequency (the TE102 mode) as high as possible. Usually a wider cavity is less dispersive, and thus has more widely spread resonating frequencies.

With the previous procedure, both filters are built with success. In the case of designing the intermediate bandwidth filter, good performance is obtained without any overall optimization; for designing the wide bandwidth filter, global optimization is necessary. However the results indicate that the previously fine tuned parameters need very little adjustment. Therefore the variation range of those parameters can be limited to obtain a fast convergence.

6. **Conclusion and Future Work**

A novel circuit model of the coupling iris for waveguide filters is proposed in this thesis for the efficient design of waveguide filters with non-resonating nodes (NRNs).

Compared to the lumped element model, which has been used for filter optimization, this novel circuit model better approximates the frequency dependence of the coupling iris within a relatively wide bandwidth.

Based on this circuit model, a systematic design procedure is developed to design the waveguide filter with NRNs with individual modules. In the thesis, two design cases indicate that designing the filter with this procedure requires much less global optimization. The bandwidth of the filter can reach as wide as 8.333%.

Furthermore, some new criteria are proposed on determining the dimensions of the waveguides which function as NRNs in order to improve the spurious free window

Future work in this area may involve integrating this novel circuit model in an automatic filter design and tuning software. With its capability to better approximate the frequency dependence of the coupling irises, a more efficient design and optimization of waveguide filters with NRNs are expected.

References

[1] A. E. Atia and A. E. Williams, “Narrow-Bandpass Waveguide Filters,” IEEE Trans. Microwave Theory Tech., vol. MTT-20, No.4, pp. 258-265, April 1972.

[2] A. E. Atia and A.E. Williams, “New Types of Waveguide Bandpass Filters for Satellite Transponders,” Comsat Tech. Review vol. 1, No.1, pp. 20-43, Fall 1971.

[3] R. J. Cameron, “General Coupling Matrix Synthesis Methods for Chebyshev Filtering Functions,” IEEE Trans. Microwave Theory Tech., vol. 47, No.4, pp. 433-442, April 1999.

[4] R. J. Cameron, “Advanced Coupling Matrix Synthesis Techniques for Microwave Filters,” IEEE Trans. Microwave Theory and Tech. vol. 51, No.1, Jan. 2003.

[5] R. J. Cameron, A. R. Harish, and C. J. Radcliffe, “Synthesis of Advanced Microwave Filters Without Diagonal Cross-Coupling,” IEEE Trans. Microwave Theory and Tech. Vol. 50, No.12, pp. 2862-2872, Dec. 2003.

[6] R. J. Cameron, J. C. Faugere, and F. Seyfert, “Coupling Matrix Synthesis for a New Class of Microwave Filter Configuration,” Microwave Symposium Digest, 2005 IEEE MTT-S International, June 2005.

[7] R. J. Cameron, R. R. Mansour, C. M. kudsia, “Theory and Design of Modern Microwave Filters and Systems Applications,” John Wiley & Sons Inc. Hoboken, New Jersey, pp.279-318, 2007.

[8] J. S. Hong, M.J. Lancaster, “Microstrip Filters for RF/Microwave Applications,” John Wiley & Sons Inc, pp104-116, 2001

[9] Ian Hunter, “Theory and design of microwave filters,” pp.61-74, IEE electromagnetic waves series; pp.48. 2001.

[10] Jorge A. Ruiz-Cruz, Kawthar A. Zaki, Jose R.. Montejo-Garai, Jesus M. Rebollar, “Rectangular waveguide elliptic filters with capacitive and inductive irises and integrated coaxial excitation,” Microwave Symposium Digest, 2005 IEEE MTT-S, June 2005.

[11] T. Shen, Heng-Tung Hsu, K. A. Zaki, A. E. Atia, “ Full-Wave Design of Canonical Waveguide Filters by Optimization”, IEEE Trans. Microwave Theory and Tech., vol. 51, No. 2, February 2003.

[12] HFSS Software Package, Pittsburg, PA. WWW.ANSOFT.COM

[13] Jan Kocbach, Kjetil Folgero, “Design Precedure for Waveguide Filters with Cross-Couplings” IEEE MTT-S Digest, 0-7803-5/02, 2002.

[14] David M. Pozar, “Microwave Engineering” 2nd Edition, John Wiley and Sons Inc., pp 211, 1998.

[15] Aravind B. Sanadi, M. Ramesh, A.T. Kalghatgi, “Simplified Design and Analysis Method for a Waveguide Iris Filter” International Journal of RF and Microwave Computer-Aided Engineering, vol 9, Issue 2, pp 150-154, John Wiley & Sons, Inc., 1999.

[16] S. Amari, “Direct Synthesis of Folded Symmetric Resonator Filters With Source-Load Coupling,” IEEE Microwave and Wireless Components Letters, vol. 11, No. 6 pp. 264-266, June 2001.

[17] Apu Sivadas, Ming Yu and Richard Cameron, “A Simplified Analysis for High Power Microwave Band pass Filter Structures,” IEEE MTT-S Digest, 0-7803-5687/00, 2000.

[18] S Amari and U. Rosenberg, “New Building Blocks for Moddular Design of Elliptic and Self-equalized Microwave Filters,” IEEE Microwave and Wireless Components Letters, vol. 14, No. 5, pp. 237-239, May 2004.

[19] S Amari, U. Rosenberg and J. Bornemann, “Singlets, Cascaded Singlets and the Non-resonating Node Model for Advanced Modular Desigh of elliptic Filters,” IEEE Trans. Microwave Theory Tech., vol. 52, No.2, pp. 234-256, Feb.2004.

[20] S Amari and G. Macchiarella, “Synthesis of Inline Filters With Arbitrarily Placed Attenuation Poles by Using Non-resonating Nodes,” IEEE Microwave Theory and Tech., vol. 53, No. 10, pp. 3075-3081, May 2005.

[21] S Amari and U. Rosenberg, “Synthesis and Design of Novel in-Line Cavity Filters with One or Two Real Transmission Zeros,” IEEE Trans. Microwave theory and tech., Vol. 2, No. 5, pp. 1464-1478, May 2004.

[22] S. Cogollos, R. J. Cameron, R. R. Mansour, M. Yu and V. E. Boria, “Synthesis and Design Precedure for High Performance Waveguide Filter based on Non-resonating Nodes,” Microwave Symposium, 2007. IEEE/MTT-S International, pp.1297 – 1300, June 2007.

[23] H. Y. Hwang and S. Yun, “The design of bandpass filters considering frequency dependence of inverters,” Microwave J. vol.45, No. 9, pp.154-163, Sept. 2002.

[24] F. M. Vanin, D. Schmitt, and R. Levy, “Dimensional Synthesis for Wide-Band Waveguide Filters and Diplexers” IEEE Trans. Microwave theory and tech. vol. 52, No. 11, November 2004.

[25] Ansoft Designer Software Package, Pittsburg, PA. WWW.ANSOFT.COM

[26] R. J. Cameron, R. R. Mansour, C. M. kudsia, “Theory and Design of Modern Microwave Filters and Systems Applications,” John Wiley & Sons Inc. Hoboken, New Jersey, pp.544-552, 2007